A study of the low spin states of ^{223}Th and ^{223}Ra as populated by α-decay.

Thesis submitted in accordance with the
requirements of the University of Liverpool
for the degree of Doctor in Philosophy.

by

Thomas Henry Hoare.

Oliver Lodge Laboratory July 1991

Abstract

The low spin states of ^{223}Th and ^{223}Ra have been populated via α-decay. The parent nucleus of ^{223}Th (^{227}U, $T_{1/2}$ $\sim$1 min) was formed in the reaction ^{208}Pb(^{22}Ne,3n)^{227}U, E_{beam} = 110 MeV. Out-of-beam measurements of α-γ and α-e coincidences were performed with the aid of a rotating target mechanism. These measurements have enabled a limited level scheme of the low-spin states in ^{223}Th to be constructed, along with tentative I^{π} assignments and α hindrance factors. The data are interpreted in terms of the geometric model assuming a static octupole deformation and compared to that for the N = 133 isotones ^{221}Ra and ^{219}Rn.

In the case of ^{223}Ra the parent nucleus (^{227}Th, $T_{1/2}$ = 19 d) was produced by the β^--decay of an ^{227}Ac ($T_{1/2}$ = 22 y) source. For this study we have designed a versatile and compact system which allows the simultaneous measurements of α-γ and α-$e_{K,L,M}$ angular correlations and hence allows the determination of internal conversion coefficients. The measurements have enabled unique spin parity values to be assigned to all bar one (315.5 keV) of the levels below 400 keV in ^{223}Ra. The results are compared to theoretical calculations that assume a static octupole deformation with β_3 $\sim$0.1.

Acknowledgements

The work described in this thesis was carried out during the academic years 1987 to 1990 and was supported by the U.K. Science and Engineering Research Council and by the Institut Interuniversitaire des Sciences Nucléaires, Brussels, Belgium. I wish to acknowledge the receipt of a S.E.R.C. postgraduate studentship and financial support (in the form of a C.A.S.E. award) from Canberra Limited.

I am grateful to Professor E. Gabathuler for allowing me to pursue my research in the Department of Physics at Liverpool.

I would especially like to thank Dr. G.D. Jones and my supervisor Dr. P.A. Butler for their guidance, encouragement and constant stream of advice and fruitful discussions.

I would also like to thank the members of the international Nuclear Structure Community who gave assistance in the running of the experiments: M.Dahlinger, A.M.Y. El-Lawindy, M. Loiselet, O. Naviliat-Cuncic, J. Vervier, R. Wadsworth, D.L. Watson and C.A. White; with particular thanks to W. Nazarewicz for his theoretical calculations and subsequent fruitful discussions. I am also grateful to the skilful technical support of Mr. C. Lowndes, his contribution to the installation and operation of the experimental equipment was invaluable.

During the course of my PhD. studies I have had the opportunity to participate in several experiments (some of which have not been directly related to my thesis work). These experiments were carried out at the Cyclone Cyclotron at the University of Louvain-la-Neuve, Belgium and the Nuclear Structure Facility, Daresbury. I should like to thank both institutions and all the people involved for their hospitality and the facilities extended to me during my visits.

My appreciation extends to the computer support staff, both at Liverpool and at Daresbury, for providing an excellent service and also to all the Lecturers and speakers that have attempted to pass on their knowledge to me during the course of my studies.

Finally, I would like to dedicate this thesis to my three children: Matthew, Rebecca and Daniel. (There you go kids fame at last, well almost.)

Contents

Introduction

The neutron-deficient light actinides (Z~88, N~132) are of interest because they lie in a transitional region where many examples of the following phenomena have now been observed:

(i) 1^- states of unusually low energy

(ii) interleaving positive and negative parity states with strong E1 transitions between them

(iii) parity doublets in odd-A nuclei

These phenomena have been cited as evidence for octupole deformation in nuclei which arise from the coupling of close-lying states with $\Delta\ell = 3$ and $\Delta j = 3$ (Sheline, 1980).

Early calculations did not allow any potential energy minima for non-zero octupole deformation, as a consequence of this the deformation was interpreted as being vibrational in nature with stabilization of the octupole shape only occurring at high spin. With the advent of the *Strutinsky method* (Strutinsky, 1967) and the use of more realistic nuclear potentials, ground state stable octupole deformation became a possibility for nuclei in the Ra region (Leander, 1982). The nuclei studied in this thesis, ^{223}Th and ^{223}Ra, both lie within the light actinide region of octupole deformation mapped out by Sheline (1987).

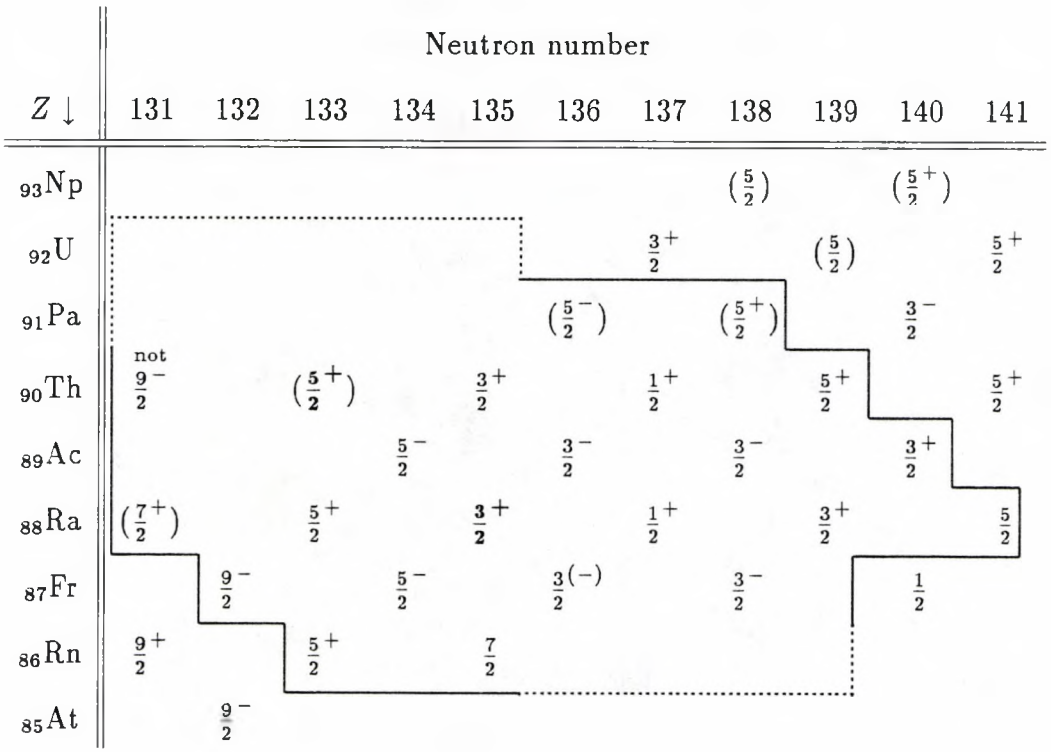

Table 1: Light actinide region of octupole deformation as mapped out by Sheline (1987) and updated by Jain *et al.* (1990).

For example, see table 1 where part of figure 32 from Jain *et al.* is reproduced. The table lists the ground state spins and parities of odd-A nuclei beyond ^{208}Pb, the region of expected octupole deformation is bounded by the solid or dotted lines.

The Strutinsky method adopts the macroscopic-microscopic approach which links together two well established nuclear models: the Liquid Drop model (LDM) and the Shell model (SM). Chapter one explains the principle of this method after first describing the models involved. The chapter also describes the rotational and vibrational excitations of the Colective model (CM). The CM is also known as the unified model since it combines certain features of the LDM and the SM. Chapter one ends with a discussion of the octupole degree of freedom with particular reference to the light actinide region.

As the title implies, the investigations of this thesis concerns the low spin structure of the light actinide nuclei ^{223}Th and ^{223}Ra. A convenient method of populating the low spin states of these nuclei is by α-decay. In chapter two α-decay is discussed with reference to the one-body formalism of Preston (1947). The concept of the hindrance factor is also explained in this chapter along with the process of internal conversion and the selection rules involved in γ-decay.

The ideas behind γ-γ angular correlations are explained in chapter three with the aid of a simple example. The general results are also quoted and extended to include the cases of α-γ and α-e angular correlations. The chapter finishes by considering the corrections that need to be added to the theory to allow for the less than ideal conditions inherent in an experimental set up.

Chapters four and five explain the experimental arrangements and the data analysis techniques used in the study of ^{223}Th and ^{223}Ra. The ^{223}Th experiment was carried out at the University of Louvain-la-Neuve, while the ^{223}Ra experiment was carried out here at the University of Liverpool. In the case of the ^{223}Th experiment the material presented in this thesis (with the exception of section 4.4—the half-life measurement of ^{227}U) has also been published in the *Journal of Physics G*, as has a preliminary report on the ^{223}Ra experiment. In this second publication the α-γ angular correlations of the 79.7 and 350.5 keV ground state transitions in ^{223}Ra were used to demonstrate the capability of the versatile and compact six-detector system of chapter five.

Finally, in chapter six the results of the above experiments are discussed in terms of static octupole deformation. In the case of the ^{223}Th experiment the level scheme is compared to those of the N = 133 isotones ^{221}Ra and ^{219}Rn. The results of the ^{223}Ra experiment are compared to the theoretical calculations of Leander and Chen (1988) and Sheline *et al.* (1988).

Chapter 1

Nuclear Models

1.1 Introduction

It is not possible to solve exactly the dynamics of any system consisting of more than two interacting bodies, however, in many cases very accurate solutions can be obtained if appropriate assumptions are made to simplify the situation (ie. effectively reduce the *many-body problem* to that of a two body interaction). For example, in the solar system the dominant interactions are those between the sun and its planets. If it is assumed that the force between the sun and any given planet is unaffected by the existence of interplanetary interactions (that are small by comparison), then solutions of planetary motions can be obtained that are in excellent agreement with the observed facts.

In the case of the atomic nucleus, where there is a dense cluster of strongly interacting particles exhibiting different forms of behaviour, things are not so simple. Finding a precise description of such a complex system is an extremely difficult task. In fact, no single treatment can be applied to predict all nuclear properties and several different models have emerged that take account of particular aspects of nuclear behaviour. Restricting a model in this way

enables it to be made simple enough to alow a proper mathematical treatment of its properties. The hope then is that the results so obtained will help in the understanding of the analogous properties of the real nucleus.

1.2 The Liquid Drop Model

Two experimental facts allow the nucleus to be likened to an incompressible liquid drop. Firstly, over a wide range of nuclei the binding energy per nucleon remains approximately constant. Secondly, since the nuclear radius is found to be given by $R = R_{\circ}A^{1/3}$, the number of nucleons per unit volume is also constant. Both of these properties arise from the short range nature of the nuclear force. This short-range nature results in bonds being formed between close neighbouring nucleons only. The force is said to *saturate*: once there are enough close neighbours the binding energy of one particular nucleon is not altered by the presence, or absence, of more distant neighbours.

The semi empirical mass formula (von Weizäcker 1935) uses the liquid drop model (LDM) to express the total binding energy, B, as a function of A and Z:

$$B(A,Z) = \underbrace{a_v A}_{1} - \underbrace{a_s A^{2/3}}_{2} - \underbrace{a_C Z^2/A^{1/3}}_{3} - \underbrace{a_{sym}(A-2Z)^2/A}_{4} - \underbrace{\delta(A)}_{5} \qquad (1.1)$$

The five terms arise as follows:

1. The volume term; this is the total binding energy of the nucleons which, since the average binding energy per nucleon is constant, is proportional to A.

2. The surface term; this arises because the nucleons near the surface are not so tightly bound as those inside the nucleus, hence the volume term

is an overestimation and must be reduced. It is therefore proportional to the surface area ($\propto R^2 \propto A^{2/3}$).

3. The Coulomb term; this corrects for coulomb repulsion between the protons, it is proportional to Z^2 and inversely proportional to the nuclear radius ($\propto A^{1/3}$).

4. The symmetry term; this is included to favour a symmetric combination of nucleons (ie N=Z).

5. The pairing term; this is included for purely empirical reasons and takes account of the fact that, compared to odd-A nuclei, those nuclei with even Z,N are more stable while those with odd Z,N are less stable. Thus, δ(A) is defined as:

$$\delta(A) \begin{cases} < 0 & \text{for even-even nuclei} \\ = 0 & \text{for odd-A nuclei} \\ > 0 & \text{for odd-odd nuclei} \end{cases} \tag{1.2}$$

The five parameters of equation 1.1 can be evaluated by fitting to the experimental data. Various sets of values have been suggested, each set differing slightly depending on the range of nuclei under investigation. One such set of values, in MeV, which result in reasonably good agreement with measurements over the whole range of A-values is given by Evans (1955):

$$\begin{aligned} a_v &= 14.1 \\ a_s &= 13 \\ a_C &= 0.595 \\ a_{sym} &= 19 \\ \delta &= 33.5/A^{3/4} \end{aligned}$$

The model outlined above is based on the assumption that the nucleus has a well defined spherical surface. Corrections to the Coulomb and surface terms can be included to take account of surface diffuseness and deviation from spherical symmetry—for further details see Myers and Swiatecki (1966).

The LDM can successfully account for the ground state stability of nuclei against deformation and the general trend of the ground state binding energies versus nuclear masses. The model cannot explain, with much accuracy, the nuclear excited states. It should also be noted that the LDM gives only an overall fit to the binding energy as a function of A and it does not predict the strong local deviations that occur at magic numbers of protons or neutrons. For this it is necessary to invoke the shell model.

1.3 The Shell Model

The behaviour of nuclear binding energy with respect to magic numbers is very reminiscent of the behaviour of atoms with respect to closed shells of electrons. It has become customary to refer to a magic number of nucleons as a closed shell, in analogy with the electrons in an atom. However, despite this superficial similarity it should be understood that the nuclear and atomic systems are physically very different. In the atom the electron motion is dominated by the Coulomb force between each electron and the nucleus, the force between the individual electrons being small by comparison. In the nucleus there is no one dominant force, each nucleon moves under the influence of all the others. The theoretical description of the *single particle* aspect of the nucleus, on which the shell model is based, was first put forward by Mayer in 1949.

The shell model (SM) starts with the drastic assumption that as far as any one nucleon is concerned, the forces exerted on it by all the other nucleons in

the nucleus can be represented, to a first approximation, by a potential well, the depth of which is roughly proportional to the density of the nucleus. This assumption immediately reduces the complex many-body problem to that of the simple problem of a single quantum mechanical particle in a potential well. But is this approximation valid? Do the nucleons in the nucleus traverse one or more orbits before undergoing a collision, as would be suggested by the solution to such a problem? The approximation is in fact quite good, because the mean free path of nucleons within the nucleus is of the order of the size of the nucleus. This is mainly due to the Pauli exclusion principle severely limiting the number of collisions causing the nucleons to be restricted to a very limited number of allowed orbits.

1.3.1 The Spherical Shell Model

In the simplest form of the shell model the nucleus is assumed to be spherical. Various shapes for the nuclear potential have been suggested and used. The Woods-Saxon and the harmonic oscillator are two such potentials. The former is considered to be more realistic because its radial dependence is closer to that of the real nuclear system, while the later has the advantage of being easier to use in calculations.

The Woods-Saxon potential is given by:

$$V(r) = -V_\circ \left\{ 1 + \exp\left(\frac{r - R_\circ}{a} \right) \right\}^{-1} \tag{1.3}$$

with, $V_\circ \approx 57$ MeV, $R_\circ \approx 1.25A^{1/3}$ fm and $a \approx 0.65$ fm (Cohen 1971).

The harmonic oscillator potential is given by:

$$V(r) = \frac{1}{2} M\omega^2 r^2 - V_\circ \tag{1.4}$$

where, ω is the oscillator frequency ($\hbar\omega \approx 40/A^{1/3}$ MeV—Burcham 1979) and M is the reduced mass of the system (core plus single nucleon).

In order to reproduce the magic numbers a strong, non-central spin-orbit coupling term needs to be added to the central static potential. This term is proportional to $\vec{\ell} \cdot \vec{s}$ and when included the single particle potential of equation 1.4 becomes:

$$V(r) = \frac{1}{2} M\omega^2 r^2 - V_\circ - C\vec{\ell} \cdot \vec{s} \tag{1.5}$$

where, $\vec{\ell}$ and $\vec{s}$ represent the orbital angular momentum vector and the spin vector, respectively, of the nucleon. With the addition of this term the potential is usually referred to as the modified oscillator (MO) potential.

The above equations ignore Coulomb effects and as such are only applicable to neutrons. For protons, the addition of the repulsive coulomb force leads to energy levels which, on an absolute scale, are higher than the neutron levels but are in other respects similar. This model provides a good description of all low-spin states seen in nuclei close to shell closures. However, as nuclei depart from the closed shell structure discrepancies begin to appear, for example mid-shell values of magnetic moments and electric quadrupole moments are at variance with experimental results.

1.3.2 The Deformed Shell Model

The nuclear electric quadrupole moment is a measure of the deviation of the nuclear charge distribution from spherical symmetry. The differences between experimental quadrupole moments and those predicted by the spherical shell model suggest the possibility of a deformed nuclear shape.

Nuclear deformations can be thought of as being due to the tendency of nuclear orbitals to orientate themselves so that the nucleons are as close as possible. This results in an asymmetric mass distribution, which in turn leads to a deformation of the shell model potential. For example; if the first nucleon

added to a closed shell nucleus occupies a horizontal orbit, then the addition of further nucleons will lead to a considerable equatorial bulge by the time a mid-shell configuration is reached. The resulting deformed potential will affect even the orbits in the closed shell (ie. the core becomes polarised) and the whole nucleus takes on an ellipsoidal shape.

Perhaps the most widely used deformed shell model is that provided by Nilsson (1955), the potential used is that of an anisotropic harmonic oscillator with the addition of an $\vec{\ell} \cdot \vec{s}$ term and an ℓ^2 term:

$$V(r) = \frac{1}{2}m(\omega_x^2 x^2 + \omega_y^2 y^2 + \omega_z^2 z^2) + C\vec{\ell} \cdot \vec{s} + D\ell^2 \tag{1.6}$$

where, x, y, z represent body fixed axes and the frequencies ω_i are related to the length of the axes defining the nuclear shape. As before the $\vec{\ell} \cdot \vec{s}$ term allows for spin-orbit coupling. The ℓ^2 term is used to depress the energies of levels with high ℓ-values to take into account the fact that the real nuclear potential is rather flat, so that the nucleons near the surface feel a stronger force than would be described by the bare oscillator potential. Figure 1.1 shows the splitting of the harmonic oscillator energy levels caused by the addition of ℓ^2 and $\vec{\ell} \cdot \vec{s}$ terms to the single particle potential.

When $\omega_x = \omega_y \neq \omega_z$, equation 1.6 describes the single particle potential of a deformed nucleus with an axis of symmetry parallel to the z-axis. If the volume of the nucleus is to remain constant then the following condition must hold:

$$\omega_x \omega_y \omega_z = \omega_0^3 = \text{constant} \tag{1.7}$$

If a deformation parameter δ is introduced so that:

$$\omega_x^2 = \omega_y^2 = \omega_\delta^2 \left(1 + \frac{2}{3}\delta\right) \tag{1.8}$$

$$\omega_z^2 = \omega_\delta^2 \left(1 + \frac{4}{3}\delta\right) \tag{1.9}$$

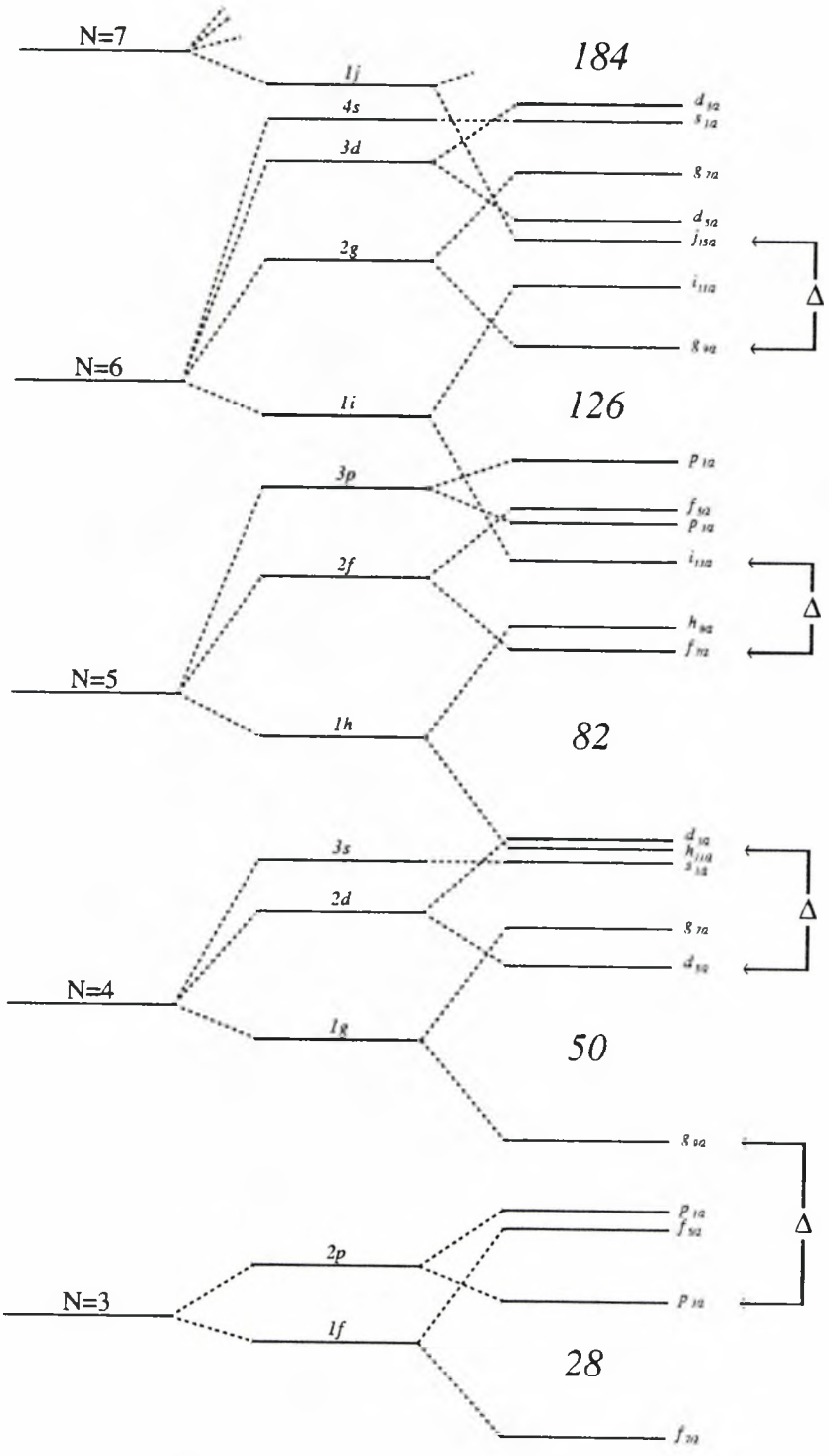

Figure 1.1: Single particle level scheme showing the effect on the harmonic oscillator levels (left) of introducing an ℓ^2 term (centre) and an $\vec{\ell} \cdot \vec{s}$ term (right). Δ indicates the levels with $\Delta\ell = \Delta j = 3$—see section 1.5.1.

the volume of the nucleus remains constant provided that:

$$\omega_\delta = \omega_\circ \left(1 - \frac{4}{3}\delta^2 - \frac{16}{27}\delta^3\right)^{-\frac{1}{6}} \tag{1.10}$$

Since spherical symmetry is broken with the introduction of deformation, orbital angular momentum is not conserved. Hence, ℓ and consequently $j\,(=|\,\vec{\ell}+\vec{s}\,|)$ are no longer good quantum numbers. However, since cylindrical symmetry is preserved the projection of j and the projection of ℓ onto the symmetry axis remain good quantum numbers. The projections are denoted by Ω and Λ respectively and are related to each other by:

$$\Omega = \Lambda + \Sigma \tag{1.11}$$

where, Σ $(= \pm 1/2)$ is the projection of the intrinsic spin onto the symmetry axis.

In the Nilsson model the levels are labelled by the so-called asymptotic quantum numbers: $\Omega^\pi[N, n_z, \Lambda]$; where $N(= n_x + n_y + n_z)$ is the total oscillator quantum number, with n_i being its component along the i-axis and π is the parity—given by $\pi = (-1)^N$. Since orbits that differ only in the sign of Ω represent the same motion in opposite directions (time reversed orbits) then each level is two fold degenerate (corresponding to $\pm\Omega$). The asymptotic quantum numbers become good in the limit of very large deformation when the ℓ^2 and $\vec{\ell}\cdot\vec{s}$ terms can be neglected.

Figures 1.2 and 1.3 (reproduced from Lederer and Shirley, 1978) show *Nilsson diagrams* for protons and neutrons in the region corresponding to actinide nuclei. These diagrams are useful in determining the ground state spin of odd-A deformed nuclei, ie. if the deformation parameter is known then the appropriate energy level can be associated with the last proton or neutron, thus ascertaining the ground state configuration.

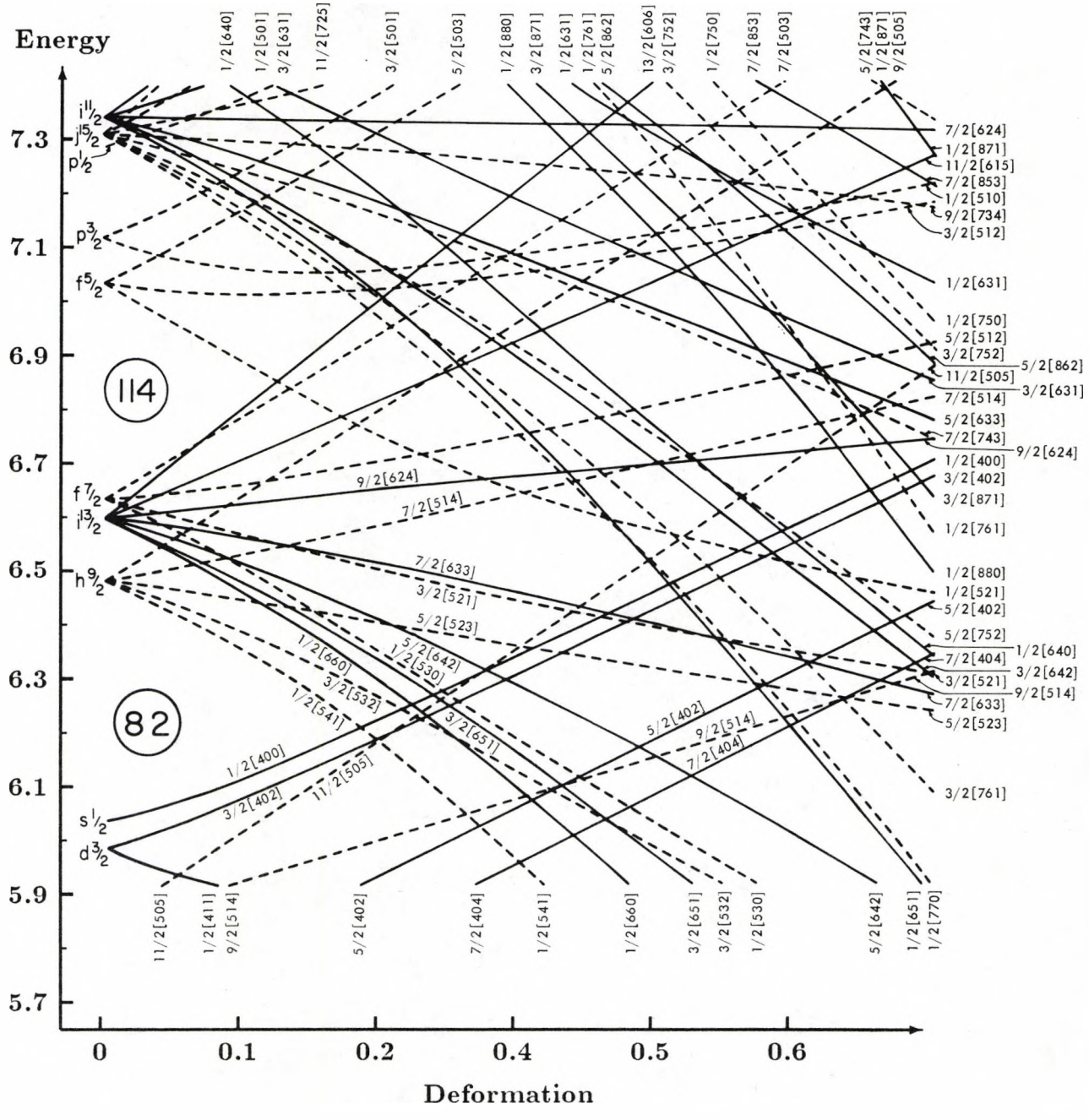

Figure 1.2: Nilsson diagram for protons showing the change in the energy (in units of $\hbar\omega_\circ$) of the single particle levels as a function of deformation.

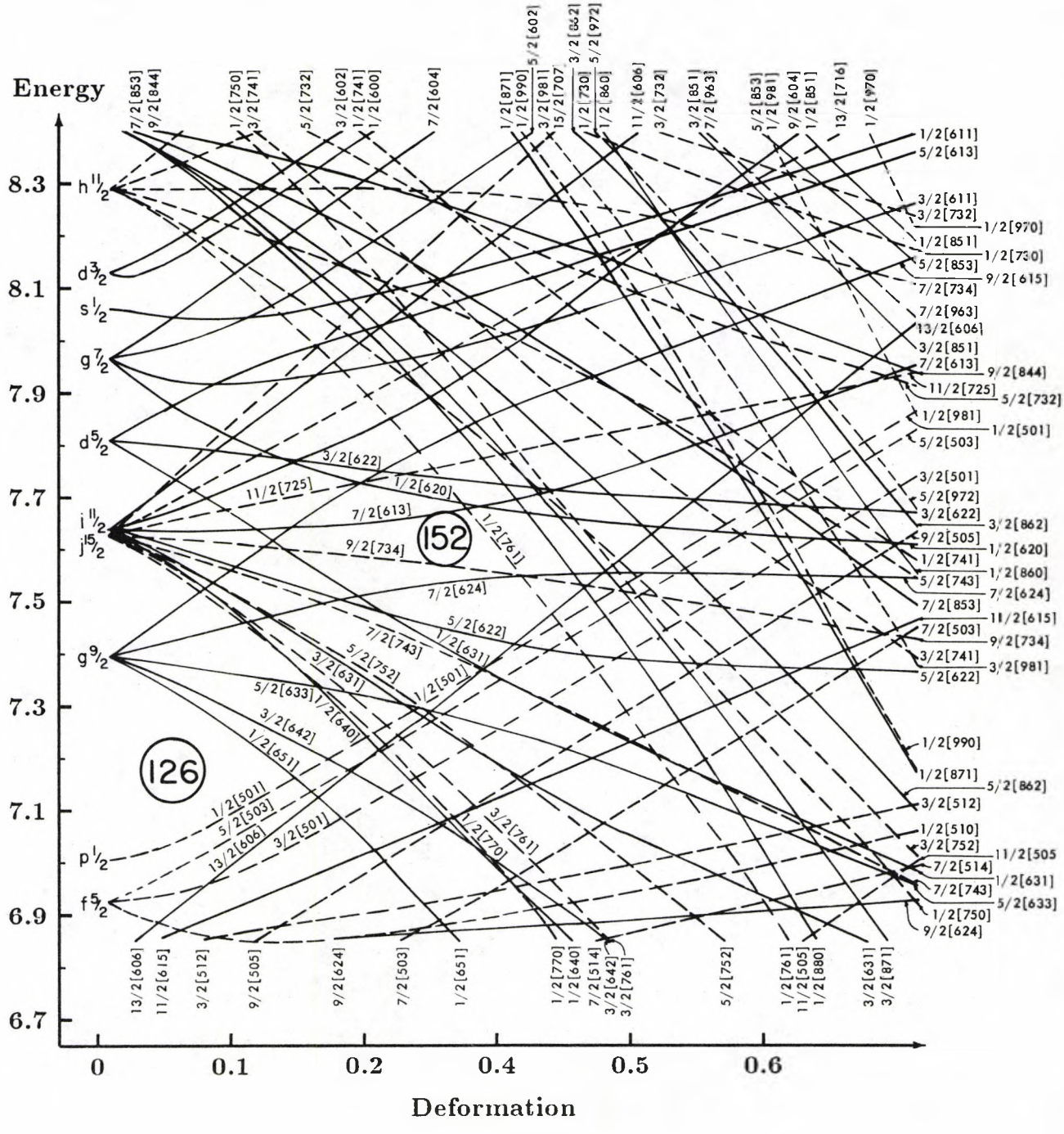

Figure 1.3: Nilsson diagram for neutrons showing the change in the energy (in units of $\hbar\omega_o$) of the single particle levels as a function of deformation.

Although the shell model can explain many of the nuclear properties it does not represent a complete picture, for example it cannot account for the low energy of the first excited state in even-even nuclei. The next step is to consider the possibility of collective motion of a large number of nucleons.

1.4 The Collective Model

The collective model (CM) combines certain features of the LDM and the SM. This unified model, as it was originally known, was first suggested by Rainwater (1950), and later developed by Bohr and Mottelson (1953). In this model the nucleons are assumed to move independently in a real potential that is capable of undergoing deformations in shape. Like the SM the nucleons fill orbits in a pairwise fashion forming an even-even core. However, in the CM this core is not inert and it can have angular momentum, this means that any odd particle is not entirely responsible for the nuclear properties as in the SM.

Nuclei that are close to the closed shell type posses spherical symmetry and they will resist any deformations impressed upon them. However, as nucleons are added (or subtracted) the restoring forces become weaker and the nucleus will pass through a state of having a soft, easily deformed structure (transitional nuclei) to become a spheroid of revolution as it approaches a mid-shell configuration.

The surface of a general shape can be written as:

$$R(\theta,\phi) = R_{\circ}\left\{1 + \sum_{\lambda=1}^{\infty}\sum_{\mu=-\lambda}^{\lambda}\alpha_{\lambda,\mu}Y_{\lambda}^{\mu}(\theta,\phi)\right\} \tag{1.12}$$

where, $R_{\circ}$ is the radius of an equivalent sphere, θ,ϕ are the polar angles with respect to arbitrary axes, Y_{λ}^{μ} are spherical harmonics of order μ,λ and the coefficients $\alpha_{\lambda,\mu}$ are used to quantify the deformation. For axially symmetric

nuclei R is independent of ϕ and $\alpha_{\lambda,\mu} = 0$ for all non-zero μ. In this case the above equation reduces to:

$$R(\theta) = R_\circ \left\{ 1 + \sum_{\lambda=1}^{\infty} \beta_\lambda Y_\lambda^0(\theta) \right\} \tag{1.13}$$

where, β_λ represents $\alpha_{\lambda,0}$.

The simplest type of deformation is ellipsoidal and, in analogy to a diatomic molecule, a nucleus possessing this type of deformation can be expected to exhibit vibrational and rotational excitation levels.

1.4.1 Rotational Excitations

When considering collective rotations it is assumed that the rotations take place with low enough angular velocity to permit the single particle orbits (which involve much higher velocities) to follow the rotation of the deformed shape. When a deformed nucleus rotates it can have two components of angular momentum: a component $\vec{R}$, due to the rotation of the deformed core and a component $\vec{j}$ due to the intrinsic angular momentum of any single particle excitations. These components will couple together to form a resultant $\vec{I}$, whose projection onto the symmetry axis is denoted by K—see figure 1.4.

For even-even nuclei in their ground state the individual particles are paired off and fall alternately into states of opposite K so that the resultant K-value is zero with even parity. Because of the symmetry about a plane perpendicular to the z-axis only even I values occur (ie $K = 0$ implies that a 180° rotation about PQ leaves the system unaltered). In this case the spin-parity values for the rotational band will be: $I = 0^+, 2^+, 4^+, \ldots$, the total angular momentum arising solely from the collective rotation.

In even-even nuclei with an intrinsic excitation and in odd-A nuclei K is non-zero and the energy levels will have spin given by: $I = K, K+1, K+$

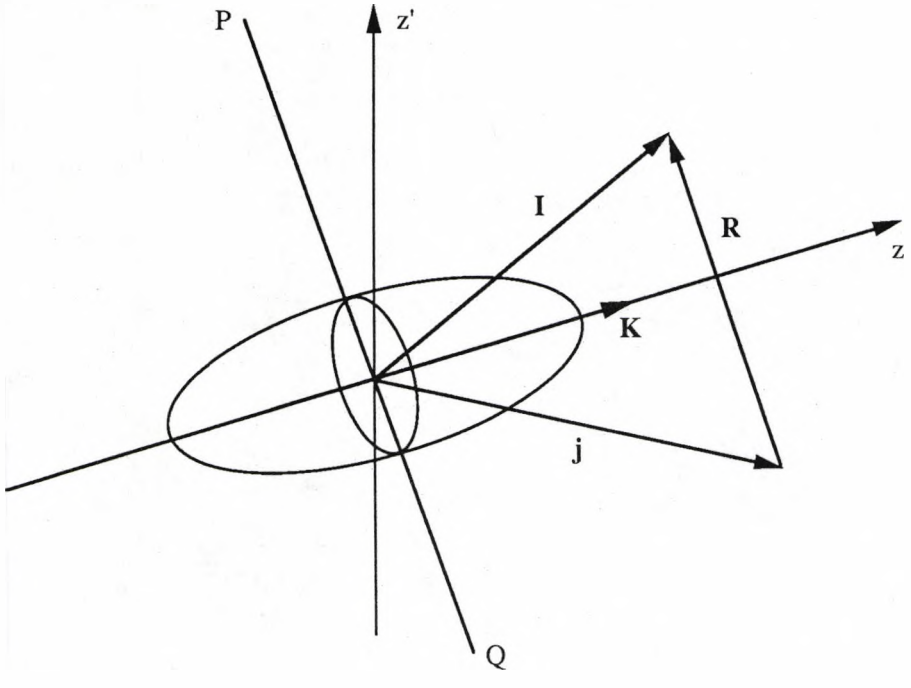

Figure 1.4: Schematic representation of an axially deformed nucleus, showing the coupling between the angular momenta of the collective rotation (about the body fixed axis PQ) and the intrinsic excitation.

$2, \ldots$ with a parity that of the intrinsic excitation. In this case there will be rotational bands built on single particle excitations, with the K-value known as the *band head.*

The energy of collective rotations is given by:

$$E_{rot} = \begin{cases} \{\hbar^2/(2\Im)\}\{I(I+1) - K^2\} & \text{for } K \neq \frac{1}{2} \\ \{\hbar^2/(2\Im)\}\{I(I+1) - K^2 + a(-1)^{I+\frac{1}{2}}(I+\frac{1}{2})\} & \text{for } K = \frac{1}{2} \end{cases} \quad (1.14)$$

where $\Im$ is a moment of inertia and a is a decoupling parameter that describes the mixing between the $K = \pm 1/2$ states, this mixing is caused by the coriolis force and depends on the single particle nature of the states.

At low spins the experimental moments of inertia are about 30–50% of the rigid body value. This is due to the fact that *pairing correlations* (see section 1.4.3) introduce a strong irrotational flow pattern into the nuclear motion, resulting in a moment of inertia whose value lies between that of a rigid body and that of an irrotational fluid.

1.4.2 Vibrational Excitations

According to the theory developed by Lord Rayleigh (in the 19th century) the shape oscillations of a macroscopic drop of liquid may be thought of in terms of standing waves on the surface of the drop consisting of an integral number of wavelengths. In equation 1.12 $\lambda = 2, 3, \ldots$ are the interesting cases and can be thought of as fundamental vibrational shapes called *normal modes.* According to classical mechanics any possible vibrational pattern can be described as a linear combination of normal modes, so that problems in vibration can be reduced to problems of understanding the vibration of each normal mode.

In a system such as a molecule or a nucleus, where quantum effects are important, vibrations are quantized into energy units of size $h\nu_\lambda$, where ν_λ

represents the frequency of vibration of order λ. These energy units are known as *phonons* and each carries an angular momentum λ and parity $(-1)^{\lambda}$. A vibrational state must contain an integral number of phonons of each λ. One-phonon states with energy $h\nu_2, h\nu_3, h\nu_4$ will have I^{π} of $2^+, 3^-, 4^+$ respectively. In the two-phonon vibration of energy $2h\nu_2$ the angular momentum of the two-phonons will couple to give a total angular momentum of 0, 2, 4 (see table 5.5 of Cohen, 1971) so there will be three states at energy $2h\nu_2$ with I^{π} of $0^+, 2^+$ and 4^+.

Many examples of such vibrational states have been found and a reasonable description of low-lying states of non-closed shell spherical nuclei is provided by vibrational motion. However, since the theoretical phonon energies have been derived using a simple harmonic oscillator potential the predictions are not accurately borne out. For example, the two-phonon states are not degenerate and the ratio of the two-phonon to one-phonon energies is not precisely 2:1. The introduction of anharmonic vibrations can remove the degeneracy of the two-phonon state and change its excitation energy relative to that of the one-phonon state.

For deformed nuclei λ is no longer a good quantum number. However, if the deformation is axially symmetric the quantum number μ (= the projection of λ onto the symmetry axis) will remain good and different μ-values (λ, $\lambda-1$, $\ldots$, $1-\lambda$, $-\lambda$) will no longer be degenerate in energy. For example, the one phonon octupole vibration has:

$$\lambda = 3 \text{ with } \mid \mu \mid = 0, 1, 2, 3 \tag{1.15}$$

This gives rise to an $I^{\pi} = 3^-$ state in the spherical case and $I^{\pi} = 0^-, 1^-, 2^-, 3^-$ states in the axially deformed case. Since, deformed nuclei must be thought of as rotating as well as vibrating this will complicate the level structure and

we can expect to see rotational bands built on vibrational states. In the above example, a rotational band built on the lowest energy octupole vibration will give rise to a $K^{\pi} = 0^{-}$ band with $I^{\pi} = 1^{-}, 3^{-}, 5^{-}, \ldots$

1.4.3 Pairing Correlations

The forces resulting from 'close encounters' between nucleons within a nucleus are known as *residual interactions*. A particular type of residual interaction is the pairing force, it is strongest between nucleons occupying time-reversed orbits (monopole pairing) and results in a lowering of the overall energy of the nucleus. On a simple level, pairing correlations can be treated in terms of collisions. That is, a collision between two like nucleons in time-reversed orbits will cause them to scatter into unoccupied time-reversed orbits, subject to the conservation of angular momentum and parity. In accordance with the uncertainty principle conservation of energy may be violated by an amount ΔE provided the violation does not last longer than a time Δt:

$$\Delta E \Delta t \simeq \hbar \tag{1.16}$$

Given that the time between collisions is at least of the order of the time taken for a nucleon to traverse its orbit then, for a medium mass nuclei (Cohen 1971), we have:

$$\Delta E \lesssim 1\text{MeV} \tag{1.17}$$

This value for ΔE is much less than the energy gap between major shells. Thus, in closed shell nuclei there can be no collisions due to the lack of available orbits to scatter into. On the other hand however, ΔE is of the order of the energy difference between orbits in the same shell. So that as the closed shell structure is departed from more scattering orbits become available, the Fermi surface becomes less well defined and both holes below it and particles above

it can co-exist—excitations that are mixtures of a hole state and a particle state are known as *quasiparticles*. This smearing out of the Fermi surface leads directly to the smooth variation of nuclear properties associated with the collective behaviour of the nucleus. That is, as a mid shell configuration is approached and nucleons are added, the Fermi surface does not jump from one single particle orbit to the next. Instead, the Fermi level is raised with only a slight modification of the occupation numbers[1] and thus the properties of the nucleus are not greatly changed.

1.5 Octupole Deformation

The discovery of very low-lying negative parity levels in certain light actinide nuclei (Stephens *et al.* 1954, 1957) has stimulated much theoretical interest and led to the introduction of an octupole degree of freedom into the collective nature of nucleonic motion. While even order deformation results in reflection symmetric nuclear shapes, octupole deformed nuclei are reflection asymmetric. For example, figure 1.5 shows the shape generated by equation 1.13 and the parameter set $\{\beta_i\}$ provided by Sheline *et al.* (1988) for the equilibrium deformation of ^{223}Ra.

The level schemes for various forms of the octupole potential are shown in figure 1.6 (reproduced from Leander *et al.* 1982). The potential on the left has a very high barrier between the reflection asymmetric shape and its mirror image. The octupole shape will be stabilised in this situation giving rise to the single band of the form: $I^\pi = 0^+, 1^-, 2^+, 3^-, \ldots$ in the even-even case (see

[1]The occupation numbers V_j^2 indicate how fully occupied the orbits are with given values of n, ℓ, j—an orbital in any given shell is completely specified by its j-value (see figure 1.1) so neither n nor ℓ are needed as subscripts.

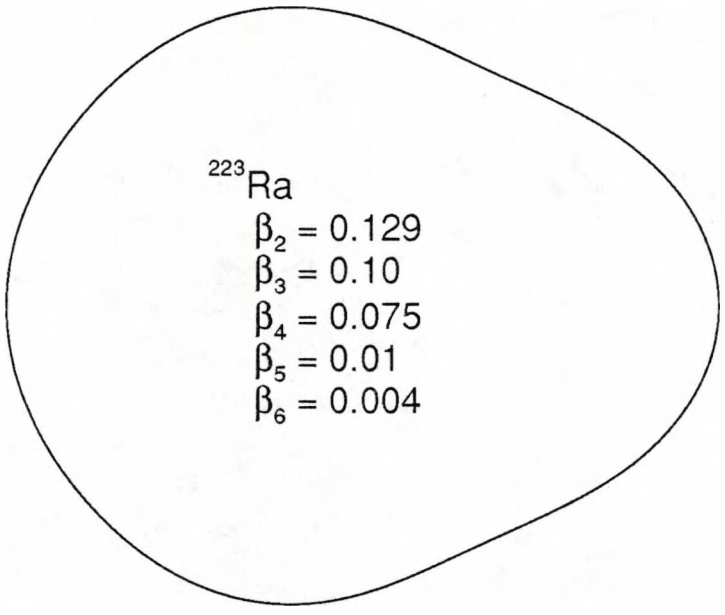

Figure 1.5: The octupole shape used in calculations by Sheline *et al.* (1988).

section 1.6.1). The potential in the centre has a more realistic finite barrier height. This allows tunnelling between the two minima, at a frequency ω_t that is strongly dependent on barrier height. In this case the negative parity states are pushed up in energy by an amount $\hbar\omega_t$. If the barrier disappears entirely ω_t becomes the vibrational frequency and the level scheme goes smoothly over to the vibrational limit.

1.5.1 Microscopic Origins

The microscopic origin of octupole deformation lies in the coupling between single particle states that differ by $\Delta\ell = \Delta j = 3$. These states lie close to each other and close to the Fermi surface at proton and neutron numbers 34, 56 ,88 and 134—see figure 1.1. In order to gain an insight as to why this is so we can

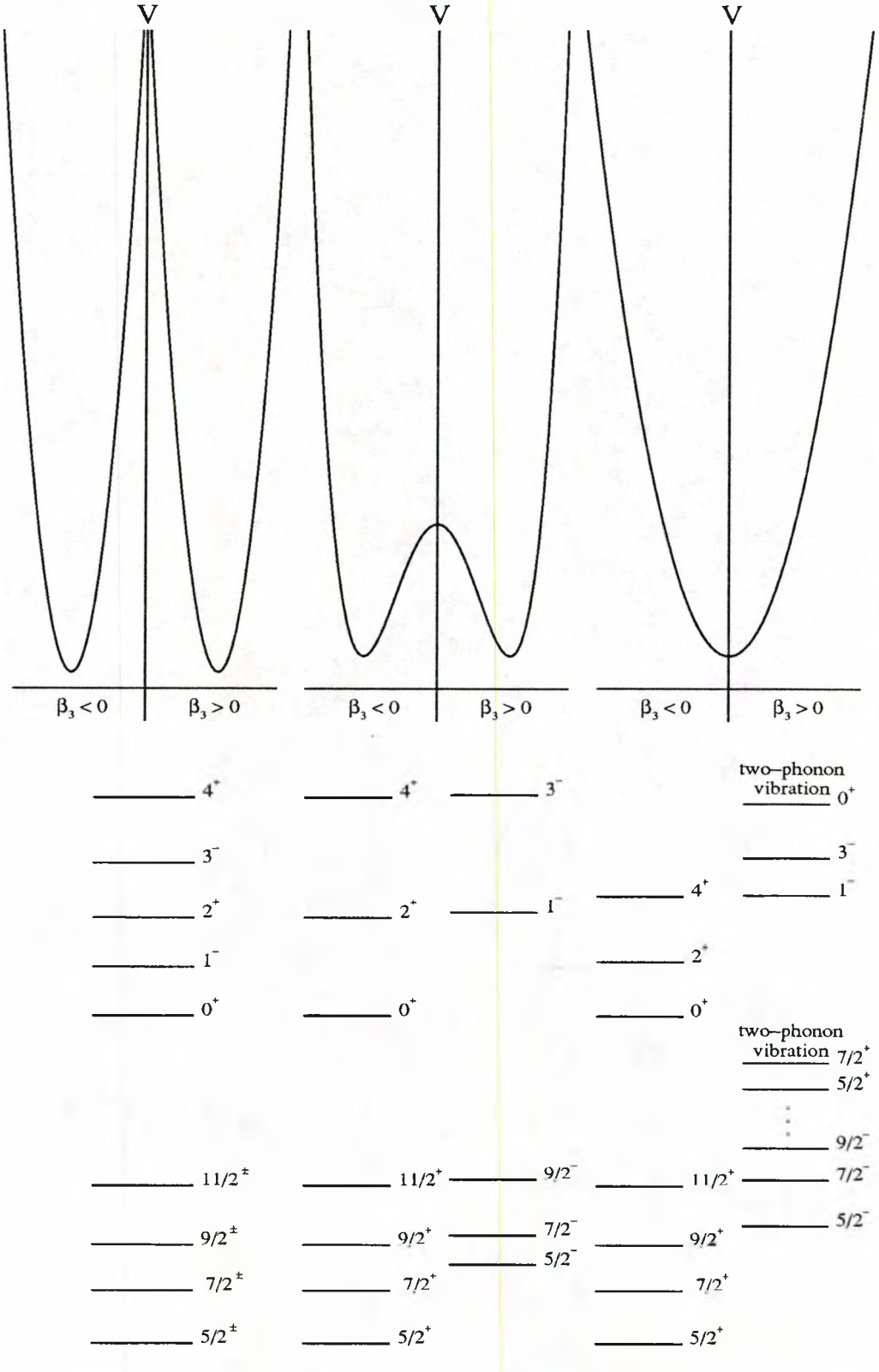

Figure 1.6: Schematic representation of octupole potentials along with the resulting level schemes.

consider the general conditions for shell structure in spherical systems given by Bohr and Mottelson (1975). They suggest that shell structure is expected when the ratio:

$$\frac{\partial\varepsilon}{\partial n} : \frac{\partial\varepsilon}{\partial\ell} = \frac{\partial\ell}{\partial n} = a : b \tag{1.18}$$

where, a and b are small integers and ε is the energy of the single particle level characterised by the radial, n, and angular, ℓ, quantum numbers. A ratio of 2:1 means that single particle states with $\Delta\ell = 2$ (or 4, 6,...) will lie energetically close together, while a ratio of 3:1 gives states with $\Delta\ell = 3$ (or 6, 9,...) lying energetically close.

Equation 1.18 can also be related to the classical trajectory, with the ratio $a : b$ corresponding to the number of radial and angular oscillations in a closed orbit. For example, $a : b = 2 : 1$ or $a : b = 3 : 1$ would imply elliptical or triangular orbits respectively. These orbits tend to line up and hence have a shape driving effect, so that elliptical orbits lead to quadrupole deformation and triangular orbits lead to octupole deformation. If this driving force is strong enough then the nucleus will achieve a permanent ground state deformation. If the driving force is not so strong however, the nucleus will be soft and the deformation will appear in the form of a vibration. The strength of the driving force will depend on how close in energy the single particle states actually are and hence on the single particle potential used.

1.6 Octupole Deformation in the Light Actinide Region

Early calculations, based mostly on the Nilsson model, came to the conclusion that although certain nuclei are soft with respect to octupole deformation,

intrinsic reflection asymmetry is never stabilised. Consequently, interpretation in terms of an octupole vibrational model were favoured. In this model the octupole deformation appears in the form of a vibration built on a reflection symmetric ground state minimum. The $I^\pi = 0^+, 2^+, 4^+, \ldots$ states arise from the usual $K^\pi = 0^+$ rotational band, while the $I^\pi = 1^-, 3^-, 5^-, \ldots$ states represent a rotational band built on the one-phonon $K^\pi = 0^-$ octupole vibration (see section 1.4.2). The vibrational model was successful in predicting the low-lying octupole states in even-even nuclei with $152 \leq A \leq 190$ (Neergard and Vogel 1970). However, when applied to the light actinide region the results were less successful. Perhaps the greatest discrepancy was the failure to observe the 0^+ two-phonon excitation expected at about twice the energy of the 1^- state.

The first hint of static octupole deformation came with the advent of the Strutinsky shell correction method (Strutinsky 1967). However, although calculations predicted potential energy minima at non-zero values of β_3 they were considered too shallow to be significantly different from the soft potentials obtained previously. It was not until 1981 that the use of more realistic potentials indicated a significant stabilisation of octupole deformation in the Ra region.

In the Strutinsky method the total nuclear energy is expressed as the sum of macroscopic and microscopic energy contributions, both of which are functions of deformation and particle number:

$$E_{tot} = E_{macro} + E_{micro} \tag{1.19}$$

The smoothly varying macroscopic energy can be calculated from the LDM, while the rapidly fluctuating microscopic energy is given by:

$$E_{micro} = E_{shell} - \tilde{E}_{shell} \tag{1.20}$$

where E_{shell} is the sum of the single particle energies and $\tilde{E}_{shell}$ is a smoothed

average of E_{shell}. In this way E_{tot} is composed of an average bulk energy (from the LDM) and a shell correction term which accounts for any oscillations, due to shell closures for example. Any other considerations, eg. pairing, can be included in an overall energy formula. The potential energy can then be minimised by varying the shape parameters to obtain the ground state deformation.

The first calculation to predict a significant potential energy minima at $\beta_3 \neq 0$ was performed by Möller and Nix (1981), on nuclei around ^{222}Ra. Further calculations by Leander *et al.* (1982) were able to show that static octupole deformation is more appropriate (than octupole vibration) for certain nuclei in the Ra region. Furthermore, with the inclusion of this octupole effect the calculations were able to explain the disagreements between experimental and theoretical nuclear masses in the Ra region. The main difference between these and earlier calculations was the use of more realistic potentials in the Strutinsky treatment. A modified LDM (modified to include surface diffuseness and the finite range of the nuclear force) and a folded Yukawa (FY) single particle potential were used to calculate the macroscopic and microscopic energy terms respectively. (For a description of the FY potential see Möller and Nix 1981.)

Other potentials that have been used to calculate the shell correction term are the MO and the WS. The effect of these different potentials on the octupole deformed minima have been calculated by Nazarewicz *et al.* (1984). The calculations cover four different regions of nuclei: (Z,N) $\approx$ (34,34); (34,56); (56,88) and (90,134), with the strongest octupole correlations occurring in the latter (light actinide) region. The results of two comparisons are reproduced in figure 1.7. The top half of the figure shows the effect of using the more realistic modified LDM, as compared to the standard LDM, for calculating the bulk

nuclear energy (in both cases the WS potential is used to calculate the shell correction term). The effect of using different single particle potentials (with the bulk contribution coming from the modified LDM) is shown in the bottom half of figure 1.7, as can be seen the calculations give similar values of β_3 at the minima, with only the actual depth of the potential varying.

1.6.1 Parity Doublets

With the introduction of octupole deformation the intrinsic nuclear Hamiltonian is no longer invariant with respect to the operators $\mathcal{P}$ and $\mathcal{R}$ ($\mathcal{P}$ is the parity operator, equivalent to space inversion, and $\mathcal{R}$ represents a rotation of 180° about an axis perpendicular to the z-axis). One symmetry that remains however, is that of reflection in a plane containing the z-axis. This is described by the operator $\mathcal{S}$ and is connected to the two broken symmetries via:

$$\mathcal{S}_x\mathcal{R}_x = \mathcal{P} \Rightarrow \mathcal{S}_x = \mathcal{P}\mathcal{R}_x^{-1} \tag{1.21}$$

where, $\mathcal{S}_x$ represents a reflection in the y-z plane and $\mathcal{R}_x$ a rotation of 180° about the x-axis. The eigenvalue of $\mathcal{S}$ is called *simplex* and is denoted by the quantum number s. The spin and parity of a level are related to s by:

$$\pi = s(-1)^I \tag{1.22}$$

where,

$$s = \begin{cases} \pm 1 & \text{for even A (i.e. integer spin)} \\ \pm i & \text{for odd A (i.e. half integer spin)} \end{cases} \tag{1.23}$$

The application of $\mathcal{S}$ to the ground state of an even-even nucleus ($K = 0$) leads to the identity:

$$\mathcal{S}\Phi_{K=0} = \Phi_{K=0} \tag{1.24}$$

where $\Phi_{K=0}$ is the intrinsic ground state wave function. Thus, $s = +1$ only and a single rotational band of the form: $I^\pi = 0^+, 1^-, 2^+, 3^-, \ldots$ occurs.

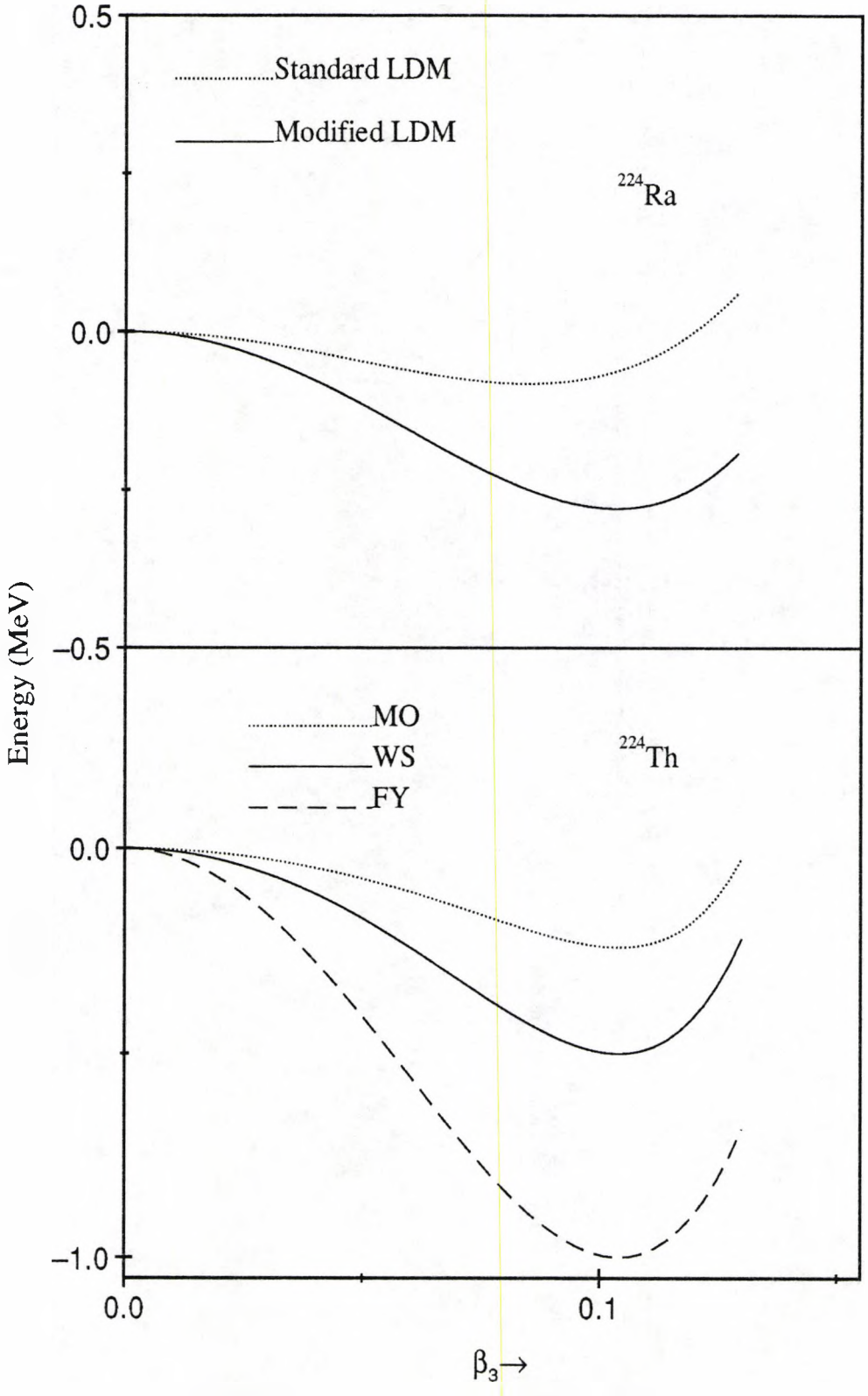

Figure 1.7: Results of calculations by Nazarewicz *et al.* (1984) using the Strutinsky method and various nuclear potentials.

For odd-A nuclei (or indeed excited states of even-even nuclei), $K \neq 0$ and the application of $\mathcal{S}$ yields:

$$\mathcal{S}\Phi_K = \Phi_{\bar{K}} \tag{1.25}$$

where $\Phi_{\bar{K}}$ represents the time reversed state with projection $-K$ onto the symmetry axis. In this case both s-values are allowed and there will be a doubling of all spin states with respect to parity. For example, if $K = 3/2$, then $s = \pm i$ with:

$$s = \begin{cases} +i & \Rightarrow I^\pi = \frac{3}{2}^+, \frac{5}{2}^-, \frac{7}{2}^+, \ldots \\ -i & \Rightarrow I^\pi = \frac{3}{2}^-, \frac{5}{2}^+, \frac{7}{2}^-, \ldots \end{cases} \tag{1.26}$$

1.6.2 Intrinsic Dipole Moments

The existence of octupole deformation is expected to give rise to a dipole moment in the intrinsic frame (ie. a frame whose orientation is defined by the instantaneous shape of the nucleus). Classically, this can be seen to be due to a separation of the centre of charge and the centre of mass within the nucleus, the protons moving towards the end of greatest curvature in analogy to the electrons in a conductor. This intrinsic dipole moment would manifest itself in the form of enhanced E1 transitions in the laboratory frame. So that, along with E2 transitions, we can expect to observe E1 transitions connecting states of opposite parity within the rotational bands of constant simplex. In fact, one of the signatures of octupole deformation is the characteristic decay pattern involving E2 transitions with two parallel E1 transitions.

Although the existence of enhanced E1 transitions is taken as an indication of octupole deformation, the magnitude of the associated E1 moment is not necessarily a measure of the amount of octupole deformation present. For example, in a theory formulated by Leander *et al.* (1986) the E1 moment of a given nuclear shape is expressed as the sum of two terms: a macroscopic liquid

drop term and a microscopic shell correction term. Since these terms may be of a similar magnitude they can enhance or cancel each other (depending on their relative sign), resulting in very different E1 moments for similarly shaped nuclei.

The results of the calculations of Leander *et al.* (1986) are reproduced in table 1.1. The calculations are of a two-step nature: first it was necessary to determine the equilibrium deformation at the appropriate spin, and then to determine the E1 moment at this equilibrium shape.

Nucleus	β_2	β_3	β_4	Q_1 (efm)	Q_2 (eb)	$\langle I \rangle$	B(E1)/B(E2) (fm^{-2})
^{218}Ra	0.02	0.08	0.013	–0.07	0.75	12	1.1×10^{-6}
	–0.06	0.08	0.037	–0.11	–2.26	12	5.0×10^{-6}
^{220}Ra	0.11	0.10	0.065	0.19	4.6	4–9	9×10^{-7}
	0.11	0.08	0.065	0.13	4.3	17	4×10^{-7}
^{222}Ra	0.12	0.11	0.071	0.18	5.2	5–12	6×10^{-7}
	0.13	0.04	0.076	0.17	5.3	21	8×10^{-8}
^{224}Ra	0.14	0.11	0.081	0.12	6.0	8	2×10^{-7}
	0.14	0.04	0.081	0	5.8	23	0
^{226}Ra	0.16	0.09	0.090	0.05	6.8	3–11	3×10^{-8}
	0.15	0.05	0.086	0.05	6.3	24	3×10^{-8}
^{220}Th	0.07	0.07	0.043	0.25	2.8	13	2.5×10^{-6}
^{222}Th	0.11	0.01	0.065	0.32	5.0	0–12	2.0×10^{-6}
	0.13	0	0.076	0	5.4	26	0
^{224}Th	0.14	0.11	0.081	0.33	5.9	5–14	1.6×10^{-6}
^{226}Th	0.15	0.11	0.086	0.29	6.6	6	9.6×10^{-7}
	0.15	0	0.086	0	6.6	20	0
^{228}Th	0.18	0.08	0.099	0.10	7.7	8	9×10^{-8}
	0.18	0	0.099	0	7.8	15	0

Table 1.1: Results of calculations by Leander *et al.* (1986) using a WS potential in the Strutinsky method. Columns 2–4 give the calculated equilibrium values of the respective deformation parameters (β_5 and β_6 were also included in the calculations but are not shown above). Columns 5 and 6 give the calculated intrinsic dipole and quadrupole moments respectively. Column 7 gives the approximate spin region over which the entries are valid. Column 8 gives the theoretical branching ratios.

Chapter 2

Alpha Decay

2.1 Introduction

Alpha decay can be used to good effect to study low-lying states of certain nuclei. Alpha transitions, in contrast to γ-transitions, are only mildly inhibited by angular momentum changes, this means that they are more likely to populate, to a significant extent, all the low-lying states of the daughter nucleus. As a spectroscopic tool α-decay suffers from two main restrictions: only certain regions of nuclei are α-active; and α transition rates exhibit an extremely sensitive exponential dependence on decay energy. The latter restriction means that in practice only low-lying states (ie. states of up to a few hundred keV in excitation) are excited in α-decay.

If the sum of the binding energies, E_{b}, of the two protons and two neutrons that occupy the last filled orbitals of the parent nucleus is less than the intrinsic binding energy, E_{b}^{α}, of an α particle (28.3 MeV) then α-decay of the nucleus will be energetically possible. However, since α-emission involves the penetration of a potential barrier α-decay will not occur at an appreciable rate until the difference between E_{b}^{α} and E_{b} is positive by several MeV. This explains the

fact that although most of the naturally occurring A > 150 nuclei are unstable with respect to α-decay, very few of them have observable α-activity.

2.2 Alpha-Particle Energetics

The total kinetic energy available from the emission of an α-particle can be obtained by applying conservation of mass-energy to α-decay:

$$Q_T = [M_{\text{parent}} - \{M_{\text{daughter}} + M_\alpha\}]c^2 \tag{2.1}$$

where, Q_T is the energy (in MeV) and the masses M are in units of MeV/c^2

Assuming α-decay is a two-body process then the available energy will be shared between the emitted α-particle and the recoiling daughter nucleus:

$$Q_T = E_\alpha + E^{\text{recoil}}_{\text{daughter}} \tag{2.2}$$

From simple two-body kinematics, this can be written:

$$Q_T = E_\alpha\,(1 + 4/A) \tag{2.3}$$

where A is the atomic number of the daughter nucleus.

Experimentally it is found that α-particles emitted from a particular nucleus do not always have the same energy. This implies that the Q-values and hence nuclear masses are multivalued. In conformity with mass-energy equivalence the effective mass of a nucleus when in an excited state is given by:

$$M_{\text{effective}} = M_{\text{g.s.}} + E_{\text{x}}/c^2 \tag{2.4}$$

where, $M_{\text{g.s.}}$ represents the ground state mass and E_{x} the energy of excitation.

Thus α-decay can leave the daughter nucleus in one of its excited states, with a Q-value depending on the excitation of the state involved. The largest

Q-value; Q_α, corresponds to decay to the ground state, so that:

$$Q_\alpha = E_\alpha (1 + 4/A) - E_x \tag{2.5}$$

The Q-value that is actually measurable is slightly lower than that given by the above equation since the α-particle must do work against the attractive force of the orbital electrons in escaping from the parent nucleus. The true Q-value can be obtained from the measured Q-value by adding a *screening correction* term (Rasmussen 1966), $\Delta E_{S.C.}$:

$$\Delta E_{S.C.} = \left\{65.3Z^{7/5} - 80Z^{2/5}\right\} \text{eV} \tag{2.6}$$

where, Z is the atomic number of the parent nucleus.

Once formed the excited states will usually de-excite (eg. by γ-ray emission or internal conversion) well within a nanosecond. This means that the α-particle and the subsequent γ-ray or conversion electron will appear in good time coincidence. Both α-γ and α-e coincidences can be recorded and used to deduce information on the daughter nucleus. For example, the α-γ coincidence data can be used to determine the level ordering of the excited states, whilst the α-e coincidence data can be used to deduce the multipolarity of transitions within the daughter nucleus.

2.3 Exponential Decay Law

Alpha decay is described by the exponential-decay law:

$$A(t) = A_o e^{-\lambda t} \tag{2.7}$$

where, A(t) is the activity (number of decays per unit time) of the parent nucleus at time t, A_o is the initial activity (A(t) at t=0) and λ, the decay constant, represents the probability per unit time of a decay occurring.

The decay constant is related to the average lifetime, τ, and the half-life, $T_{1/2}$, of the parent nucleus:

$$\lambda = \frac{1}{\tau} = \frac{\ln 2}{T_{1/2}} \tag{2.8}$$

If additional modes of decay are possible (eg. β-decay, γ-decay etc.) then:

$$\lambda = \lambda_\alpha + \lambda_\beta + \lambda_\gamma + \cdots \tag{2.9}$$

$$= \frac{1}{\tau_\alpha} + \frac{1}{\tau_\beta} + \frac{1}{\tau_\gamma} + \cdots \tag{2.10}$$

$$= \frac{\ln 2}{T^\alpha_{1/2}} + \frac{\ln 2}{T^\beta_{1/2}} + \frac{\ln 2}{T^\gamma_{1/2}} + \cdots \tag{2.11}$$

where, $\lambda_{\alpha,\beta,\gamma,\ldots}$, $\tau_{\alpha,\beta,\gamma,\ldots}$ and $T^{\alpha,\beta,\gamma,\cdots}_{1/2}$, are the *partial* decay constants, lifetimes and half-lives respectively.

When dealing with nuclei that can only decay by α emission then:

$$\lambda = \lambda_\alpha = \sum_i \lambda_i \tag{2.12}$$

where, i refers to a decay to a particular state of the daughter nucleus, λ_i is the partial decay constant to state i and can be expressed in terms of the total decay constant λ_α:

$$\lambda_i = a_i \lambda_\alpha \tag{2.13}$$

where, a_i represents the fraction of the decay to state i and:

$$\sum_i a_i = 1 \tag{2.14}$$

2.4 The Concept of the Hindrance Factor

Experimentally it is found that the α-decay constant varies extremely rapidly with decay energy—the least energetic α-particles coming from nuclides with the longest half-lives (and vice-versa). This energy-lifetime relationship was displayed in a useful form by Geiger and Nuttall (1911). They showed that

for the even-even α emitters known at the time a good straight line fit could be obtained by plotting the logarithm of the half-life against the range of the α-particles in air. This is known as the Geiger-Nuttall relationship:

$$\log \lambda = A(Z) + B(Z) \log R \tag{2.15}$$

where, A and B are empirical quantities (constant for a given Z), and R is the range (in cm) of the α-particles in air.

Since E_α is related to R, this relation can be expressed as follows:

$$\log T^i_{1/2} = \frac{A'(Z)}{\sqrt{E_\alpha}} + B'(Z) \tag{2.16}$$

Figure 2.1 shows a plot of experimental points for even-even nuclides, the lines on the plot are connecting points of the same Z. With the exception of two isotopes of Rn and three of Po, whose decay involves a magic number, all the points corresponding to α-decay to ground states are seen to lie very close to the empirical lines.

If a corresponding plot is made for non-even-even nuclides then great departures from the straight lines of figure 2.1 are seen to occur. Figure 2.2 shows a plot for even-Z, odd-N nuclides; in no case is the half-life shorter than for an even-even nuclide of the same Z and same E_α and in many cases half-lives are longer by two to three orders of magnitude.

The empirical facts highlighted by the plots shown in figures 2.1 and 2.2 have led to the concept of the *hindrance factor*. In non-even-even nuclides any α-transition that is slower than the ground state transition, of the same energy, in nearby even-even α emitters is said to be *hindered*. The degree of slowness can be expressed in terms of the hindrance factor HF:

$$HF = \lambda_o / \lambda_i \tag{2.17}$$

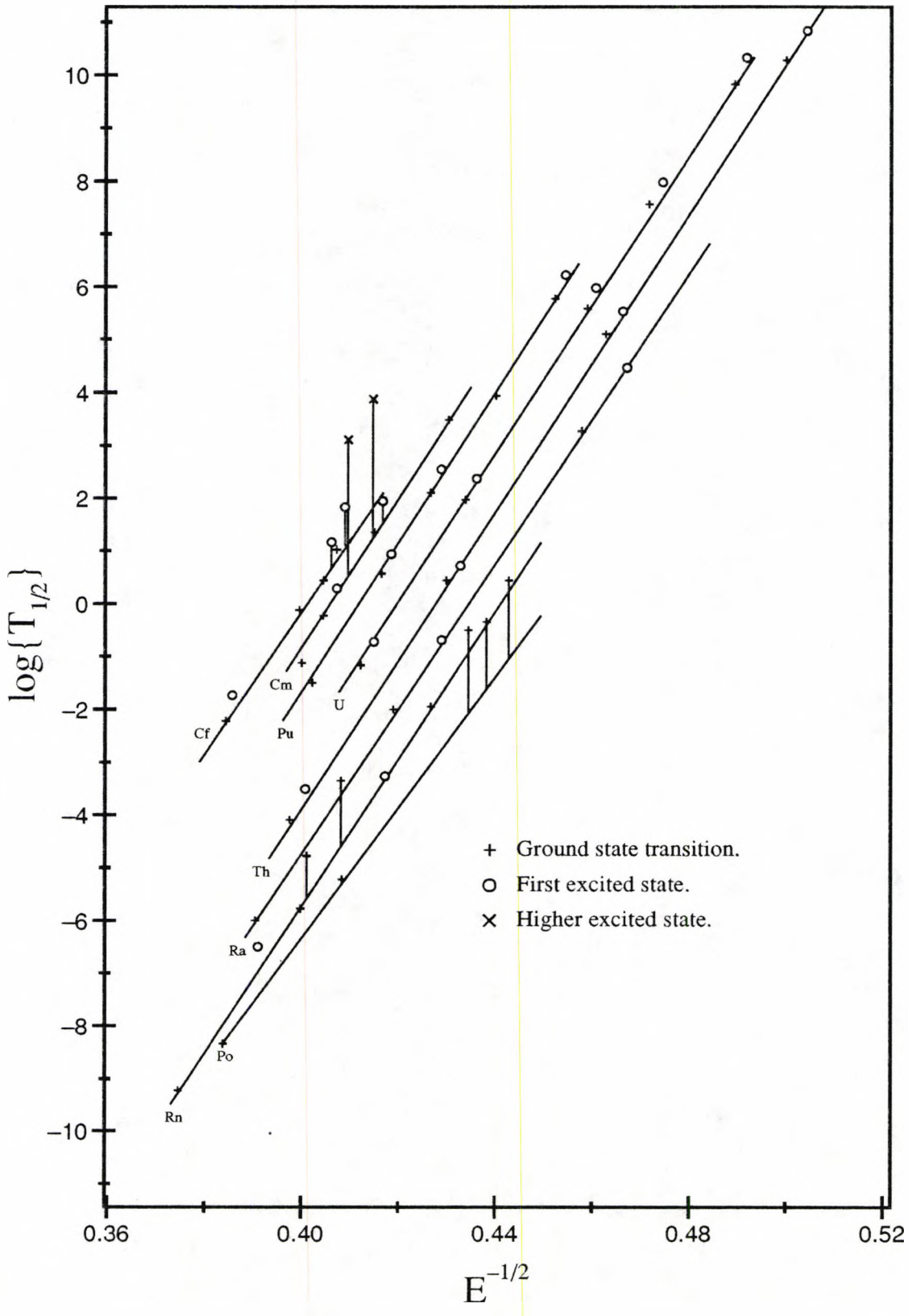

Figure 2.1: Plot of experimental points for even-even nuclides—Preston (1947).

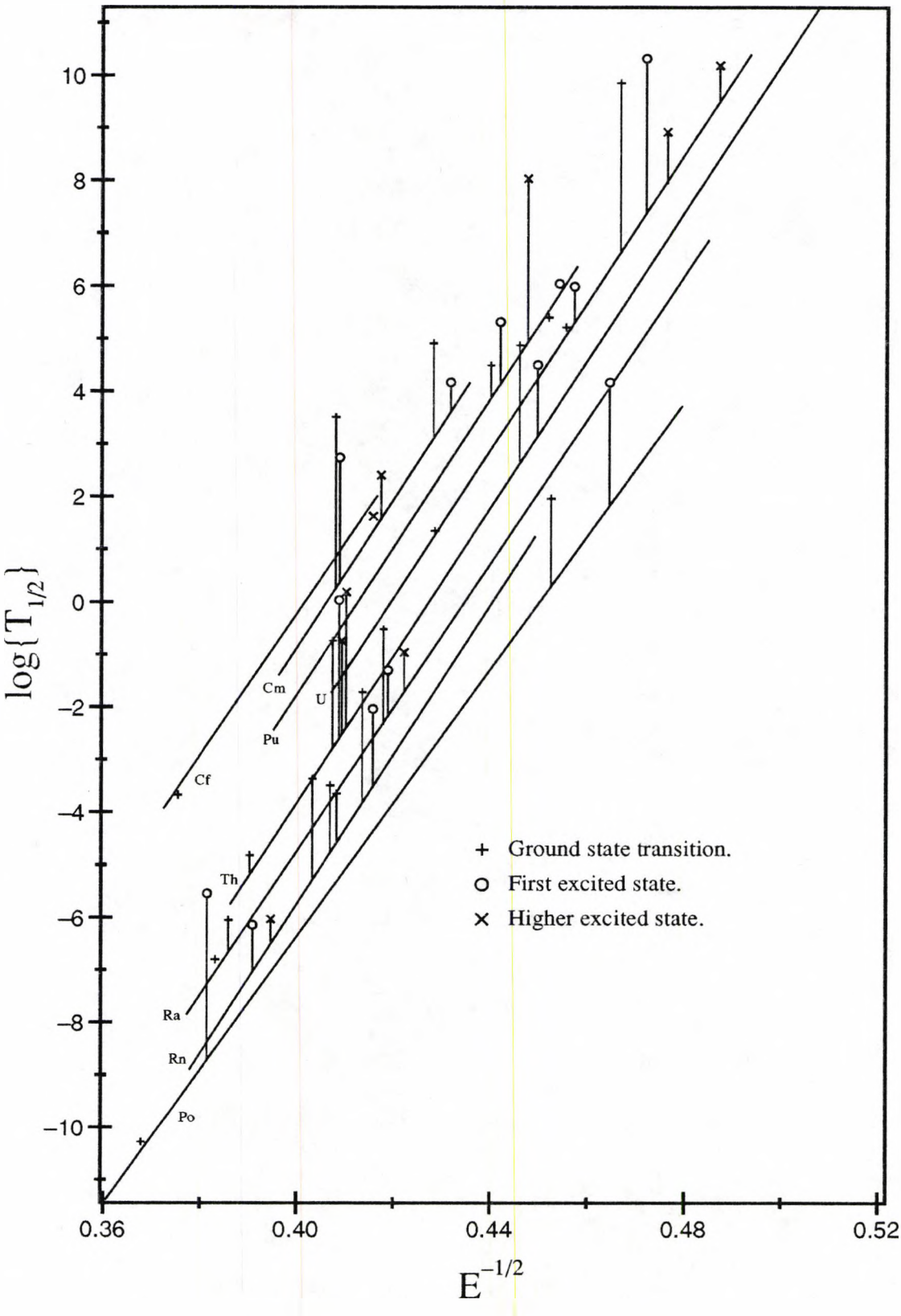

Figure 2.2: Plot of experimental points for even-Z, odd-N nuclides—Preston (1947).

where, λ_i represents the partial decay constant of the odd-A α-emitter and λ_o represents the decay constant predicted by the empirical even-even line.

Hindrance factors can be defined for α-decays to excited states of even-even nuclides by a formula identical to the one above. In this case the partial decay constants, λ_i and λ_o are those to the excited state and ground state respectively.

Since there is no apparent correlation between hindrance and transition energy, the hindrance factor is seen as a way of removing the strong energy dependence of α transition rates so that comparisons can be made between α-decays. For example hindrance factors can be used to deduce a measure of the overlap between the parent wave function prior to α-emission and the daughters immediately after.

2.5 The One-Body Model of Alpha-Decay

In the one-body model of α-decay, it is assumed that the α-particle exists preformed within the nucleus and that the action of the nucleus on the α-particle can be represented by a rectangular potential well. This potential is expressed graphically in figure 2.3 and mathematically as follows:

$$V = \begin{cases} U & \text{for } r < r_o \\ 2Ze^2/r & \text{for } r > r_o \end{cases} \tag{2.18}$$

where, Z and r_o are the atomic number and nuclear radius of the daughter nucleus respectively.

The nuclear surface is assumed to be well defined, so the potential consists of two distinct parts. Outside the nucleus the potential is that due to the Coulomb force, whilst inside the nucleus it is assumed that the potential can be represented by an average value U, which remains constant throughout the

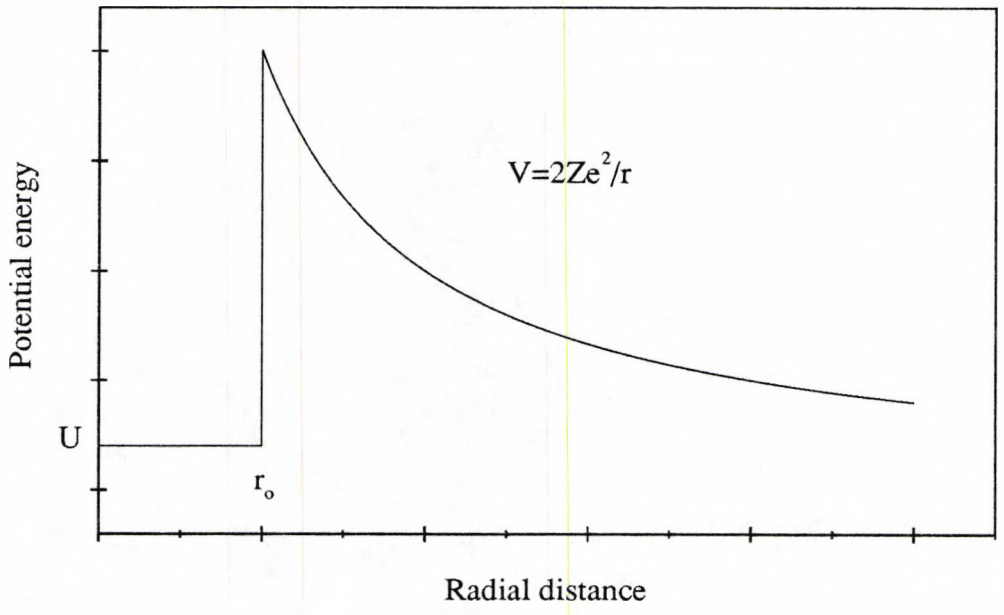

Figure 2.3: Graphical representation of the potential used in the one-body model of α-decay.

nuclear volume. The nuclear surface represents a potential barrier through which the α-particle has a finite probability of tunnelling, even though it may be moving inside the nucleus with a kinetic energy less than the barrier height.

Hindrance factors are calculated using the one-body formalism of Preston (1947). In his attempts to obtain a formula expressing the $E_\alpha - \lambda$ relationship which is valid for non-zero values of α-particle angular momentum, Preston found it necessary to re-derive the case for $\ell = 0$ in a more rigorous manner. The results of this re-derivation are represented by the following two equations:

$$\mu = -\tan\alpha_\circ \tan(\mu k r_\circ) \tag{2.19}$$

$$\lambda = \frac{2v}{r_\circ}\frac{\mu^2 \tan\alpha_\circ}{\mu^2 + \tan^2\alpha_\circ} e^{-2\omega_\circ} \tag{2.20}$$

where:

$$\mu = \sqrt{1 + \frac{U}{E_\alpha}}$$

$$\alpha_o = \cos^{-1}\left(\sqrt{\frac{mv^2 r_o}{4e^2 Z}}\right)$$

$$k = \frac{mv}{\hbar}$$

m is the reduced mass of the α particle and daughter nucleus and v is their relative velocity

$$\omega_o = \frac{4e^2 Z}{\hbar v}(\alpha_o - \sin\alpha_o \cos\alpha_o)$$

In calculating hindrance factors the above formulae are used twice: first to calculate an effective nuclear radius, r_o, of the parent, using the known values of E_α and λ for even-even ground state transitions; and second, retaining this value of r_o, to calculate a value of λ using the measured E_α of the transition for which the hindrance factor is being determined. The hindrance factor is then given by the ratio of this calculated value to that of the measured experimental value. In the case of a non-even-even nuclide the effective nuclear radius of the parent is taken to be the mean of the values calculated for its even-even neighbours.

The probability that an α-active nuclide will decay can be expressed as the product of three quantities:

$$\lambda = pfP \tag{2.21}$$

where, p is the probability of formation of an α-particle within the nucleus, f is the frequency with which the α-particle strikes the potential barrier and P is the barrier penetrability factor (ie. the probability that on striking the barrier, the α-particle will tunnel through). The one-body model assumes $p = 1$ (ie. a preformed α-particle), with the decay constant representing the probability of the α-particle escaping from the potential well. The justification of the above assumption is borne out, to a certain extent, by the consistency of the values of r_o obtained for even-even nuclei using equations 2.19 and

2.20. This consistency (eg. see table 4.3 in Hyde, Perlman and Seaborg 1964) demonstrates the dominance of the barrier penetration process and that all other factors are essentially constant. It should be noted however, that r_o is a model dependent parameter and as such represents an "effective nuclear radius for α-decay".

2.6 Limitations of the One-Body Model

The simple one-body model of α-decay provides sufficient treatment of ground state transitions in even-even nuclei. However, this model represents an ideal situation in which the following factors have been ignored:

- non-zero values of α-particle angular momentum.
- non-central forces.
- formation factors.

Non-Zero Values of Alpha Angular Momentum. The effect of angular momentum is to reduce the probability of α emission since the potential barrier is increased by a centrifugal contribution. This change in barrier penetrability can be allowed for by the addition of a centrifugal term to the potential outside the nucleus, so that for $r > 0$ the potential becomes:

$$V = \frac{2Ze^2}{r} + \frac{\hbar^2 \ell(\ell+1)}{2m_\alpha r^2} \tag{2.22}$$

Retaining the quantum mechanical rigor used in re-defining the $\ell = 0$ case, Preston went on to produce formulae, similar to equations 2.19 and 2.20, valid for $\ell > 0$. However, as pointed out by Preston, when these formulae are used to calculate λ for a given r_o and E_α the values of λ show an initial increase

with ℓ. This predicted increase is at variance with later theoretical calculations involving more realistic potentials (eg. Winslow 1954) in which the α-particles existence within the nucleus is limited to the surface region. Perhaps the best way to allow for $\ell \neq 0$ is to correct for the change in barrier penetrability separately. One such method is provided by Rasmussen (1959), he offers the following approximate formula:

$$\frac{P_\ell}{P_0} = \exp\left\{\frac{-2.027\,\ell(\ell+1)}{Z^{1/2}A^{1/6}}\right\} \tag{2.23}$$

where, Z and A are the atomic number and mass number of the daughter nucleus and P_ℓ, P_0 are the barrier penetrability factors for non-zero and zero α-particle angular momentum, respectively. Hindrance factors calculated in this way (ie. with the angular momentum dependence removed) are known as *reduced hindrance factors.*

Non-Central Forces. A particular case of a non-central force is the quadrupole interaction. If an even-even nucleus undergoes its ground state transition emitting an α-particle of zero angular momentum then the resulting daughter nucleus will be in its 0^+ ground state. Now, before the α-particle has fully penetrated the potential barrier, the quadrupole interaction can excite the daughter nucleus to a 2^+ state, simultaneously changing the kinetic energy and angular momentum of the α-particle. The energy of the α-particle would now be the same as that of one involved in a "one-step" $0^+ \rightarrow 2^+$ transition but, since the potential barrier would have been penetrated at two different energies, the value of λ will be different—presumably it will have a value somewhere between those of the "true" $0^+ \rightarrow 0^+$ and $0^+ \rightarrow 2^+$ transitions, ie. lower than expected. This effect, along with the increased intensity of the excited state transitions at the expense of the ground state transitions, will tend to reduce the hindrance factor of the excited state transition.

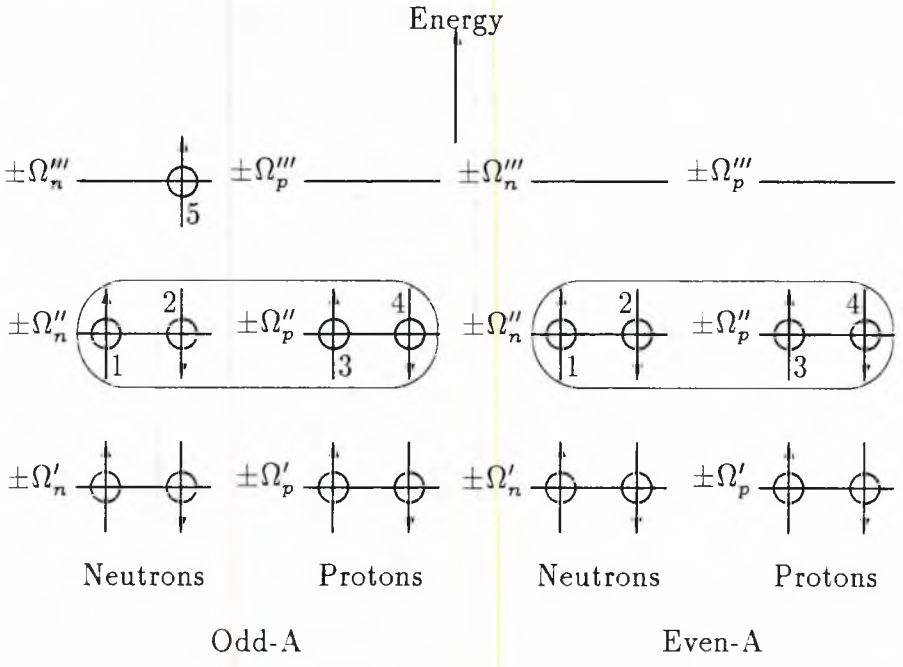

Figure 2.4: Schematic diagram of the nucleon states involved in α-decay. The diagram is a reproduction of figure 4.15 from Hyde, Perlman and Seaborg (1964), it shows the last Nilsson states to be filled in a spheroidal nucleus.

Formation Factors. As previously stated the one-body model of α-decay assumes a preformed α-particle moving within the nuclear interior. A more realistic treatment is provided by Brussard and Tolhoek (1958). They suggest a *nucleon overlap* model, where the α-particle is formed in the nuclear surface region from individual nucleon states depending on the overlap of their wavefunctions. A schematic representation of the nucleon states is given in figure 2.4. Neutrons 1 and 2, and protons 3 and 4 are in paired states with maximum overlap, consequentially formation of an α-particle from these nucleons would represent a favoured α-decay. In the odd-A case this would leave the odd nucleon occupying state 5 in both the parent and the daughter nuclei. For this reason a hindrance factor ≤ 4 is usually taken to imply that the excited state has the same I^π as the parent ground state. Formation of the α-particle from nucleons 1,2,3 and 5 might correspond to the ground state

decay (the most energetic α-particle), but since nucleon states 3 and 5 will have a small overlap the probability of this combination is likely to be small.

Of the effects not treated in the one-body model it is the variation in the formation factor that causes the greatest variation in half lives, it is the only effect that is likely to be capable of producing variations of an order of magnitude or more in the half life (Preston 1964). Thus, it is usual not to attempt to correct for non-zero values of α-particle angular momentum and non-central forces but to continue using the one-body formalism of Preston (1947) and treat the hindrance factors obtained as: "merely a number that is the order of magnitude of the ratio of the formation factor of an even-even nucleus to that of the nucleus in question"—Preston (1964).

2.7 Gamma Decay

One mode of decay available to all excited states of nuclei is that of γ decay. The possible decays are governed by the selection rules that arise from applying the conservation of angular momentum and parity to the system of nucleus plus γ-rays. The possible multipolarity of the radiation emitted in a transition between initial, (I_i, π_i) and final (I_f, π_f) states is given by:

$$| I_i - I_f | \leq L \leq I_i + I_f \tag{2.24}$$

$$\Delta\pi = \pi_i/\pi_f = \begin{cases} (-1)^L & \text{for EL radiation} \\ (-1)^{L-1} & \text{for ML radiation} \end{cases} \tag{2.25}$$

where, L is the angular momentum (in units of $\hbar$) carried off by each γ-ray and is used to classify the radiation in terms of multipole order. From the limitations imposed on L we can see that $I_i = I_f = 0$ would mean that $L = 0$, this is not allowed however, since an emitted γ-ray must carry off at least one unit of angular momentum.

For most known nuclear γ-transitions the probability for decay decreases rapidly with increasing multipole order so that it is usually sufficient to consider only the lowest one or two L-values; L and $L+1$, where:

$$L = \Delta I = \mid I_i - I_f \mid \tag{2.26}$$

When it is necessary to consider two L-values a multipole mixing ratio δ is introduced. The ratio of intensities of the (L+1)-pole radiation to that of the L-pole radiation being equivalent to δ^2.

In this work only radiation of pure M1, E1, E2 and mixed E2/M1 multipolarity are considered. The E2/M1 mixture arises because magnetic transition rates are significantly smaller than electric transitions of the same order. Therefore it is possible for E(L+1) radiation to compete favourably with ML radiation.

When the multipolarity[1] of a transition is known, along with one of (I_i, I_f), then the selection rules can be used to place restrictions on the unknown of (I_i, I_f). For example, an E1 transition with $I_f = 3/2^+$ implies that $I_i = 1/2^-$, $3/2^-$, or $5/2^-$.

2.8 Internal Conversion

The existence of orbital electrons provide a nucleus with a method of de-excitation that competes with γ-ray emission. The field of the nuclear multipole will act on any electron that is in the vicinity of the nucleus, the full transition energy can be communicated to the electron causing it to be ejected from the atom (provided of course that this transition energy is greater than the electron binding energy). This process is referred to as *internal conversion*,

[1]The term multipolarity is commonly used to specify the kind of radiation as to both class and order.

it is distinct from, and competes with, γ-ray emission. There is no intermediate γ-ray emitted and later converted as the term erroneously implies (this is a possible process, but much less likely).

The competition between internal conversion and γ-decay is expressed in terms of an *internal conversion coefficient*, α:

$$\alpha = \frac{\lambda_e}{\lambda_\gamma} \tag{2.27}$$

where λ_e and λ_γ are the total probabilities for the emission of electrons and γ-rays respectively.

Since electrons from different atomic shells have finite probability densities close to the nucleus, electrons may be emitted from the K, L, M, ...shells of the atom. The total probability for internal conversion λ_e is then composed of partial probabilities for the different shells:

$$\lambda_e = \lambda_e(K) + \lambda_e(L) + \lambda_e(M) + \cdots \tag{2.28}$$

and similarly for the L, M, ...sub-shells, for example:

$$\lambda_e(L) = \lambda_e(L_I) + \lambda_e(L_{II}) + \lambda_e(L_{III}) \tag{2.29}$$

so that:

$$\alpha = \alpha(K) + \alpha(L) + \alpha(M) + \cdots \tag{2.30}$$

This forms a rapidly converging series, since the outer electrons do not normally get close enough to the nucleus to strongly interact with the nuclear multipole field.

Calculations of internal conversion coefficients reveal a dependence on the Z-value of the atom and on the energy and the multipolarity of the transition (these latter factors control the field strength involved in the process). Blatt and Weiskopf (1952) have given

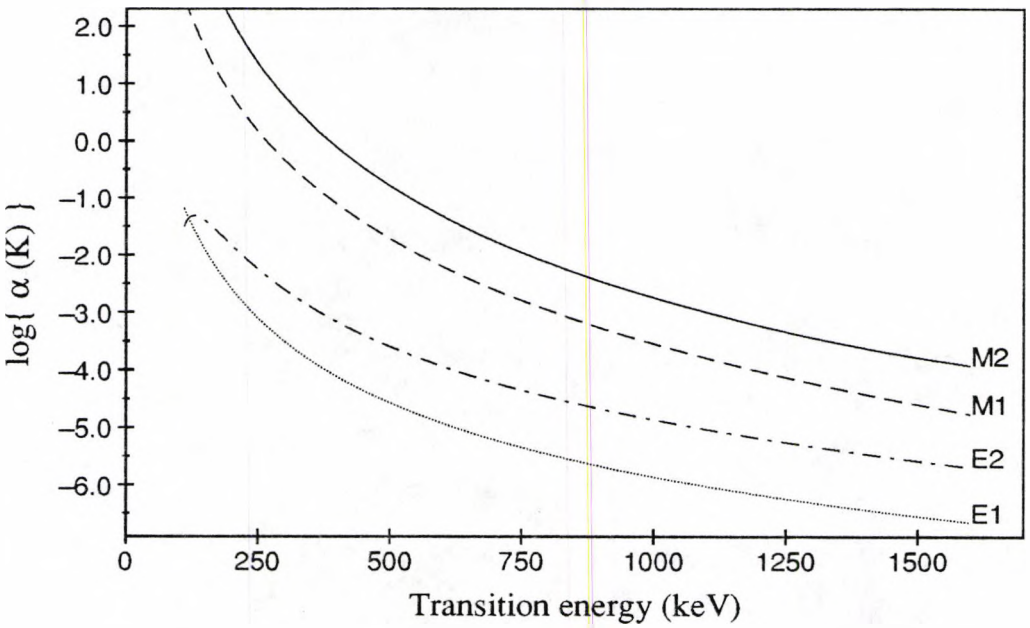

Figure 2.5: K shell conversion coefficients for Z = 90.

an approximate formula for $\alpha(K)$, when the binding energy of the K-electron is small compared to the transition energy:

$$\alpha(K) \cong Z^3 \left\{\frac{e^2}{\hbar c}\right\}^4 \frac{L}{L+1} \left\{\frac{2m_o c^2}{\hbar\omega}\right\}^{L+\frac{5}{2}} \tag{2.31}$$

where Z is the atomic number, L the angular momentum and $\hbar\omega$ is the energy of the transition in units of $m_o c^2$.

As a consequence of this dependence internal conversion has its greatest relative importance for low-energy transitions in high-Z nuclei. This dependence is shown graphically in figures 2.5–2.7, where values of conversion coefficients for Z = 90 (obtained from Hager and Selzter 1968) are plotted as a function of transition energy.

The theory of internal conversion and the details of the calculations involved in obtaining conversion coefficients can be found in numerous references (eg. Rose 1966).

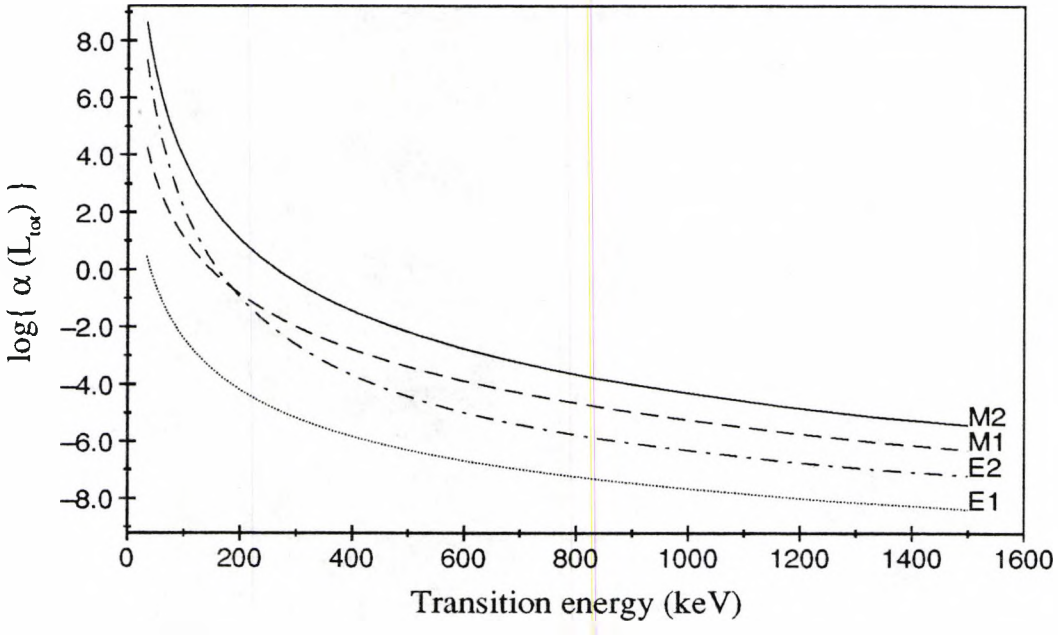

Figure 2.6: Total L shell conversion coefficients for Z = 90.

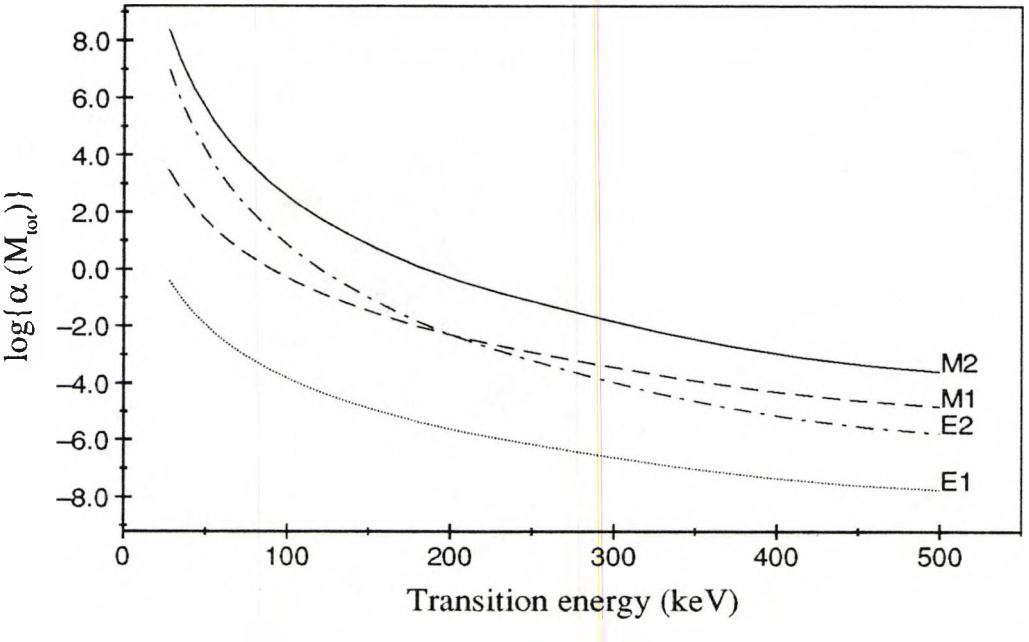

Figure 2.7: Total M shell conversion coefficients for Z = 90.

The energy of a conversion electron E_e is given by:

$$E_e = E_o - E_b \tag{2.32}$$

where E_o is the energy of the transition and E_b is the binding energy of the electron. Thus, electrons from different shells will be experimentally distinguishable because of the difference in E_b and an internal conversion electron spectrum will contain several peaks corresponding to each transition. If the intensities of these conversion peaks are measured for a particular transition, along with the intensity of the associated γ-ray peak, then the conversion coefficient can be calculated. This experimental value can then be compared with the tabulated theoretical values to determine the multipolarity of the transition. The conversion coefficients for different multipoles often differ by an order of magnitude so an unambiguous determination is usually possible.

It is possible, and sometimes desirable, to obtain information on the multipolarity of a transition by consideration of electron data alone. For example, a measurement of the K to L conversion ratio has the advantage of reducing the error introduced when corrections are made for detection efficiency—only relative electron efficiency need be calculated. In the case of two different multipoles (eg. E1, M1) having similar K:L ratios a measurement of ratios within the L shell (provided the electron spectra exhibit the required energy resolution) may distinguish between the two cases. This has the added advantage of simplifying efficiency calculations even further: the energies within the L sub-shell differ by only a few keV, over which range the electron efficiency is expected to vary very little.

For transitions of mixed multipolarity internal conversion measurements can be used to obtain a value for the multipole mixing ratio δ^2. For example,

the conversion coefficient for an E2/M1 mixture can be written:

$$\alpha(X, E2/M1) = a\alpha(X, E2) + b\alpha(X, M1) \tag{2.33}$$

where X=K,L,M,..., the mixture parameters a, b clearly being the same for all shells and sub-shells. Since $a+b = 1$ and $a/b = \delta^2$, a and b can be expressed separately in terms of δ^2, allowing the above equation to be rewritten:

$$\alpha(X, E2/M1) = \frac{\delta^2\alpha(X, E2) + \alpha(X, M1)}{1 + \delta^2} \tag{2.34}$$

In this way δ^2 can be expressed in terms of an experimentally measured conversion coefficient or conversion ratio, eg:

$$\delta^2 = \frac{\alpha(K, M1) - \alpha_K}{\alpha_K - \alpha(K, E2)} \tag{2.35}$$

or:

$$\delta^2 = \frac{\alpha(K, M1) - (\text{K:L})\alpha(L, M1)}{(\text{K:L})\alpha(L, E2) - \alpha(K, E2)} \tag{2.36}$$

where $\alpha(K, M1)$, etc. are the theoretical conversion coefficients and α_K, (K:L) represent the experimentally measured K conversion coefficient and K to L conversion ratio respectively.

Chapter 3

Angular Correlations

3.1 Introduction

The theory of angular correlations is well developed and the details of this complex theory can be found in many references; eg. Rose and Brink (1967), Frauenfelder and Steffen (1966). The following discussion follows the formalism of the latter reference.

The energy flow of the radiation from an oscillating multipole is given by *Poynting's vector*:

$$\left(\frac{1}{4\pi c}\right) \Re\{\vec{E}_{LM} \times \vec{H}_{LM}\} \tag{3.1}$$

where, L is the multipole order and M is the z-component of the angular momentum. Calculations (Preston 1964), using the *vector potential* $\vec{A}$, show that for a fixed M, the angular distribution is proportional to:

$$\begin{aligned} S_{LM}(\theta) \;=\; & \{2L(L+1)\}^{-1} \times \{[L(L+1) - M(M+1)] \mid Y_L^{M+1} \mid^2 \\ & + 2M^2 \mid Y_L^M \mid^2 + [L(L+1) - M(M-1)] \mid Y_L^{M-1} \mid^2\} \end{aligned} \tag{3.2}$$

where, Y_L^M ($= Y_L^M(\theta, \phi)$[1]) are spherical harmonics. Since electric and magnetic

[1]The ϕ dependence of Y_L^M is in the form of a multiplicative term $e^{iM\phi}$ that cancels out when $\mid Y_L^M \mid^2$ is calculated, hence S_{LM} is independent of ϕ

multipoles differ mathematically only in their parity and physically only in their plane of polarization, equation 3.2 holds for both types of multipole.

For radiative transitions between nuclear states the L,M of the emitted radiation is given by the selection rules:

$$\mid I_i - I_f \mid \leq L \leq I_i + I_f \tag{3.3}$$

$$m_i - m_f = M \tag{3.4}$$

where $I_{i,f}$ are the initial and final spins of the levels each having $2I_{i,f} + 1$ magnetic substates $m_{i,f}$.

The angular distribution arising from a transition between a particular pair of substates m_i, m_f is given by:

$$W(\theta) = P(m_i)G(m_i m_f)S_{L,M} \tag{3.5}$$

where $P(m_i)$ is the relative population of the substate m_i and $G(m_i m_f)$ is the relative probability for the transition $m_i \rightarrow m_f$. $G(m_i m_f)$ is defined in terms of the Clebsh-Gordan coefficient for the vector addition $\vec{I}_i = \vec{I}_f + \vec{L}$, $m_i = m_f + M$:

$$G(m_i m_f) = \langle I_f m_f LM \mid I_i m_i \rangle^2 \tag{3.6}$$

In the nuclear case, it is not normally possible to detect transitions between individual substates, instead an unresolved line is observed and the total angular distribution is given by summing over all possible pairs of m_i, m_f values:

$$W(\theta) = \sum_{m,m_i} P(m_i)\langle I_f m_f LM \mid I_i m_i \rangle^2 S_{LM}(\theta) \tag{3.7}$$

Consider the particular case of a dipole transition, where a state B ($I_B = 1$; $m_B = 0, \pm 1$) decays to a state C ($I_C = 0$; $m_C = 0$) in the presence of a magnetic field. Except at strong fields and very low temperatures ($\approx 0.01^\circ K$)

the population of the magnetic substates of B will be equal, furthermore, since one of the combining vectors ($\vec{I}_f$) is zero the vector addition coefficients will be unity.Thus, equation 3.7 reduces to:

$$W(\theta) = \sum_M S_{LM}(\theta) \tag{3.8}$$

substituting $L = 1$, $M = 0, \pm 1$ into equation 3.2 and using the definition for Y_L^M given by Blatt and Weiskopf (1952), gives:

$$S_{1,0} = \frac{3}{8\pi}(1 - \cos^2\theta) \tag{3.9}$$

$$S_{1,\pm 1} = \frac{3}{16\pi}(1 + \cos^2\theta) \tag{3.10}$$

$$\Rightarrow \sum_m S_{LM} = \text{constant} \tag{3.11}$$

that is, $W(\theta)$ is isotropic. From this we see that the observation of an anisotropic angular distribution depends on the ability to obtain a non-uniform population of substates. One way to achieve this is to observe the angular distribution of sequential radiations.

3.2 A Simple Case of Gamma-Gamma Angular Correlation

Consider again the previous example, but imagine that the state B is populated from a higher lying state A ($I_A = 0$; $m_A = 0$), via another dipole transition. The population of the substates of B will now depend on the angular distribution of the radiation from state A, in the general case:

$$P(m_B) = \sum_{m_A} \langle I_B m_B L_1 M_1 \mid I_A m_A \rangle^2 S_{L_1 M_1}(\theta) \tag{3.12}$$

where, $M_1 = m_A - m_B$.

In this particular example this reduces to:

$$P(m_B) = S_{1,-m_B}(\theta) \tag{3.13}$$

Now, in the absence of a magnetic field the choice of the quantisation axis is arbitrary and without loss of generality we may choose our $\theta = 0$ direction as that of the first γ-ray. With this choice of axis the function $S_{1,0}(0) = 0$ ($\Rightarrow P(m_B) = 0$, ie. the $m_B = 0$ substate is not populated) and, provided the state B is sufficiently short-lived, the directional correlation between the two γ-rays is seen to be (from equations 3.7 and 3.12):

$$\begin{aligned} W(\theta) &= S_{1,-1}(0)S_{1,1}(\theta) + S_{1,1}(0)S_{1,-1}(\theta) \\ &\propto (1 + \cos^2\theta) \end{aligned} \tag{3.14}$$

ie. an anisotropic angular distribution.

From the above example we see that $P(m_B) = P(-m_B)$, this is a general feature and means that for $I_B = 1/2$ the two magnetic substates, $m_B = \pm 1/2$, will be equally populated and so can only give rise to an isotropic distribution. Similarly, if $I_B = 0$ there is only one magnetic substate ($m_B = 0$) and the distribution is again isotropic.

3.3 The General Angular Correlation Function

A similar analysis can, in principle, be carried out in the general case $I_i \rightarrow I \rightarrow I_f$ giving the result:

$$W(\theta) = \sum_{kk} A_{kk} P_k(\cos\theta) \tag{3.15}$$

where, P is the Legendre polynomial; $0 \leq k \leq min\{2I, 2m_i, 2m_f\}$, with k being even (the odd k terms disappear because the intermediate state is aligned[2]) and:

$$A_{kk} = A_k(L_1 I_i I) A_k(L_2 I I_f) \tag{3.16}$$

The above equation defines A_{kk} under the assumption that the detected radiations are of *pure* multipolarity and represent consecutive γ-rays in a double cascade. In fact, allowances can be made for the possibility of the multipolarity being of a mixed nature (ie E2/M1) and for the existence of unobserved transitions between the two coincident γ-rays. For example, in the triple cascade: $I_i \rightarrow I_A \rightarrow I_B \rightarrow I_f$, where the intermediate γ-ray is unobserved, the above equation is modified by the inclusion of a U_k term:

$$A_{kk} = A_k(L_1 I_i I_A) U_k(I_A I_B) A_k(L_3 I_f I_B) \tag{3.17}$$

In the case of mixed multipoles it is usually sufficient to consider only the lowest two multipole orders L and L', where $L' = L + 1$ (see section 2.7). In this case we have:

$$A_{kk} = A_k(L_1 L_1' I_i I) A_k(L_2 L_2' I_f I) \tag{3.18}$$

where,

$$A_k(L_1 L_1' I_i I) = \frac{F_k(L_1 L_1) + 2\delta_1 F_k(L_1 L_1') + \delta_1^2 F_k(L_1' L_1')}{1 + \delta_1^2} \tag{3.19}$$

and:

$$A_k(L_2 L_2' I I_f) = \frac{F_k(L_2 L_2) + 2\delta_2 F_k(L_2 L_2') + \delta_2^2 F_k(L_2' L_2')}{1 + \delta_2^2} \tag{3.20}$$

where δ_1, δ_2 are the multipole mixing ratios for the first and second radiations and the F_k coefficients represent the normalised A_k terms, eg:

$$F_k(LL) = F_k(LLI_iI) = \frac{A_k(LLI_iI)}{A_0(LLI_iI)} \tag{3.21}$$

[2]The state I is said to be aligned if $P(m_j) = P(-m_j)$ for all m_j and $P(m_j) \neq P(m_k)$ for all $j \neq k$.

The F_k coefficients can be expressed in terms of Clebsh-Gordan and Racha coefficients, for which formula and numerical values are available (eg. Condon and Shortley 1951). Hence, F_k-values can be calculated for any desired case. Alternatively, several authors (eg. Ferentz and Rosenzwieg, 1954) have provided tables of selected F_k coefficients allowing their values to be obtained directly.

Experimentally, angular correlations of this type will at best yield the two constants F_{22} and F_{44} (certainly, the maximum value of γ-ray multipolarity considered in this work is $L = 2 \Rightarrow k_{max} \leq 4$). In this case the angular distribution is usually written:

$$W(\theta) = A_0 + A_2 P_2(cos\theta) + A_4 P_4(cos\theta) \tag{3.22}$$

or, normalising to A_0:

$$W(\theta) = 1 + a_2 P_2(cos\theta) + a_4 P_4(cos\theta) \tag{3.23}$$

where a_2 and a_4 are experimental values (obtained from a Legendre polynomial fit to the data) that can be compared to theoretical F_k coefficients for various spin hypotheses.

3.4 Alpha-Gamma and Alpha-Electron Angular Correlations

By convention the γ-γ correlation function is adopted as the standard representation of the 'geometry' of the correlation process. Angular correlations between different pairs of nuclear radiations can be obtained from this standard representation by the introduction of a *particle parameter*, $b_k(LL';x)$: $x = \alpha, \mathrm{e}, \beta \ldots$

If the radiation detectors posses cylindrical symmetry (with respect to the propagation direction of the radiation) then:

$$b_k(LL';x) = \frac{c_{k0}(LL';x)}{c_{k0}(LL';\gamma)} \tag{3.24}$$

where, the c_{k0} terms are *Racah radiation parameters*, they are the only terms that enter into the derivation of the angular correlation function that depend on the nature of the radiation. From this we see that the b_k coefficients merely serve to replace one set of radiation parameters with another and in so doing, transform the standard γ-γ correlation function to an α-γ correlation function, for example.

The correlations of interest in this work are α-γ and α-e (where e represents an internal conversion electron). For these cases we have:

$$A_{kk} = \begin{cases} A_k(L_1L_1'I_iI;\alpha)A_k(L_2L_2'I_fI;\gamma) & \text{for } \alpha\text{-}\gamma \text{ correlations} \\ A_k(L_1L_1'I_iI;\alpha)A_k(L_2L_2'I_fI;\mathrm{e}) & \text{for } \alpha\text{-e correlations} \end{cases} \tag{3.25}$$

For pure transitions ($L' = L$) we have:

$$A_k(LLI_iI;x) = b_k(LL;x)A_k(LLI_iI;\gamma) \tag{3.26}$$

while for mixed transitions we have:

$$A_k(LL'I_iI;\alpha) =$$

$$\frac{b_k(LL)F_k(LL) + [b_k(LL') + b_k(L'L)]\delta_\alpha F_k(LL') + \delta_\alpha^2 b_k(L'L')F_k(L'L')}{1+\delta_\alpha^2} \tag{3.27}$$

and:

$$A_k(LL'I_iI;\mathrm{e}) =$$

$$\frac{b_k(LL)F_k(LL) + 2\delta_\mathrm{e} b_k(L'L)F_k(LL') + \delta_\mathrm{e}^2 b_k(L'L')F_k(L'L')}{1+\delta_\mathrm{e}^2} \tag{3.28}$$

with,

$$\delta_\mathrm{e} = \delta_\gamma \sqrt{\frac{\alpha_{ic}(L')}{\alpha_{ic}(L)}} \tag{3.29}$$

where, $\alpha_{ic}(L')$ and $\alpha_{ic}(L)$ are the internal conversion coefficients of the two competing multipoles—the equations and tabulated values for the particle parameters can be found in several references eg Biedenharn and Rose (1953).

In the case of α transitions $L' = L + 2$, since the parity selection rule for α-decay ($\Delta\pi = (-1)^L$) only permits mixtures of L-values differing by an even number of units (ie. $(L' = L+2,\ L+4, \ldots)$. Usually it is sufficient to consider only the lowest two multipole orders. However, if $I_i = 0$ or $1/2$ the transition must be of pure multipolarity. That is, the angular momentum selection rule:

$$\mid I_i - I_f \mid \leq L \leq I_i + I_f \tag{3.30}$$

only allows one L-value for $I_i = 0$ $(L = I_f)$ and two L-values for $I_i = 1/2$ $(L = I_f \pm 1/2)$, each of which differ by a single unit and so are not allowed to mix.

Equation 3.15 represents a somewhat idealised situation, in that $W(\theta)$ gives the distribution at a point and it is assumed that the intermediate state is sufficiently short lived so that its population is unaffected by the existence of any extranuclear fields. These shortcomings can be remedied by the inclusion of solid angle correction factors Q_{kk} and attenuation parameters G_{kk}. Equation 3.15 is then rewritten:

$$W(\theta) = \sum_{kk} A_{kk} Q_{kk} G_{kk} P_k\ (\cos\theta) \tag{3.31}$$

3.5 Attenuation Parameters

The attenuation parameters G_{kk} describe the influence of extranuclear fields on the angular correlation. If the intermediate state in the cascade $I_i \rightarrow I \rightarrow I_f$ is sufficiently short lived, so that the relative population of its substates (imposed on it by the previous transition) remains unaltered, then the G_{kk} parameters

will be unity. If this is not the case then interactions can occur between the magnetic dipole moment or the electric quadrupole moment of the nucleus and any extranuclear fields present. These interactions will cause transitions among the m-states of I and lead to an attenuation of the angular correlation ($G_{kk} < 1$).

The fact that the daughter nucleus can recoil through the source material following α-decay will expose it to quite considerable electric field gradients, both as it recoils and when it comes to rest—since it is unlikely to do so at a regular lattice site. A further source of extranuclear fields is provided when the α-particle passes through the cloud of orbital electrons, this can have the effect of leaving the electrons in unpaired configurations which then produce magnetic fields and electric field gradients at the nucleus.

The interaction of the nucleus with its surroundings is a very complex situation and a theoretical discussion of the G_{kk} terms can be found in Frauenfelder and Steffen (1966). Experimentally, an indication of the amount of attenuation occurring can be gained by measuring the angular correlation of a cascade in which all the factors are known. The data can then be fitted and a value obtained for G_{kk}. Alternatively, G_{kk} can be treated as a free parameter and varied alongside A_k and δ^2 to obtain the best fit to the total data set.

3.6 Solid Angle Correction Factors

The solid angle correction factors, Q_{kk} enable us to allow for the finite size of our radiation detectors, where:

$$Q_{kk} = \begin{cases} Q_k(\gamma)Q_k(\alpha) & \text{for } \alpha\text{-}\gamma \text{ correlations} \\ Q_k(\gamma)Q_k(\mathrm{e}) & \text{for } \alpha\text{-e correlations} \end{cases} \tag{3.32}$$

The correction factors will vary inversely with the solid angle, Ω, subtended

by the detector. For example, $Q_k = 1$ for a point-like detector ($\Omega = 0$) and $Q_k = 0$ for a detector totally surrounding the source ($\Omega = 4\pi$). For detectors with axial symmetry Yates (1966) has obtained the following expression for Q_k:

$$Q_k = \frac{J_k}{J_0} \tag{3.33}$$

$$J_k = \int_0^{\phi} P_k(\cos\varphi)\varepsilon(\varphi)\sin\varphi\, d\varphi \tag{3.34}$$

where, φ is the angle at which the radiation enters the detector, ϕ is the half angle subtended by the detector at the source of the radiation (ie. φ_{max}) and $\varepsilon(\varphi)$ represents the detector efficiency.

If ε is independent of φ then, substituting x for $\cos\varphi$, we get:

$$J_k = \varepsilon \int_{\cos\phi}^{1} P_k(x)\, dx \tag{3.35}$$

For $k = 0$, 2 and 4 this gives:

$$J_0 = \varepsilon(1 - \cos\phi) \tag{3.36}$$

$$J_2 = \frac{1}{2}\varepsilon(\cos\phi - \cos^3\phi) \tag{3.37}$$

$$J_4 = \frac{1}{8}\varepsilon(-3\cos\phi + 10\cos^3\phi - 7\cos^5\phi) \tag{3.38}$$

and so,

$$Q_0 = 1 \tag{3.39}$$

$$Q_2 = \frac{1}{2}\cos\phi(1 + \cos\phi) \tag{3.40}$$

$$Q_4 = \frac{1}{4}Q_2(7\cos^2\phi - 3) \tag{3.41}$$

Chapter 4

The ^{223}Th Experiment

4.1 Introduction

The nucleus ^{223}Th has been investigated in a recent in-beam experiment (Dahlinger *et al.* 1988). The presence of two equal intensity bands of alternating parity, connected by strong E1 transitions, was revealed. The two $K = 5/2$ bands were established up to spin $33/2^+$, and were interpreted in terms of an octupole deformed core and an unpaired nucleon. The reflection asymmetric rotor model with octupole deformation predicts a band based upon a K = 3/2 orbital which lies close to the K = 5/2 ground state (Leander and Chen 1988); the non-yrast members of this band were not observed by Dahlinger *et al.* (1988). Both bands have been observed in a recent study of the isotone ^{221}Ra where low lying states were populated via the α-decay of ^{225}Th (Ackermann *et al.* 1989). In this experiment comparable α hindrance factors to opposite parity members were observed. Observation of similar phenomena in ^{223}Th would allow the behaviour of the single neutron in an octupole field to be probed in a region where the octupole correlations are strongest. In an attempt to observe the above effects a study has been performed in which the

low-spin states of ^{223}Th were populated by the α-decay of ^{227}U ($T_{1/2} \sim 1$ min).

4.2 Experimental Details

The parent nucleus ^{227}U was produced using the reaction ^{208}Pb(^{22}Ne,3n)^{227}U. The cross section for this reaction is $\approx 10\,\mu$b (Ter-Akop'yan). Two $4\,\mathrm{mg\,cm^{-2}}$, isotopically pure ^{208}Pb targets were alternately bombarded by a 110 MeV ^{22}Ne beam supplied by the cyclotron facility, CYCLONE, Louvain-la-Neuve, Belgium. The target thickness was chosen to be both thick enough to trap the recoiling ^{227}U nuclei and thin enough to allow α-particles and conversion electrons to escape without the occurrence of excessive straggling. All measurements were made in an out of beam mode with the aid of a rotating target assembly. Alpha-electron and alpha-gamma coincidences were collected, along with information on the time of arrival, and associated energy, of each α-particle, for a total of 51 hours, during which time the average beam current was 26 particle nA.

4.2.1 The Windmill—a Moving Target Mechanism

In order to reduce the background from the prompt radiations, a moving target technique was employed (figure 4.1). In this method a target is irradiated for a fixed period of time and then transported to a measuring station. It remains there for a further fixed period, after which time it is returned to its original in-beam position and the cycle repeated. In order to fully utilise the available beam time two targets were employed, so that simultaneous measurement (of one target) and irradiation (of the other) could take place.

The target transport mechanism consisted of a twenty pole stepper motor and a centrally pivoted, rotating arm, with a target fixed to either end. The

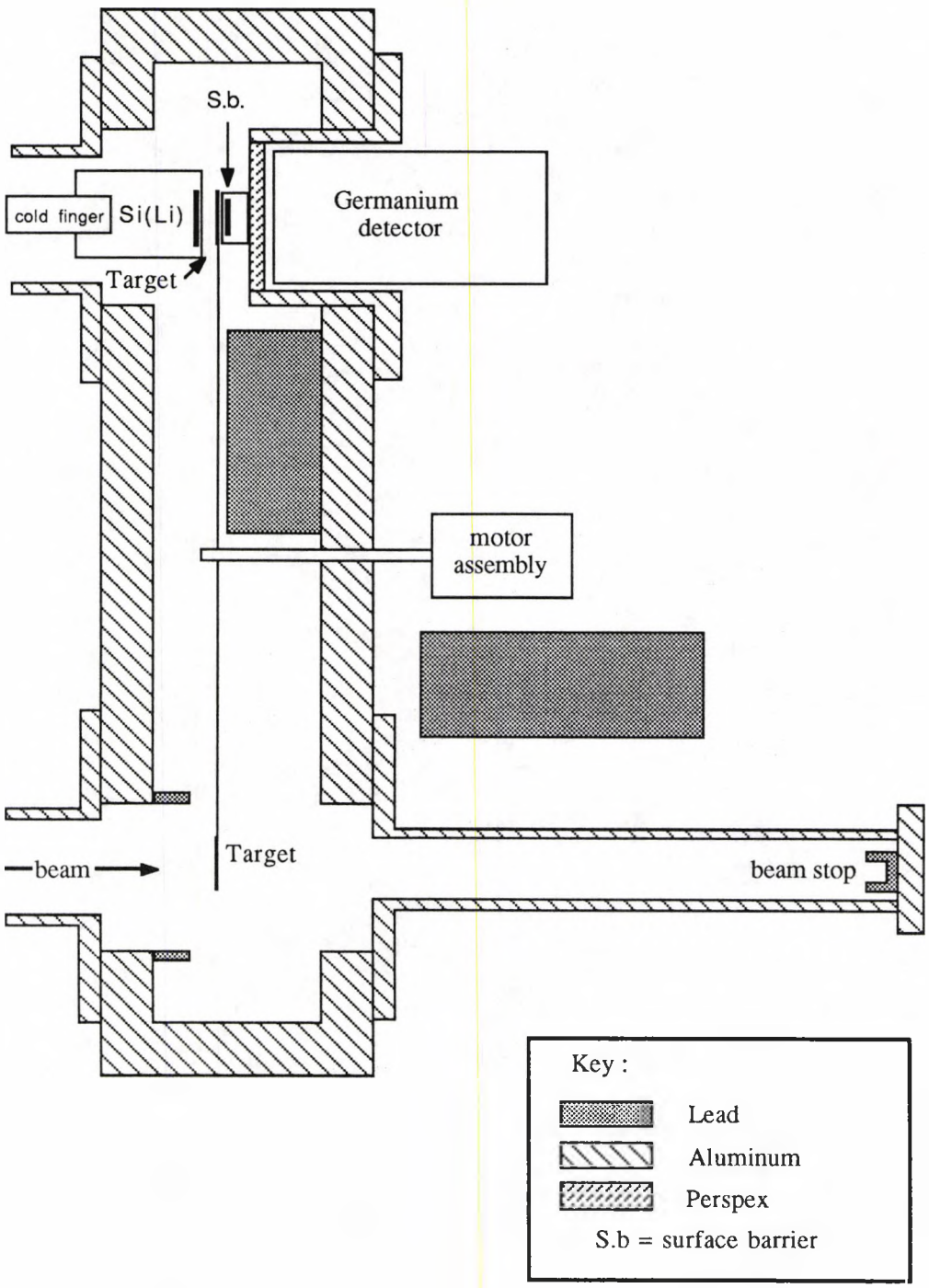

Figure 4.1: Schematic representation of the rotating target mechanism.

target arm was attached to the rotating axis of the motor in a vertical plane. The arm was cranked from its stationary position by a driving pulse and stopped, after a rotation of 180°, by a pre-set pulse rate counter. It was then rotated through a further 180°, and stopped again, this time by a photocell device. The time between successive rotations was chosen to be 30s. To prevent backlash on stopping, the arm was attached to the motor via a gearbox with a velocity ratio of 10:1.

During measurement the target was positioned between a 500 mm^2 cooled Si(Li) detector and a 200 mm^2 surface barrier Si detector. A 25% efficient (measured with respect to a 75x75 mm NaI detector for 1.33 MeV γ radiation) intrinsic n-type Ge detector was also placed in the counting position, adjacent to the surface barrier detector. The Si(Li) and surface barrier detectors subtended angles of approximately 145° and 139°, respectively, at the centre of the target.

Energy calibration was carried out using the following sources: ^{152}Eu and ^{133}Ba γ-ray sources; a ^{207}Bi electron source and a ^{228}Th α source. The α-particle energy resolution was 65 keV (full width at half maximum) at 6.297 MeV (measured using the ^{228}Th source).

4.2.2 Data Acquisition

The portable data acquisition system used was based around an IBM-PC. Additional pieces of hardware included a purpose built Octal ADC Interface unit and a Perex 'Peridata 4510' tape drive. The system was capable of controlling up to eight ADCs, in singles and coincidence mode. Multiparameter data were collected onto 15Mbyte capacity tape cartridges, and later transferred to standard 6250 bpi magnetic tape. While data collection was in progress it was

possible to perform simple on-line analysis and save any results, along with any singles spectra collected, to floppy disc. After the experiment all data collected were transferred to the GEC 4190 mini-computer at Liverpool for subsequent sorting and analysis.

4.2.3 Signal Processing

A block diagram of the electronics used is shown in figure 4.2. The energy signals from each preamplifier were fed into analogue to digital converters via spectroscopy amplifiers, while timing filter amplifiers and constant fraction discriminators processed the timing signals. Two time to amplitude convertors (TACs) were employed to generate time spectra for α-γ and α-e coincidences, the Si detector provided the start signal while the Ge and Si(Li) detectors provided the stop. The event trigger was defined to be any α-γ or α-e coincidence and was obtained by combining together an output from each TAC. In order to obtain half-life selection a time digitiser unit (TAU) was used. This enabled the time of arrival, and associated energy, of each α-particle to be written to tape.

The TAU unit was developed and used by Jones *et al.* (1980) to measure lifetimes of nuclear reaction products from μs upwards. Upon the application of a start signal (in this case the arrival of an irradiated target at the counting position) the unit begins to count internally generated clock pulses. The detection of an α-particle causes a synchronous transfer of the current count to an address register and then to the output via a digital to analogue convertor. The counter carries on incrementing, irrespective of any transfer, until it is reset by the application of a new start signal. This means that all α-particles detected will be tagged with their time of arrival. The internal clock runs at a

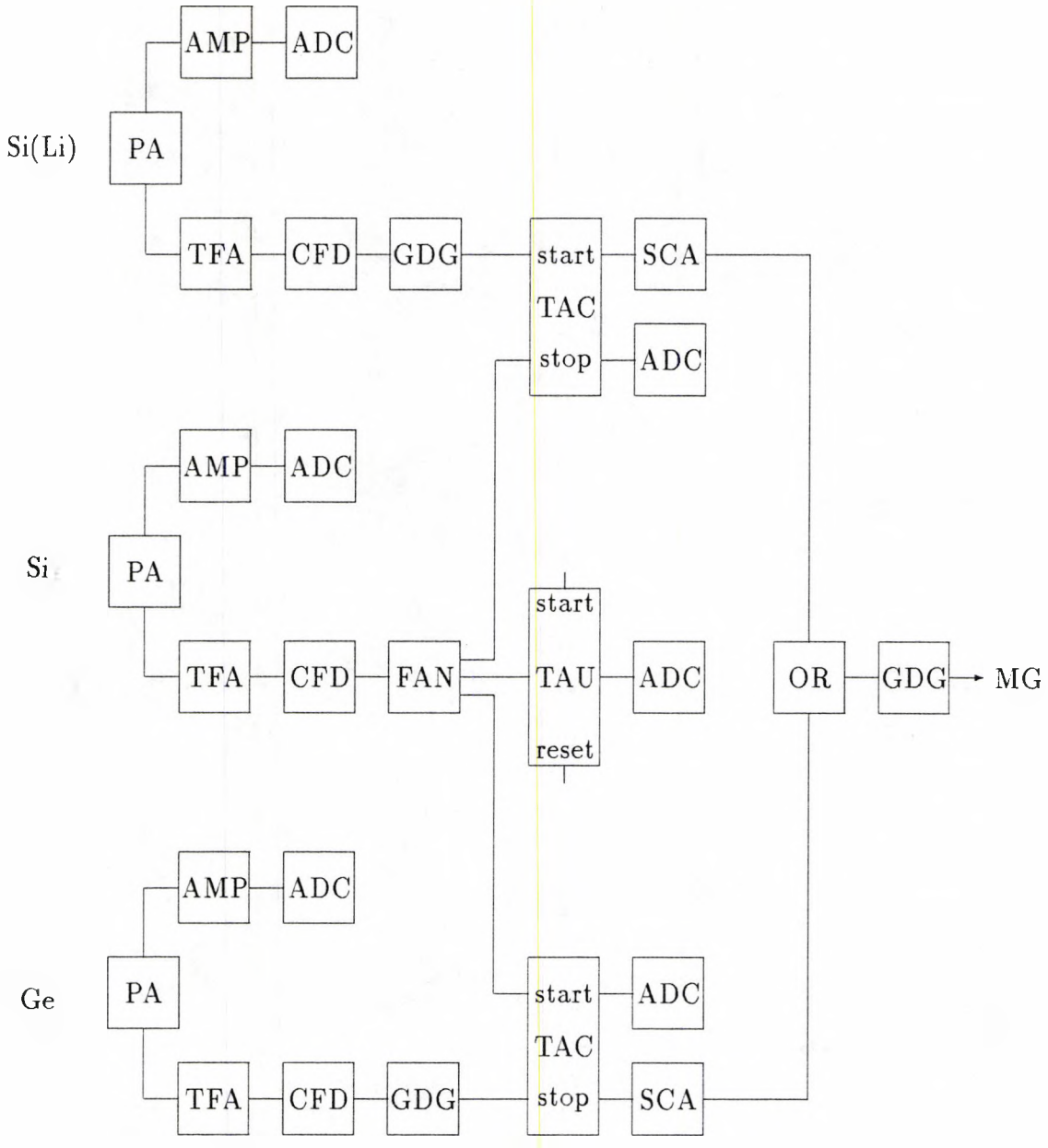

Figure 4.2: Block Diagram of the Electronics. PA = preamplifier, AMP = amplifier, ADC = analogue to digital convertor, TFA = timing filter amplifier, CFD = constant fraction discriminator, GDG = gate and delay generator, FAN = logic fan in/fan out, TAC = time to amplitude convertor, TAU = time digitiser, SCA = single channel analyser, OR = slow coincidence unit, with coincidence requirement set to one, MG = master gate.

frequency of 1 MHz, but the time period between the pulses presented to the counter can be selected, eight options are available from 1 μs to 10 s in factors of ten. In this work a period of 0.1 s was chosen.

4.3 Data Analysis

Prior to this work the only information available for α-decay into ^{223}Th was the work of Valli *et al.* (1970). From previous work it was not clear which α-energies should be associated with the decay of ^{227}U. A spectrum of all γ-rays in coincidence with α particles of energy 5.34–8.79 MeV is shown in figure 4.3. Known transitions arising from the population of channels other than the 3n channel were identified. On elimination of these known γ-rays a 247 keV transition emerged as the likeliest candidate for a decay in ^{223}Th.

From the possible open channels two 246 keV transitions are already known from α-decay studies: a $7/2^+ \rightarrow 7/2^+$ transition in ^{221}Ra and a $1^- \rightarrow 0^+$ transition in ^{224}Th. The α-particle energies corresponding to these transitions are 6.51 and 6.44 MeV respectively. The ^{224}Th channel, which corresponds to primary population of ^{228}U via the (^{22}Ne,2n) reaction, is expected to be very weak (see later). The α-particle energy corresponding to a 247 keV transition to the ground state in ^{223}Th is expected to be 6.83 MeV—based on Q_α = 7.2 MeV obtained from systematics (Lederer and Shirley 1978). Contributions from other channels could therefore be eliminated by choosing a suitable α window for generation of the γ-ray spectrum. The window chosen was 6.76–6.92 MeV.

The contribution due to the 177 keV (E_α = 7.00 MeV) transition from ^{220}Ra was reduced by requiring that the time of arrival of α-particles was $\geq$ 7 s, since the major population of this level occurred via the decay of ^{224}Th ($T_{1/2} \sim 1$ s)

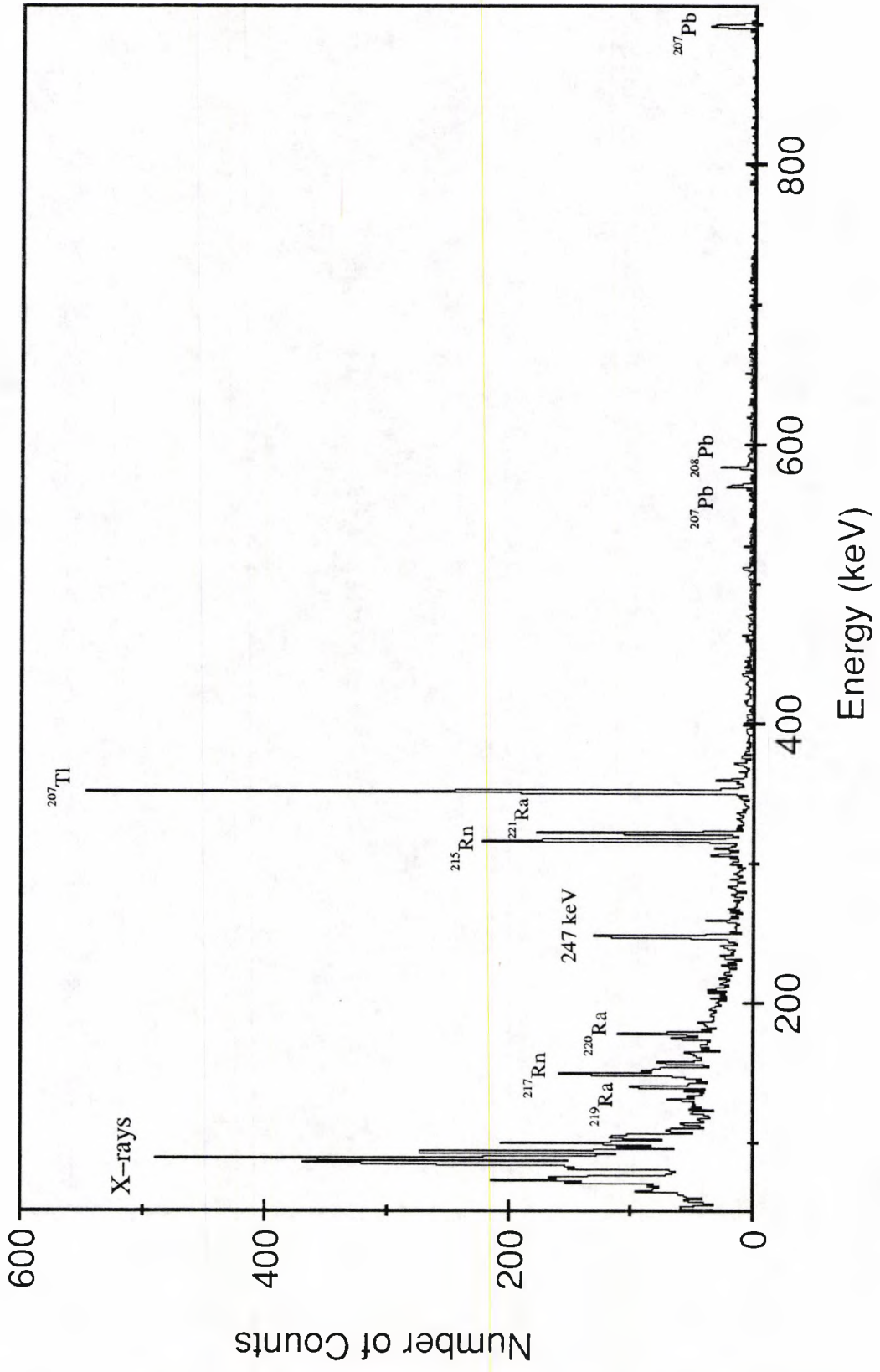

Figure 4.3: Spectrum of all γ-rays in coincidence with α-particles of energy 5.34–8.79 MeV.

which was directly populated through the (α 2n) channel.

The contribution due to the strong 152 and 140 keV (E_α = 7.3 MeV) and weaker transitions in ^{219}Ra were reduced by a two-stage normalisation and subtraction process. A spectrum was generated for ^{219}Ra and was found to contain, along with the 152 and 140 keV transitions, a 316 keV transition from ^{215}Rn. It was therefore necessary to generate a second spectrum containing only the 316 keV transition. This second spectrum was then normalised and subtracted from the first, thus removing the 316 keV peak and leaving a pure α-γ spectrum for ^{219}Ra, which was then normalised and used to reduce the contributions from ^{219}Ra.

The resulting γ-ray spectrum is shown in Figure 4.4. The presence of Th x-rays in this spectrum adds confidence to the assignment of the γ-rays to ^{223}Th. An associated electron spectrum was generated and is shown in figure 4.5. Table 4.1 shows the experimental conversion coefficients deduced from these spectra and compares them to the expected theoretical values (Hager and Seltzer 1968) for M1, E1, and E2 transitions. It can be seen from this table that all the transitions are consistent with M1 multipolarity, although E2 mixing cannot be ruled out, especially for the 158 and 209 keV transitions.

It should be noted that figures 4.4 and 4.5 do not represent pure spectra for ^{223}Th. For example, γ-rays corresponding to 68 and 75 keV transitions in ^{219}Ra and x-rays from Ra (80 and 83 keV) and possibly Tl or Pb (72 keV) can be seen, thus indicating an incomplete subtraction process. If the γ-rays observed at 68 and 75 keV are indeed due to transitions in ^{219}Ra then this would account for approximately 50% (using the multipolarity assignments of E1 from the work of El-Lawindy 1986, with conversion coefficients taken from Hager and Seltzer 1968) of the counts in the broad electron peak around 65 keV as being due to L (50–60 keV) and M (63–72 keV) conversion.

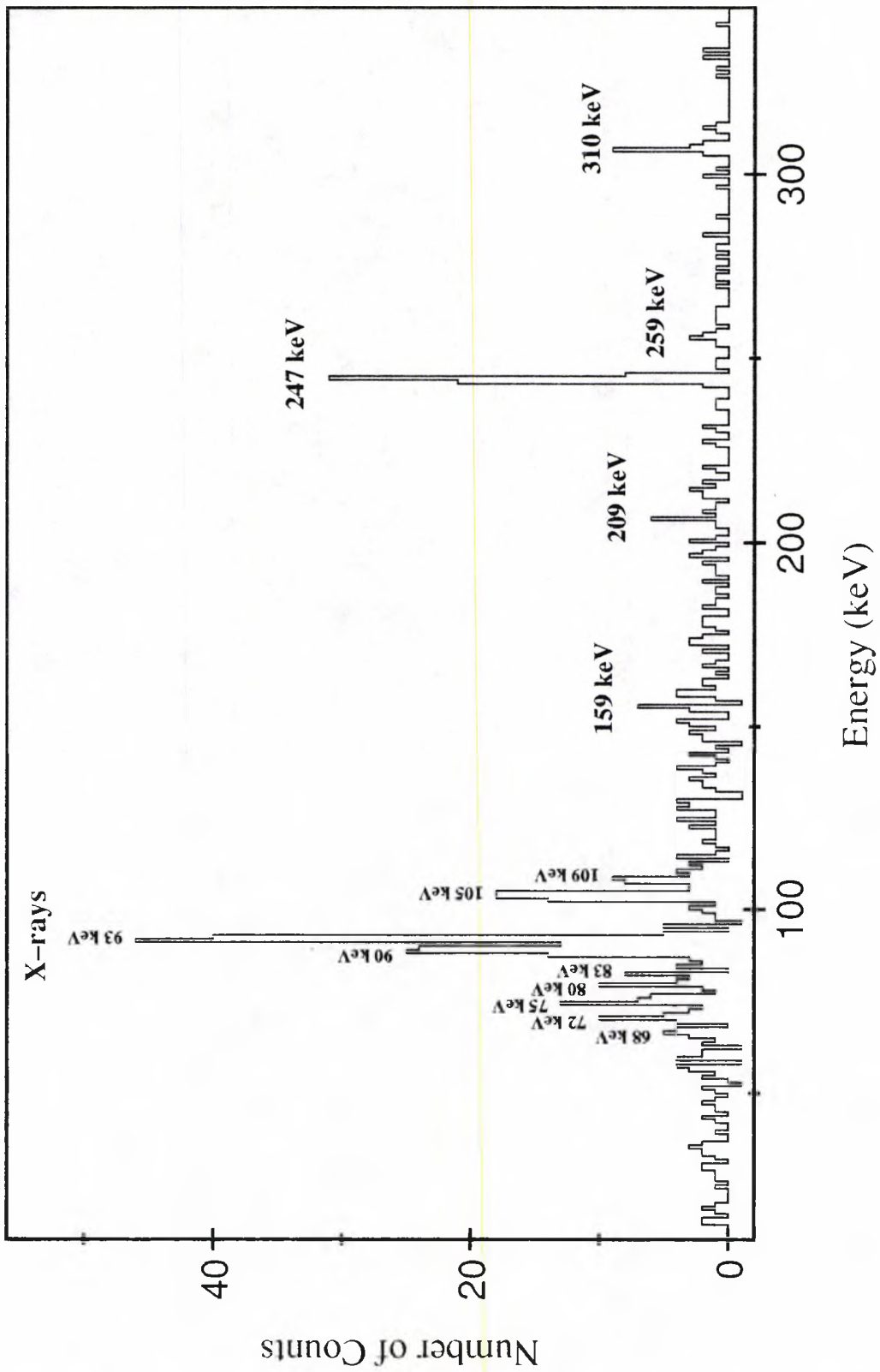

Figure 4.4: γ-ray spectrum of ^{223}Th (E_α = 6.76–6.92 MeV) as described in the text.

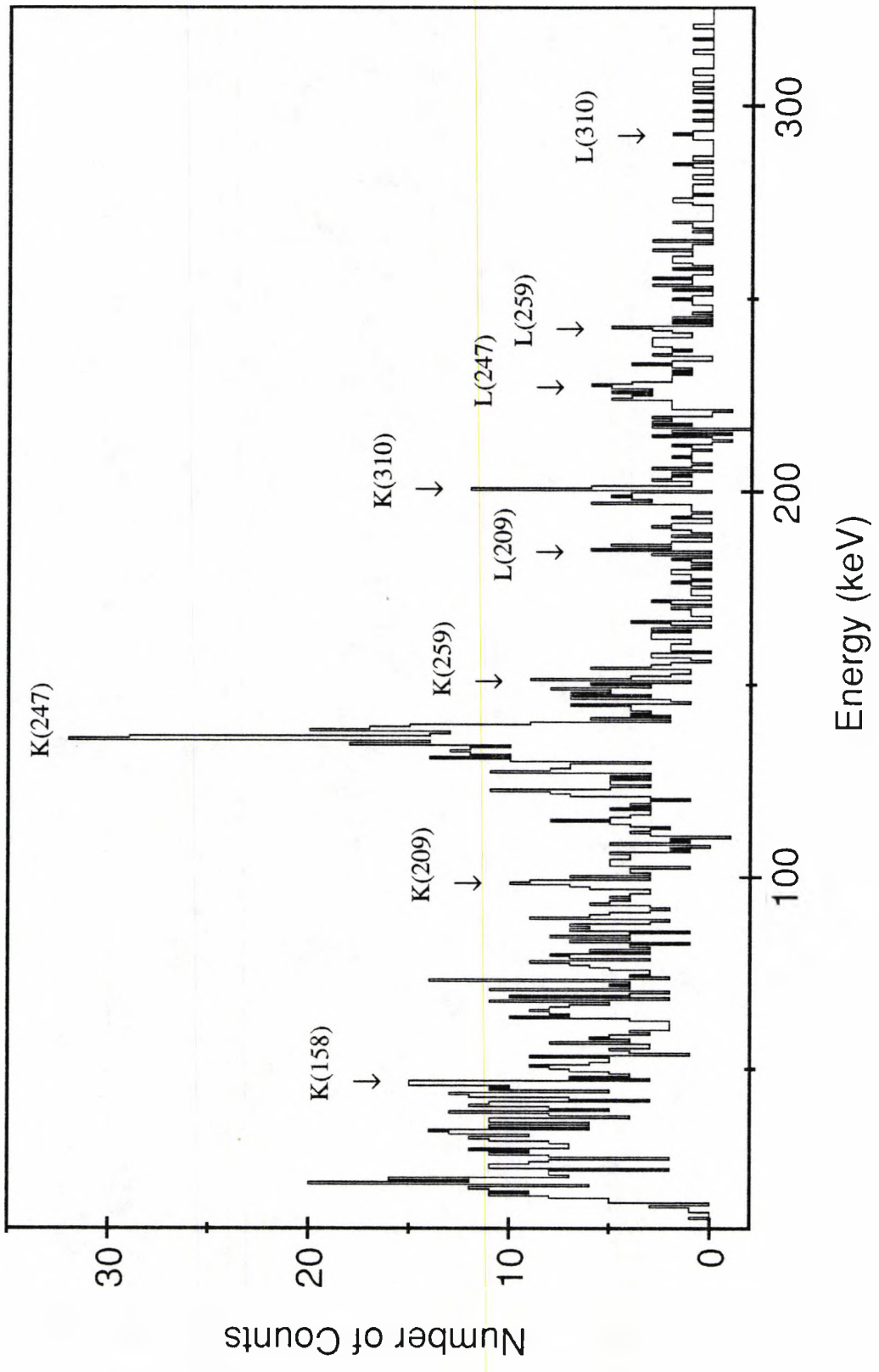

Figure 4.5: Conversion-electron spectrum associated with figure 4.4

Shell	E_γ(keV)	Expt.	M1	E2	E1
K	158	1.72(66)	4.36	0.237	0.134
	209	0.80(44)	1.95	0.150	0.0682
	247	1.24(28)	1.22	0.109	0.0465
	259	1.58(75)	1.07	0.0998	0.0418
	310	0.65(24)	0.656	0.0742	0.0285
L_{total}	158	-	-	-	-
	209	0.69(28)	0.349	0.287	0.0129
	247	0.297(74)	0.251	0.175	0.00960
	259	0.46(28)	0.218	0.143	0.00850
	310	0.092(46)	0.116	0.0582	0.00496
M_{total}	247	0.074(28)	0.0598	0.0469	0.00229

Table 4.1: Experimental and theoretical internal conversion coefficients for ^{223}Th.

E_γ (keV)	E_α (Mev)	I_{trans}
158	6.91(6)	14(5)
209	6.90(6)	14(5)
247	6.86(3)	100(13)
259	6.74(4)	15(6)
310	6.74(5)	18(6)

Table 4.2: Relative transition intensities and α energies associated with the γ-rays belonging to ^{223}Th.

If it is assumed that the five γ-rays (157–310 keV) observed in figure 4.4 all belong to ^{223}Th and their associated α-particle energies are measured, then a decay scheme (figure 4.6) can be constructed. Table 4.2 shows the α energies associated with the γ-rays in figure 4.4, along with relative γ-ray intensities.

A low-lying level 51.3 keV above the ground state was observed by Dahlinger *et al.* (1988); his assumption of a $5/2^+$ ground state and a $7/2^+$ first excited state is followed here. The assumption of a $5/2^+$ ground state is based on the experimental assignment of 5/2 to the ground state spin in ^{221}Ra (Ahmad *et al.* 1983) and the theoretical assignments given by both Leander and Chen (1988) and subsequently by Ćwiok and Nazarewicz (1989). The 247 keV transition has M1 multipolarity and is placed in the decay scheme as originating from a 247 keV level decaying to the ground state. This level has $I^\pi = 3/2^+, 5/2^+$ or $7/2^+$.

A level is placed at 310 keV with decays of 310 keV and 259 keV to the ground state ($5/2^+$) and first excited state ($7/2^+$) respectively. These transitions are both consistent with M1 multipolarity which restricts the I^π of the

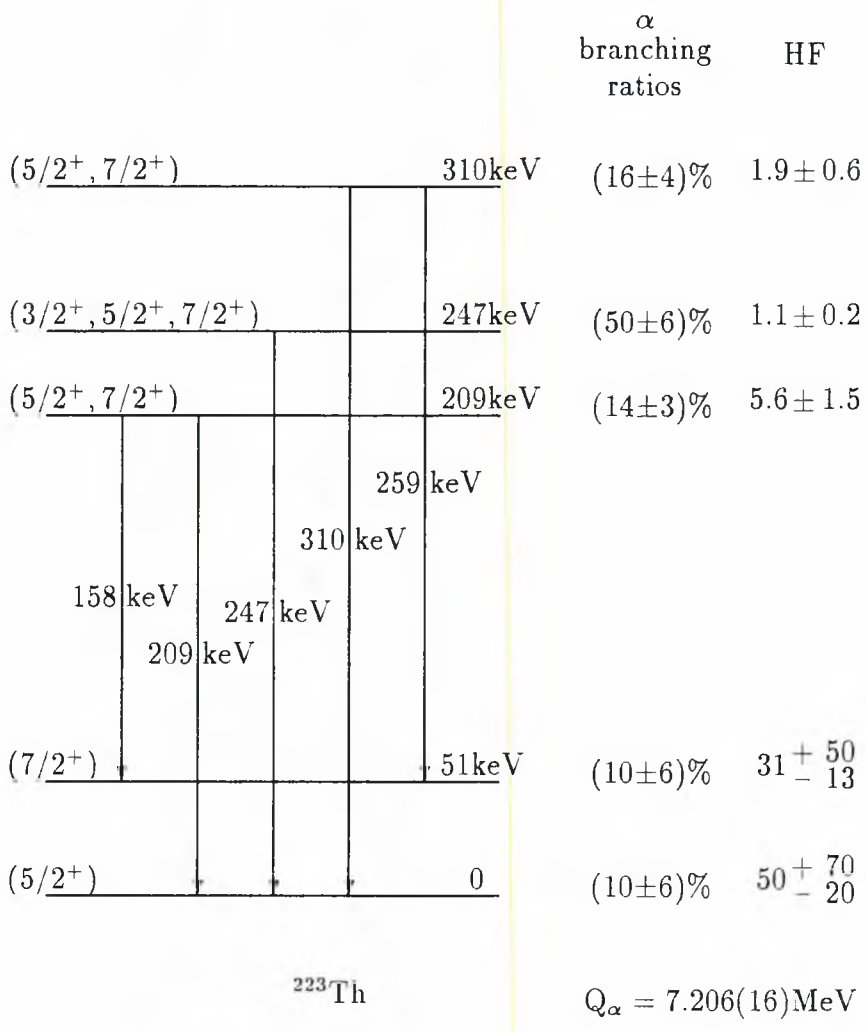

Figure 4.6: Proposed level scheme of ^{223}Th as populated in the α-decay of ^{227}U. Hindrance factors were calculated using the one-body theory of Preston (1947) with $R_o = 9.647$ fm and $T_{1/2} = 66$ s for ^{227}U.

level to $5/2^+$ or $7/2^+$.

A level is placed at 209 keV with decays of 209 keV and 158 keV to the ground state ($5/2^+$) and first excited state ($7/2^+$), respectively. These transitions are both consistent with M1 multipolarity which again restricts I^π of the level to $5/2^+$ or $7/2^+$.

The relative intensities of the five transitions given in table 4.2 were obtained from the measured γ-ray intensities by correction for internal conversion (using the values obtained in this work). In order to accurately determine the α-branching ratios to these states the intensities of the ^{223}Th γ-rays are required without any restriction on α-particle energy (ie. too restrictive an α gate on the 247 keV γ-ray would result in missing intensity from the 209 and 310 keV levels). It was therefore necessary to determine what fraction of the 246/247 keV peak was due to ^{223}Th, since the other γ-rays assigned to ^{223}Th are too weak to be used for normalisation. The contribution to this peak from ^{224}Th decay was determined by looking for the 152 keV transition corresponding to the 33% branch to the 2^+ state, which should be seen in addition to the 246 keV 1^- to 2^+ transition (Lederer and Shirley 1978). A measurement of the intensity of this 152 keV transition would allow the intensity of the 246 keV transition, and hence its contribution to the 246/247 keV peak, to be calculated. Unfortunately a 152 keV transition was also observed in ^{219}Ra so a direct measurement was not possible. However, the relative intensities of the 113 keV, 140 keV and 152 keV transitions (all belonging to ^{219}Ra) are known from the work of El-Lawindy (1986), so it was possible to determine the expected intensity of the 152 keV peak due to ^{224}Th decay alone, relative to that of the 247 keV transition in ^{223}Th. It was estimated that a maximum of 2% of the total 246/247 keV peak arises from a contribution from ^{224}Th. Further evidence that the ^{224}Th component is weak is provided by the pre-

dictions of the computer code ALICE (Blann 1966): the population of ^{224}Th is expected to be less than 0.4% of that for ^{223}Th. It was possible to deduce the contribution from the 246 keV transition in ^{221}Ra to the 246/247 keV peak by measuring the intensity of the 321.4 keV transition (also in ^{221}Ra) observed in this work, since the relative intensities of these transitions are accurately known from the work of Ackermann *et al.* (1989); this fraction was 21(3)% .

The total α-decay strength observed in the ^{227}U chain can be obtained using the measured intensity (corrected for germanium detector efficiency and internal conversion) of the 315.8 keV transition in ^{215}Rn and the known α-branching ratio (El-Lawindy 1986) to this level. In order to avoid problems over direct population of nuclei in the chain via α xn exit channels the first 7 s of each 30 s measuring period was excluded. In this way the sum of the α-branching ratios to the ground state and the 51 keV level can be deduced. The α-branching ratios to the ground state and first excited state could not be individually determined in that no transition from the 51 keV level was actually observed. The relative intensity to each state has been arbitrarily apportioned as 50/50, on the grounds that the α-branching ratios to the ground state and first excited state of ^{221}Ra are of a similar magnitude: 7% and 9%, respectively (Lederer and Shirley 1978). These values along with α-branching ratios to the excited states, are given in figure 4.6, together with deduced hindrance factors using the formalism of Preston (1947).

The Q-value given in figure 4.6 is the mean of the values obtained by measuring the α-particle energies in coincidence with γ-decays from the 209, 247 and 310 keV levels to the ground state. The α-particle energies were calibrated relative to decays from a ^{228}Th source and a measurement of the Q-value is then given by $E_\alpha + E_R + E_\gamma$, where E_α is the α-particle energy measured in coincidence with a γ-ray of energy E_γ and E_R is the energy of the

recoiling nucleus.

Due to the close geometry of the particle detectors with the target (necessary because of the low cross section) there is the possibility of pulse summing of correlated particles in the surface barrier and Si(Li) detectors. This problem has been largely circumvented by utilising windows on γ-ray spectra to generate α-particle yields. Summing in the Si(Li) detector was fortuitously avoided since a build up of contamination on the front surface of the detector during calibration, prior to the start of the experiment, precluded both direct detection of L or M electrons from the highly converted 51 keV transition as well as indirectly via summed events.

4.4 Half-life measurement of ^{227}U

We have also attempted to measure the half-life of ^{227}U. Ideally, in this type of measurement data should be collected over a period of time equivalent to several half-lives of the parent nucleus. However, since the main aim of this experiment was to obtain as much α-γ and α-e coincidence data as possible within the available time, irradiation/count periods of 30 s/30 s were chosen. The TAU unit can be used to generate a time versus count rate spectrum for a particular group of α-particle energies. A decay curve can be fitted to this spectrum and the half-life of the parent nucleus determined.

The α-particle energies, branching ratios and half-lives for the α-decay chain of ^{227}U (Lederer and Shirley 1978) is shown in figure 4.7. Since the α-decay of ^{215}Rn to ^{211}Po is well separated in energy from other decay chains seen in this work, the 8.67 MeV α group was used for the half-life measurement. Although the preceding half-lives are $\ll$ 66 s (the dominant half-life of the chain due to the ^{227}U precursor), ^{223}Th was also, to some extent, pop-

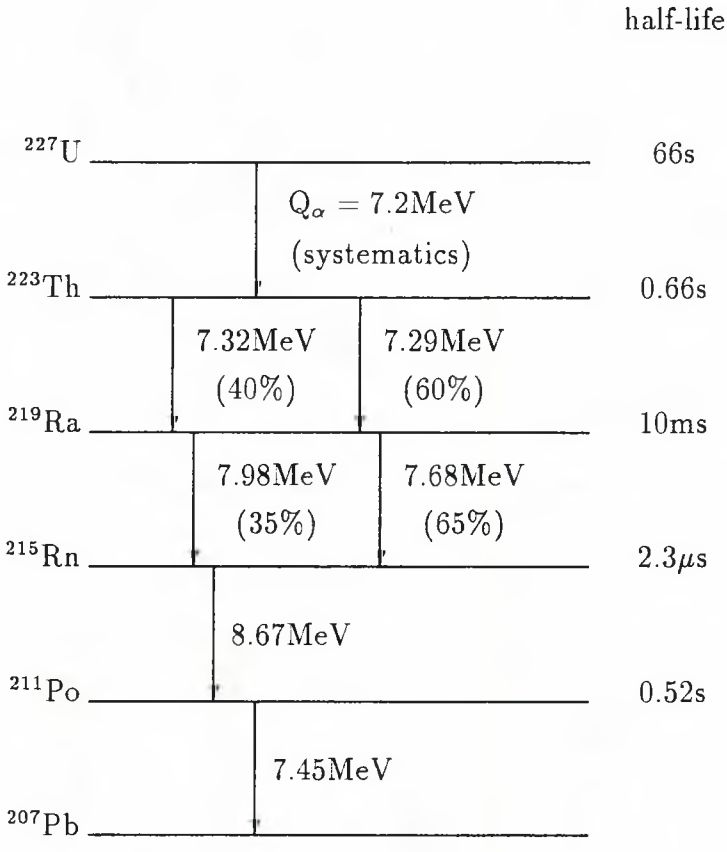

Figure 4.7: The α decay chain from the parent nucleus ^{227}U.

ulated directly via the α n exit channel. This meant that the timer spectrum contained both a fast and a slow component. A collection time of 30s made extraction of the slow component quite difficult by conventional means. Because of this a slightly different method of analysis was adopted. The first 7 s of the timer data was excluded ($\sim$ 10 half-lives of ^{223}Th—thus allowing time for any direct population to decay away) and twelve α spectra were generated—each spectrum corresponding to an equal time interval (of $\sim$ 1.9 s) ranging from 7 to 30 s. The spectra were integrated over the energy range 8.05–9.02 MeV to produce a count rate versus time plot. This was then fitted using a non-linear least squares fit to produce a half-life of 45 $\pm$ 5 s. This is somewhat shorter

than the value of 66 ± 6 s, obtained by Hann *et al.* (1969), but the difference is not sufficient to unduly influence determination of α-hindrance factors (because of a logarithmic dependence), which were calculated using the one body formalism of Preston (1947).

Chapter 5

The ^{223}Ra Experiment

5.1 Introduction

Over the past thirty or so years a wealth of experimental data has been accumulated for the nucleus ^{223}Ra. This information has been well summarised in publications such as Nuclear Data Sheets (Maples 1977). The data comes from the α-decay of ^{227}Th and from the β-decay of ^{223}Fr. As pointed out by Sheline *et al.* (1988), the complexity of this data is highlighted by noting that there are 46 α-groups and 240 γ-rays following the α-decay of ^{227}Th with a further 56 γ-rays following the β-decay of ^{223}Fr. This has lead to the assignment of 44 levels in ^{223}Ra, one of which is tentative. However, the I^{π} values assigned to these levels are now known to be incorrect since they were based on the assumption that ^{223}Ra has a ground state spin of 1/2. A measurement by Ahmad *et al.* (1983) has shown that the ground state spin of ^{223}Ra is in fact 3/2.

In an attempt to reassign I^{π} values to at least some of these levels, a study has been performed in which the low-lying states of ^{223}Ra were populated by the α-decay of ^{227}Th. It was also hoped that the level structure and the new

I^{π} values could be understood in terms of octupole deformation since ^{223}Ra lies in the middle of the region where octupole correlations are expected to be strongest.

5.2 Experimental Details

Since ^{227}Th has a half-life of only 19 days an ^{227}Ac source was used, this has a half-life of 22 years and β-decays to ^{227}Th. The source consisted of $\sim$10 μCi of ^{227}Ac evaporated onto a gold backing. Gold has a simple cubic crystalline structure and was chosen to reduce hyperfine field effects on recoiling ^{223}Ra nuclei following α-decay. The γ-rays were detected with a Be windowed, low energy, hyperpure Ge detector, while internal conversion electrons were detected using a 100 mm^2, 3 mm thick, Si(Li) detector. The α-particles were detected using low-cost silicon PIN diodes with an active area of 1.5 cm^2.

The name PIN arises from the diodes so-called p-i-n structure. The diodes consist of a highly pure wafer of silicon whose front and rear faces have been doped to form p-type and n-type layers respectively, leaving a high-resistance *intrinsic* region in between. Figure 5.1 (reproduced from HAMAMATSU 1987) shows a schematic of the cross-section and the external dimensional details of the Hamamatsu S1723 photodiode. The diodes were originally intended for use with scintillators as a solid-state alternative for photomultiplier tubes, hence the references to light. The actual diodes used were type S1723–04N and were supplied with detachable perspex squares in place of the resin windows.

In the work of Gooda and Gilboy (1987) spurious satellite peaks were observed that were found to be due to edge effects in the diodes. To avoid the possible occurrence of this problem and to ensure that equations 3.24 and 3.34 remain valid, circular collimators (with 8 mm diameter holes) were used

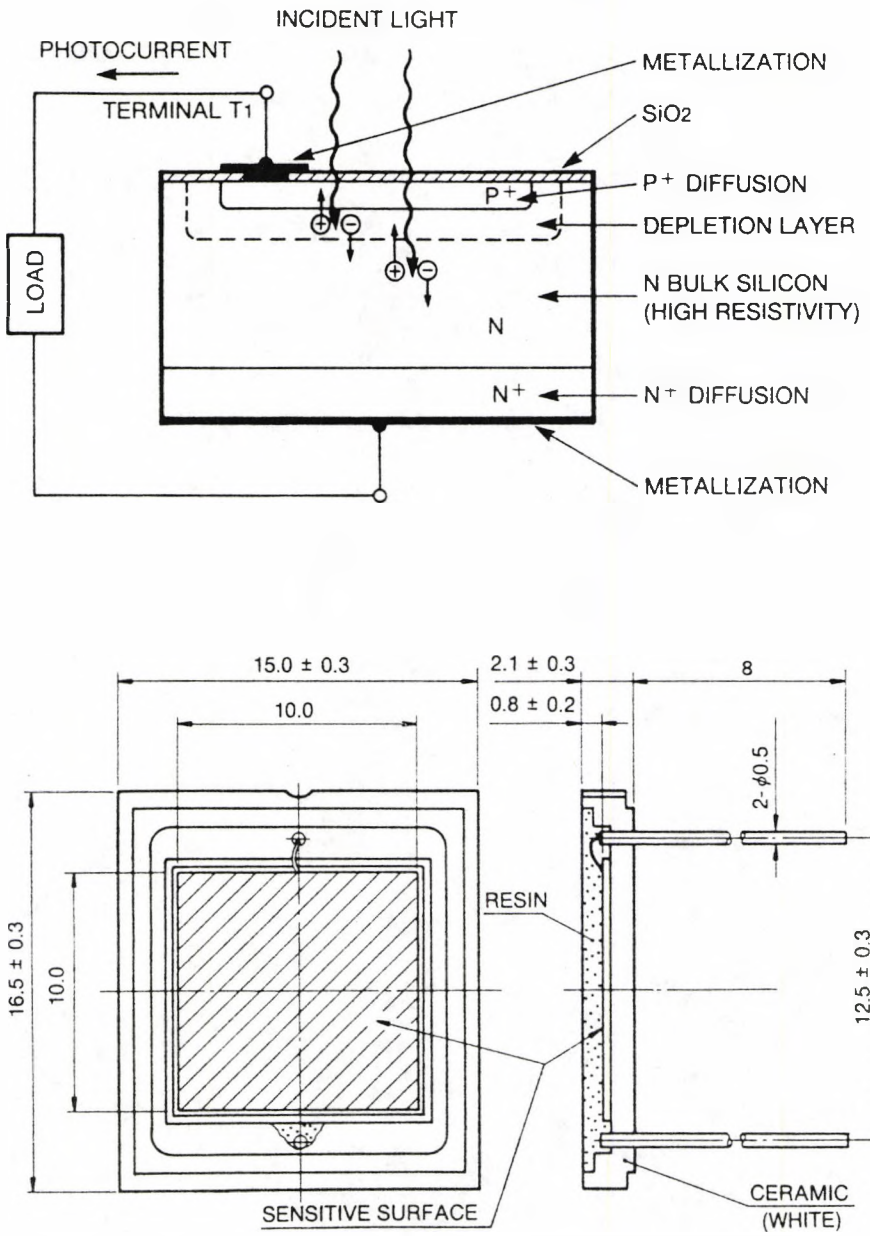

Figure 5.1: The Hamamatsu S1723 photodiode. The diodes used in this work were supplied without the resin windows.

with the PIN diodes. The collimators both mask the edges of the diodes and ensure that their exposed area is cylindrically symmetric.

Energy calibration of the Ge and Si(Li) detectors was carried out using ^{152}Eu and ^{133}Ba γ-ray sources and a ^{207}Bi electron source. Since the α energies involved in the ^{227}Th decay chain are well known, the ^{227}Ac source itself was used for energy calibration of the PIN diodes. The α-particle energy resolution was typically $\sim$25 keV and the γ-ray resolution for transitions less than 250 keV was typically 1 keV. The low energy γ-ray cut-off was $\sim$4 keV. The electron resolution was $\sim$2.5 keV at electron energies of $\sim$150 keV.

5.2.1 The Vacuum Chamber

The usual experimental arrangement for performing angular correlation measurements involves a source of radiation and two radiation detectors. One of the detectors remains fixed opposite the source defining a $\theta = 0$ direction. The second detector then occupies a number of co-planar positions about this axis allowing the coincidence intensity distribution to be recorded. In the case of α-γ or α-e correlations the particle detectors and the source must be placed in some sort of vacuum chamber. The γ detector may be positioned outside the chamber provided that the severe attenuation of low energy γ-rays can be tolerated.

In order to overcome the technical problems imposed by such a system (particularly in the α-e case) we have developed a versatile and compact six detector system which allows the simultaneous measurement of α-γ and α-e correlations. The system consists of a vacuum chamber with provision for mounting a radioactive source, upto five PIN diodes (with collimators) and two apertures for accommodating Ge or Si(Li) detectors. The system is shown

schematically in figure 5.2 and has been used in two specific arrangements: set-up I and set-up II. The figure shows five positions labelled 1 to 5, separated by 25° or 45° from their nearest neighbours, at which PIN diodes, in transmission mounts 3 cm from the centre of the chamber were placed. The positions A and B allow a Be-windowed Ge detector and a cooled Si(Li) detector to protrude into the 16 cm diameter vacuum chamber for the detection of low energy γ-rays and internal conversion electrons.

Set-up I A single-sided source was positioned facing the PIN diodes, position B was unused and position A was occupied by a low energy γ-ray detector 9 cm from the source. Coincident signals between any of the detectors in positions 1 to 5 with the Ge detector were recorded event by event. The $\theta = 0$ direction was defined to be that between the Ge detector and the source, the PIN diodes 1 to 5 then occupied angles: –25°, 0°, 45°, 90° and 115°. As the data are expressed in terms of $\cos^2\theta$ these angles are equivalent to: 25°, 0°, 45°, 90° and 65°. A more equal separation of points, in terms of $\cos^2\theta$, would be obtained if position 1 were separated from position 2 (and 4 from 5) by 30° but experimentally it was found that slight rotation of the source holder could lead to severe degradation of the α-particle resolution in the detectors at positions 1 or 5 so the indicated separation was adopted.

The only γ-ray attenuation suffered in this arrangement is through the 300 μm of PIN diode 2 and the very thin (0.2 mm thick Al) α-particle collimators. Since the Be windowed Ge detector at position A is fixed no differential γ-ray absorption occurs for different correlation angles as happens in the case of more conventional arrangements. Relative normalisation of the angular correlation yields was obtained from simultaneous collection of the α-particle singles yields in detectors 1 to 5. Coincidence data were accumulated during

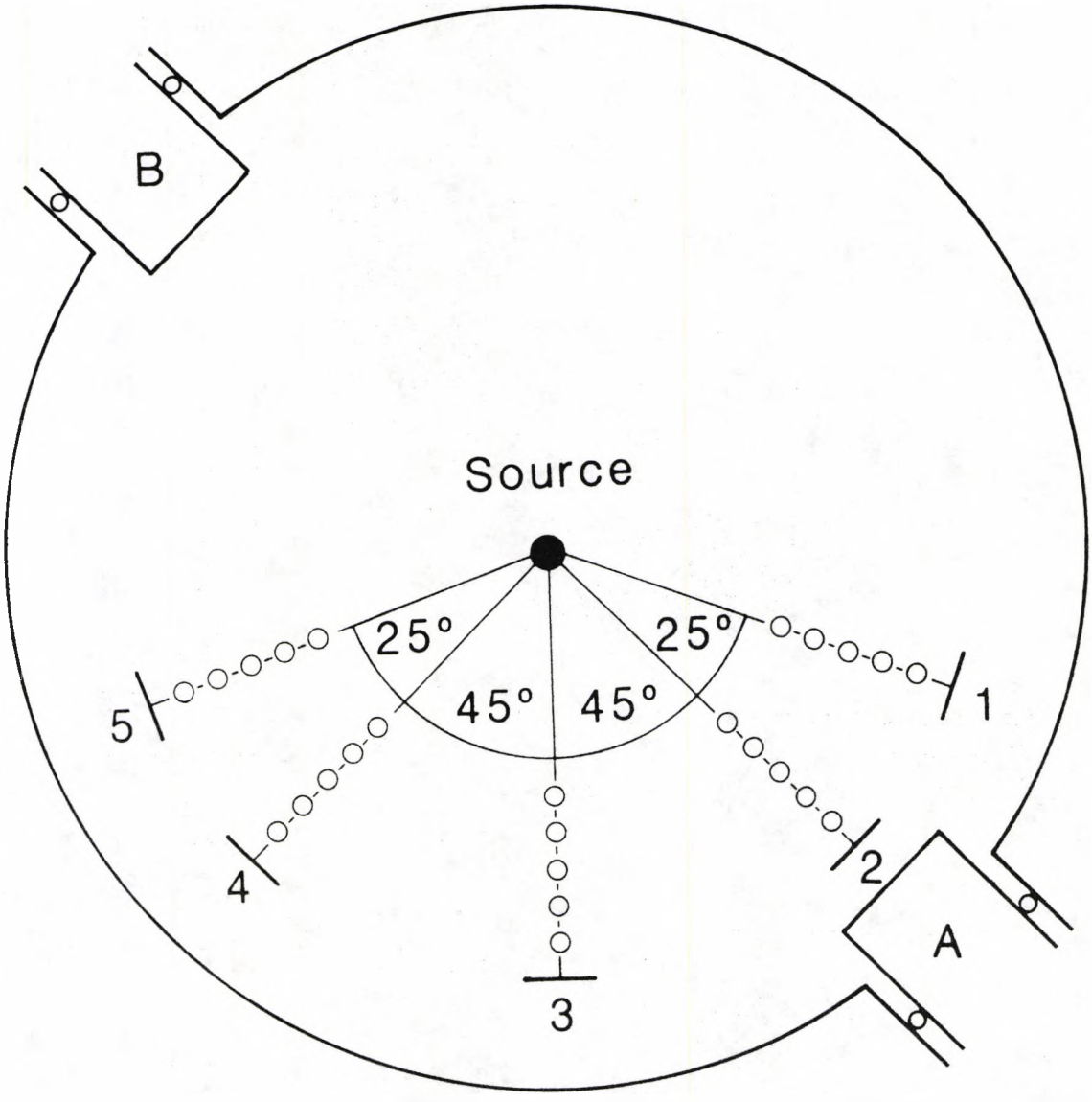

Figure 5.2: Sketch showing possible locations for PIN diodes, Ge and Si(Li) detectors

two weeks of continuous running.

Set-up II In perhaps its most versatile configuration the PIN diode at position 2 was removed, position A was occupied by a cooled Si(Li) detector, 5.5 cm from the source, for electron detection and position B was occupied by a Be windowed low energy Ge detector. Four point α-γ and α-e correlations were obtained simultaneously permitting various theoretical fitting options. With the appropriate efficiency calibrations internal conversion coefficients were also obtained from the conversion electron/γ-ray yield ratios. Coincidence data were accumulated during one week of continuous running.

5.2.2 Data Acquisition and Signal Processing

Data acquisition was performed using the portable PC based system described in chapter 4. In set-up I the event trigger (or master gate) was defined to be any α-γ coincidence, while in set-up II it was defined to be any α-γ or α-e coincidence. Standard NIM electronics modules were used for the signal processing. Block diagrams of both set-ups are shown in figures 5.3 and 5.4.

The energy signals from each preamplifier were fed into analogue to digital convertors via spectroscopy amplifiers, the timing signals were processed by timing filter amplifiers and constant fraction discriminators. In set-up I, one time to amplitude convertor was used to generate a time spectrum for α-γ coincidences and, after suitable processing by a timing single channel analyser, to provide the event trigger. In set-up II, two time to amplitude convertors were employed, the output of both being combined in a summing amplifier resulting in a single α-γ/α-e coincidence time spectrum. Appropriate adjustment of the relative delay between the Ge and Si(Li) timing signals, provided by the gate and delay generators, ensured that the α-γ and the α-e peaks

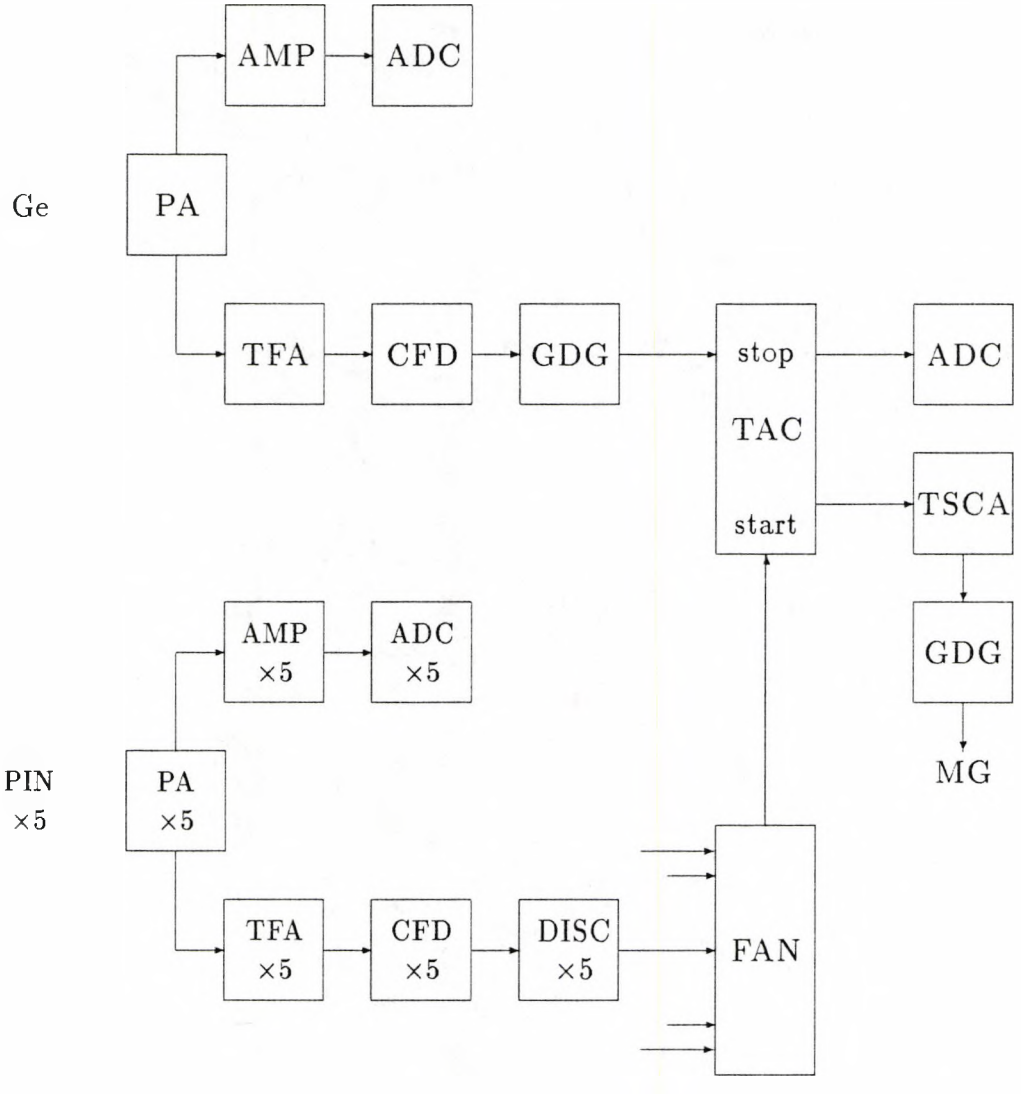

Figure 5.3: Block diagram of the electronics for set-up I. PA = preamplifier, AMP = amplifier, ADC = analogue to digital convertor, TFA = timing filter amplifier, CFD = constant fraction discriminator, GDG = gate and delay generator, FAN = logic fan in/fan out, TAC = time to amplitude convertor, TSCA = timing single channel analyser, SA = summing amplifier, DISC = discriminator, MG = master gate.

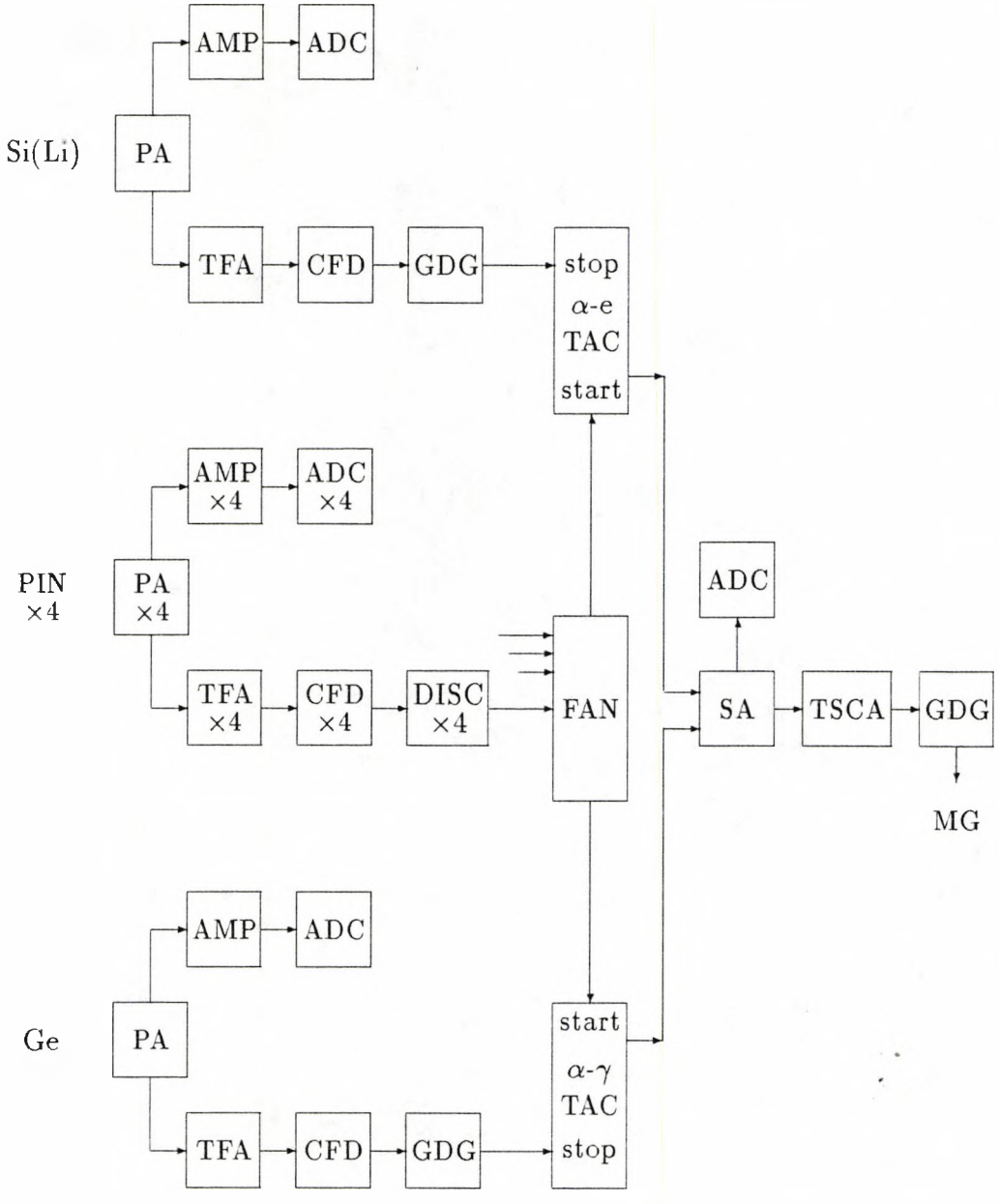

Figure 5.4: Block diagram of the electronics for set-up II. See figure 5.3 for key.

were well separated. The PIN diode timing signals were fed through Le Croy discriminators and combined in a logic fan in/fan out unit. The discriminators provided adjustment for compensating for any differential delay experienced by the diode timing signals in their propagation through the system up to this point; this adjustment ensures that the peaks in the time spectra are as well defined as possible.

5.3 Data Analysis

The original aim of this study was to make it as self-contained as possible. For example, set-up II was specifically designed to allow the measurement of α-γ and α-$e_{K,L,M}$ angular correlations, as well as measuring some or all of e_K/e_L, e_L/e_M, e_K/γ and e_L/γ conversion ratios. In this way the spins of the levels could be determined by the correlation data, the parities of the levels by the conversion ratios and the multipole mixing ratios by a combination of both. However, on a preliminary analysis of the electron data it became apparent that the results of Briançon and Vieu (1971) could not be improved upon. It was therefore decided that their multipole assignments and multipole mixing ratios would be used in the analysis of our α-γ correlation data.

5.3.1 Transition Intensities

In a recent publication by Briançon *et al.* (1990) best-fit values for the energies of transitions in ^{223}Ra are presented. The energies were obtained from the high-precision internal conversion electron spectra of an earlier study (Briançon and Vieu 1971). The error associated with any resolved transition is quoted as lying between 10 and 60 eV, depending on the transition intensity. In the light of these high-precision measurements all of the energies quoted in this work were

taken from the above reference.

Figure 5.5 represents a γ-ray spectrum for ^{223}Ra. It shows all γ-rays in coincidence with α-particles in the energy range 5.51–6.04 MeV. This range includes α energies corresponding to transitions in ^{219}Rn, consequently ^{219}Rn γ-rays and Rn x-rays can also be seen in this spectrum. Table 5.1 shows the measured intensities of ^{223}Ra γ-rays obtained from this spectrum. The intensities have been normalised so that the 236.0 keV ground state transition has an intensity of 1000.

It was not possible to make a direct measurement of the intensities of the 93.9 and 94.9 keV γ-rays because of the large contribution from Rn $K_{\beta 3}$ and $K_{\beta 1}$ x-rays (94.24 and 94.87 keV). Instead, the expected intensity of these x-rays were calculated from the measured intensity of the 84.09 keV Rn $K_{\alpha 1}$ x-ray with the difference being taken to be due to the ^{223}Ra γ-rays. This problem did not arise when measuring the α-γ distributions of these γ-rays since in each case the window on the α-particle energy excluded the Rn K x-rays (ie. the difference in energy of the α-particles corresponding to these transitions and the α-particles corresponding to the nearest transitions that produce Rn K x-rays is at least 120 keV). The intensity of the 100.3 keV γ-ray was calculated in a similar manner: the expected intensity of the $K_{\beta 3}$ and $K_{\beta 1}$ Ra x-rays (99.43 and 100.13 keV) were calculated from the measured intensity of the $K_{\alpha 1}$ Ra x-ray (88.47 keV).

Table 5.2 shows the α-branching ratios to the levels in ^{223}Ra. The total α-decay strength observed in the ^{227}Th chain was obtained by measuring the intensity of the 271.2 keV ground state transition in ^{215}Po. The multipole assignment and mixing ratio for this transition together with the α-branching ratio to the 271.2 keV level was taken from the work of Davidson and Connor (1970).

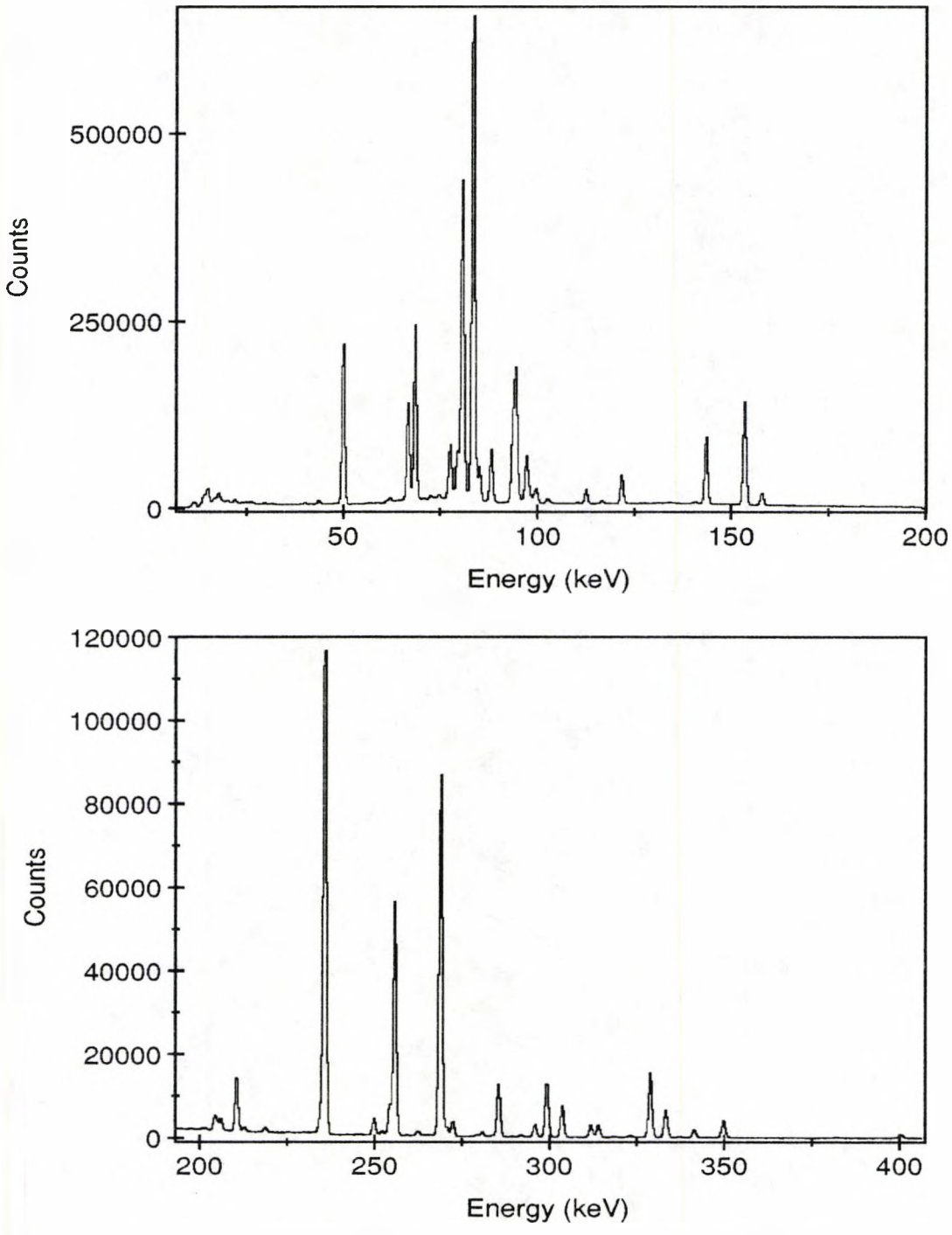

Figure 5.5: Spectrum of all γ-rays in coincidence with α-particles in the energy range 5.51–6.04 MeV.

E_γ(keV)	I_γ	I_γ^{NDS}	E_γ(keV)	I_γ	I_γ^{NDS}
20.3	16.1(14)	18(5)	212.6	6.0(5)	6.3(13)
29.6 29.9	8.4(7)	9(3)	218.8 219.0	8.4(8)	8.9(14)
31.6	7.8(7)	7.1(18)	234.8	37(4)	40(4)
43.7	19.1(17)	21(3)	**236.0**	**1000**	**1000**
49.9 50.1	760(60)	780(50)	250.1 250.4	45(4)	45(8)
61.4	6.8(7)	7.1(18)	252.5	8.6(7)	9.8(18)
62.3 62.5	20.4(17)	22(3)	254.7	65(6)	71(10)
64.4	2.9(2)	2.5(9)	256.3	530(50)	610(50)
72.7	2.28(19)	2.5(5)	262.8	8.6(8)	8.9(10)
73.7	2.0(2)	1.7(3)	272.9	38(4)	44(5)
79.7	170(20)	188(13)	279.7	5.2(7)	6.3(18)
93.9 94.9	140(60)	126(13)	281.3	13.4(14)	14.3(11)
100.3	16(7)	7.7(9)	284.3	4.1(4)	4.5(18)
113.1 113.2	61(5)	66(5)	286.1	140(12)	141(4)
117.2	13.7(12)	15.2(12)	292.4	6.2(7)	5.4(9)
134.5	2.0(2)	2.4(3)	296.5	39(4)	38(3)
140.9 141.5	12.6(10)	14.5(12)	300.0 300.4	196(15)	200(20)
168.1	1.38(14)	1.25(19)	304.5	96(10)	94(13)
173.4	1.32(13)	1.2(3)	312.7	47(6)	43(5)
184.7	3.1(3)	2.9(4)	314.8	45(5)	41(5)
201.7	2.3(3)	1.8(4)	319.2	2.5(3)	2.0(3)
204.2	21(2)	21(3)	329.9	240(20)	246(19)
205.0	11.2(11)	13(3)	334.4	102(11)	89(10)
206.1	22(2)	21(2)	342.5	30(3)	31(4)
210.6	99(8)	101(9)	350.5	12.2(15)	9.8(10)

Table 5.1: Relative γ-ray intensities for transitions in ^{223}Ra. The values obtained in this work are compared to those given in Nuclear Data Sheets (NDS).

E_{level}(keV)	I_α(%)	I_α^{NDS}(%)
0	25(3)	24.5(10)
29.9	2.8(7)	2.90(15)
50.1	—	0.002(13)
61.4	23.3(17)	23.4(10)
79.7	2.9(3)	3.00(15)
123.8	0.81(8)	0.78(3)
130.2	0.15(2)	0.174(8)
174.6	2.1(2)	2.42(10)
234.8	1.23(14)	1.27(2)
247.4	0.33(4)	0.311(5)
280.2	0.24(3)	0.228(10)
286.1	20.6(15)	20.3(10)
315.5	—	0.034(3)
329.9	5.5(5)	4.9(2)
334.4	7.8(8)	8.2(3)
342.6	3.6(3)	3.6(2)
350.5	1.59(18)	1.50(10)
369.3	0.067(11)	0.057(4)
376.3	2.07(17)	2.06(12)

Table 5.2: Experimental α intensities compared to the values given in Nuclear Data Sheets—see text for details.

The easiest way of obtaining the α intensities was to gate on the α-group populating a level and measure the intensity of each of the depopulating γ-rays. These intensities were then corrected for Ge detector efficiency and internal conversion and the results summed to give the α-branch to that level.

In the case of overlapping α peaks corresponding to unresolved γ-rays, the converse of the above procedure was used. Take for example the 250.1 and 250.4 keV transitions, it was not possible to resolve these two γ-rays and the energies of the corresponding α-particles differed by only 50 keV. If we were to gate on one of the α-groups then, even with an α resolution of 25 keV (FWHM), it would not be possible to prevent α-particles from the other group causing a contribution to the γ-peak at 250 keV. On the other hand however, it is a relatively simple matter to gate on the γ-ray at 250 keV and measure the intensity of both α-groups with the aid of a peak-fitting routine (ie. see figure 5.6).

Care must be taken when using this method however, if there are transitions connecting the two levels. Since the lifetimes of the levels are shorter than the coincidence resolving time of the signal processing circuits it is possible to record a coincidence between an α-particle populating the higher level and a γ-ray depopulating the lower level if the intermediate γ-ray is not detected. This is more likely if the connecting transition is highly converted and will result in an excess in the measured α intensity of the higher energy group.

A further problem is posed by highly converted transitions: if the γ-ray intensity is too low to be measured, but the total intensity is significant then this will result in missing 'depopulating' intensity and hence a reduced α-branch.

In cases where any of the above problems are expected to occur the measurements of the suspect transitions were not included in the determination

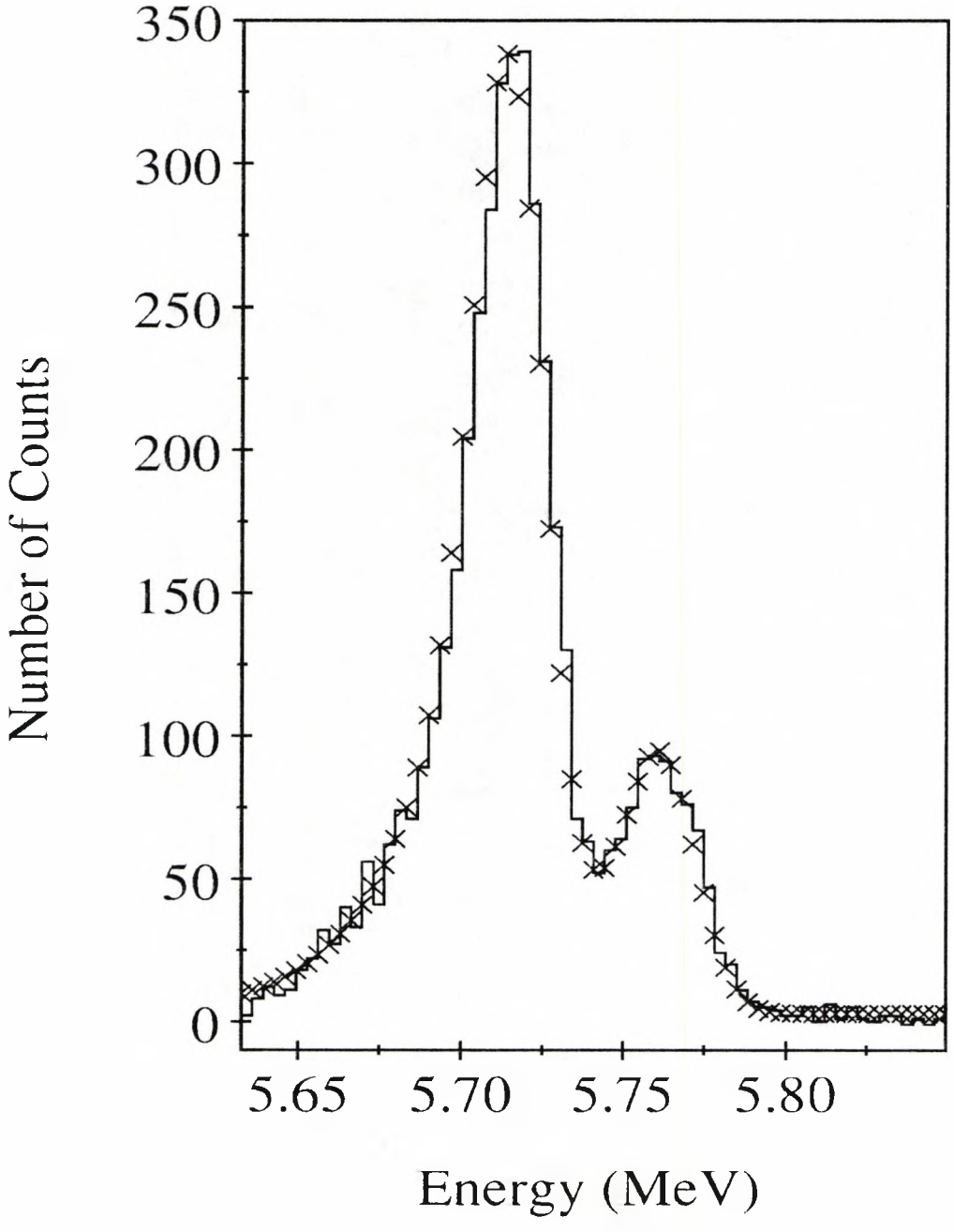

Figure 5.6: Spectrum of α-particles in coincidence with the 250 keV γ-ray. The crosses show the result of a peak fitting routine. The two peaks correspond to the α-groups populating the 329.9 and 280.2 keV levels in ^{223}Ra.

of the α-branching ratios. Instead, the values for the intensities of these γ-transitions given in Nuclear Data Sheets (Maples 1977) were used, after normalising to the measured intensities of transitions from the same level (to ensure that the intensity corresponded to that part due to population via α-decay). In this sense the figures in table 5.2 do not represent totally independent measurements. However, since these values are well known this was not considered to be a problem and their measurement here merely serves as an indication that there are no serious flaws in our experimental technique.

5.3.2 Alpha-Gamma Angular Correlations

The ground state spin of ^{225}Ra (the isotone of ^{227}Th) has been measured by Ahmad *et al.* (1983) to be 1/2 which along with theoretical calculations (Leander and Chen 1988) suggests a spin of 1/2 for the ground state ^{227}Th. Clearly a definitive measurement of the ground state spin of ^{227}Th would be welcome, but if we follow Jain *et al.* (1990) and assume that the ground state I^{π} of ^{227}Th is $1/2^{+}$ with a ground state I^{π} for ^{223}Ra of $3/2^{+}$ then the α-γ correlation analysis becomes particularly simple: there will be no mixing of α-particle angular momenta. That is, conservation of angular momentum and parity implies that α transitions to states in the daughter nucleus can only proceed by a single pure even L transition to positive parity states and by a single pure odd L transition to negative parity states—see section 3.4.

The standard procedure in the analysis of angular correlation data is to first normalise the coincidence data to the singles rate in order to remove any angle dependent efficiency. The coincidence intensity of each transition is then plotted as a function of $\cos^2\theta$. A Legendre polynomial is then fitted to the data, using a computer code, resulting in experimental values for the

angular distribution coefficients A_0, A_2 and A_4. These can then be compared to the theoretical values obtained for a given spin hypothesis. The sum of the squares of the residuals (S^2) between the Legendre polynomial with the theoretical coefficients and the actual data points is then computed. In the case of mixed multipoles the program also gives the value of δ_γ that allows the best fit to the experimental data.

The number of experimental degrees of freedom (ν) together with S^2 is taken as a measure of the agreement between experiment and theory. For example, with set-up I we have five data points, for a transition of pure multipolarity and a fully aligned intermediate state the only variable parameter is A_0. In this case $\nu = 5 - 1 = 4$. Consulting table C-4 in Bevington (1969) we see that for a value of $S^2 \geq 13.28$ the given spin hypothesis can be rejected at the 99% confidence level. Similarly, for an E2/M1 mixture with δ_γ unknown then $\nu = 3$ and $S^2 \geq 11.34$ would again imply rejection at the 99% confidence level.

In this work the Legendre polynomial fits were performed by the computer code STAG (Butler 1974). The program was not specifically designed for use with α-γ angular correlation data, however it can be used to fit the angular distribution of γ-rays emitted from aligned (eg. see Litherland and Ferguson, 1961) states formed by nuclear reactions. The amount of alignment is included in the calculation either as a fixed value or as a free parameter that is varied during the fitting procedure. Since we are assuming a parent spin of 1/2 we can expect the alignment of the intermediate state to be high[1] and we can initially fix the alignment parameters to 1. The program can then be used to

[1]Since an α-particle is spinless it can have no component of angular momentum in its direction of travel (ie. $\vec{\ell} = \vec{r} \times \vec{p} \Rightarrow \vec{\ell} \cdot \vec{p} = 0$); if this direction is taken as the z-axis then $m_i = m_f$ and only the $\pm 1/2$ magnetic substates of the daughter nucleus will be populated.

fit the measured distribution for the spin sequence $I \xrightarrow{\gamma} I_f$, where one of (I, I_f) is known. The program uses a non-linear least squares fitting procedure on each hypothesis in turn. In the case of an E2/M1 multipole mixture the value of δ_γ is allowed to vary over a specified range and an iterative procedure is carried out leading to the identification of any local minima in S^2. It should be noted that the sign of δ_γ obtained from our angular correlation measurements may be opposite to those obtained from some γ-γ angular distribution analyses (Yamazaki 1967). To avoid any confusion the phase consistent sign convention of Rose and Brink (1967) is adhered to in this work.

Since δ_γ can have any value between $\pm\infty$ it is easer to deal with the quantity $\arctan(\delta_\gamma)$. This takes on values between $\pm 90°$ and allows the results to expressed graphically in a S^2 vs $\arctan(\delta_\gamma)$ plot. This method is demonstrated by fitting the α-γ angular correlation data for the 61.4 keV ground state transition. The multipolarity of this transition is known to be E2, which along with a ground state of $3/2^+$ restricts the I^π of the 61.4 keV level to $7/2^+$, nevertheless for illustrative purposes the data were fitted for the four hypotheses: 1/2, 3/2, 5/2 and 7/2 for the 61.4 keV level. For two of these values $\arctan(\delta_\gamma)$ was varied over the range $\pm 85°$. The top half of figure 5.7 shows S^2 plotted as a function of $\arctan(\delta_\gamma)$ while the bottom half shows the Legendre polynomial fits to the experimental data. The fits for the 3/2 and 5/2 spins represent the best fit with $\arctan(\delta_\gamma) = -74°$ and $-24°$ respectively.

In the analysis of the angular correlation data the fits were all carried out twice. Initially the alignment parameters were all fixed to 1 (ie no dealignment). In each case this resulted in a single favoured spin hypothesis (the other possibilities being rejected at the 99% confidence level). The fits were then performed again, this time the alignment parameters for the previously rejected possibilities were allowed to vary between 0.8 and 1.0 (ie up to 20%

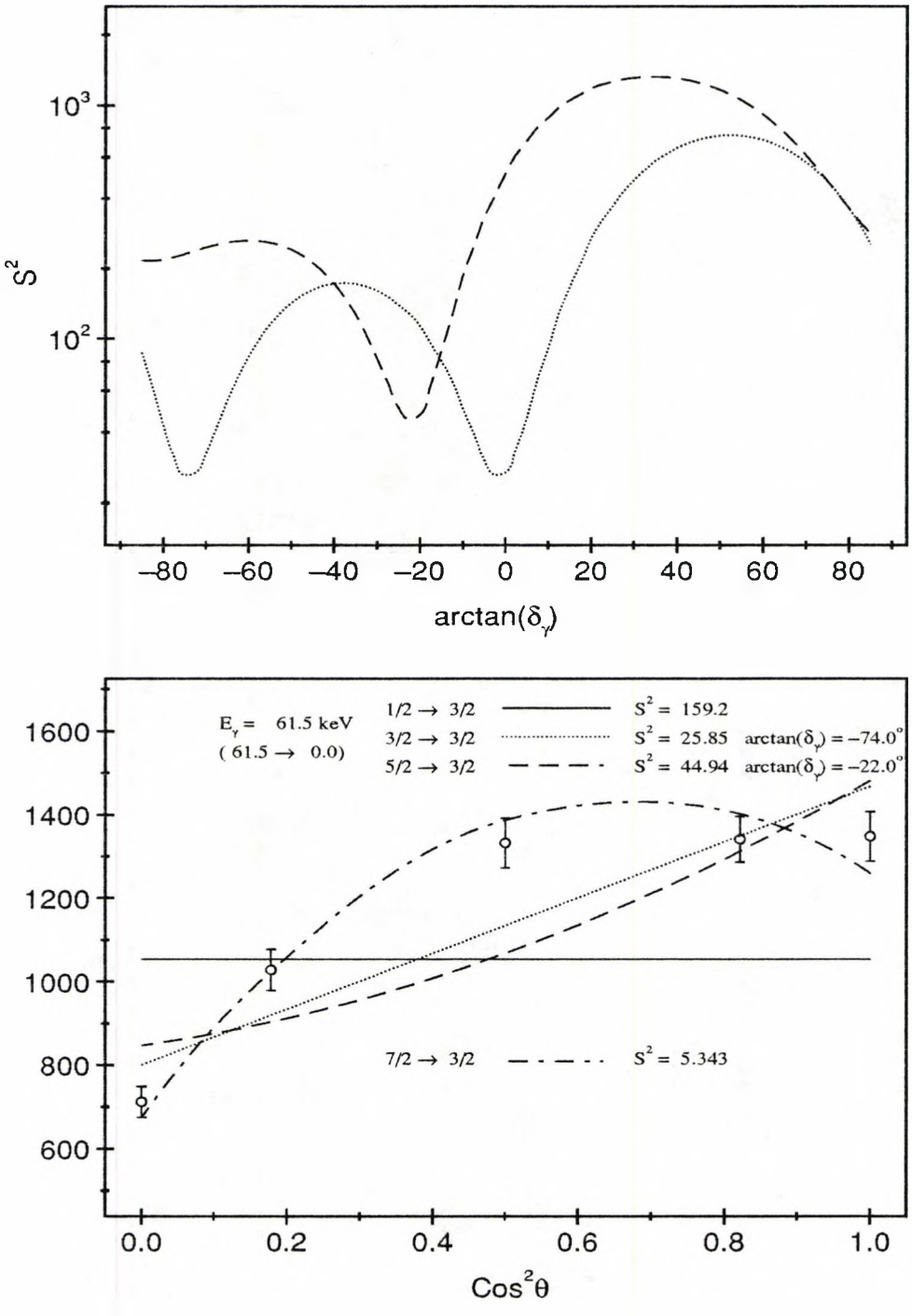

Figure 5.7: Top: S^2 vs arctan(δ_γ) plot for the 61.4 keV ground state transition. The dotted and dashed curves represent the spin sequences $1/2 \xrightarrow{\alpha} 3/2 \xrightarrow{\gamma} 3/2$ and $1/2 \xrightarrow{\alpha} 5/2 \xrightarrow{\gamma} 3/2$ respectively. Bottom: Theoretical fits for the indicated spin sequences ($1/2 \xrightarrow{\alpha} I \xrightarrow{\gamma} I_f$) and multipole mixing ratios.

$$\frac{1}{2}^{+} \xrightarrow{\alpha} I^{\pi} \xrightarrow{\gamma} \frac{3}{2}^{+}$$

E_{level}	multipolarity	I^{π}	a_2	a_4
61.4	E2	$7/2^{+}$	+0.47(4)	-0.26(5)
79.7	E1	$5/2^{-}$	-0.41(3)	-
234.8	M1	$5/2^{+}$	-0.33(5)	-
329.9	E1	$3/2^{-}$	+0.32(4)	-
334.4	E2/M1	$5/2^{+}$	+0.68(5)	+0.18(6)
342.5	E2/M1	$3/2^{+}$	-0.57(4)	+0.03(4)
350.5	E1	$1/2^{-}$	+0.07(3)	-

Table 5.3: I^{π} assignments and experimental correlation coefficients arising from ground state transitions in ^{223}Ra.

dealignment). Although in many cases the S^2 values for the rejected possibilities improved, in no case did it decrease enough to necessitate reconsideration.

Using ground state I^{π} values of $1/2^{+}$ and $3/2^{+}$ for ^{227}Th and ^{223}Ra respectively, and using the multipolarity assignments and mixing ratios of Briançon and Vieu (1971), then the α-γ angular correlation data of this work can be used to assign definite I^{π} values to twenty levels in ^{223}Ra. With exception of the level at 315.5 keV this accounts for all of the levels up to 376.3 keV in energy. Tables 5.3 and 5.4 show the I^{π} assignments along with the experimental a_2 and a_4 coefficients. A selection of the theoretical fits to the experimental data are shown on pages 110 to 114. For the 334.4 and 342.5 keV E2/M1 transitions S^2 vs arctan(δ_γ) plots are also shown. The horizontal error bars on these plots mark the 99% confidence level and the relevant[2] value of arctan(δ_γ) $\pm 2\sigma$ taken

[2]Of course, internal conversion measurements only yield $\mid \delta_\gamma \mid$ the sign is determined from the S^2 vs arctan(δ_γ) plots.

$$\frac{1}{2}^{+} \xrightarrow{\alpha} I^{\pi} \xrightarrow{\gamma} I_f^{\pi}$$

E_{level}	I^{π}_{level}	$E \xrightarrow[multipolarity]{E\gamma} E_f$			a_2	a_4
29.9	$5/2^+$	123.8	$\xrightarrow[E1]{93.9}$	29.9	−0.33(3)	–
		234.8	$\xrightarrow[E1]{205.0}$	29.9	+0.42(5)	–
50.1	$3/2^-$	234.8	$\xrightarrow[E1]{184.7}$	50.1	−0.47(6)	–
		342.5	$\xrightarrow[E1]{292.4}$	50.1	+0.48(8)	–
123.8	$7/2^-$	123.8	$\xrightarrow[E1]{62.3}$	61.4	+0.39(11)	–
		329.9	$\xrightarrow[E2]{206.1}$	123.8	+0.11(4)	+0.09(5)
		334.4	$\xrightarrow[E1]{210.6}$	123.8	−0.10(3)	–
130.2	$9/2^+$	334.4	$\xrightarrow[E2]{204.2}$	130.2	+0.24(4)	+0.01(4)
		130.2	$\xrightarrow[E2]{100.3}$	29.9	+0.48(11)	−0.14(12)
174.58	$9/2^-$	174.58	$\xrightarrow[E2]{94.9}$	79.7	+0.38(5)	−0.26(5)
174.62	$11/2^+$	247.4	$\xrightarrow[E1]{72.7}$	174.62	+0.37(9)	–
247.4	$11/2^-$	247.4	$\xrightarrow[E1]{117.2}$	130.2	−0.34(7)	–
280.2	$7/2^+$	280.2	$\xrightarrow[M1]{250.4}$	29.9	−0.37(3)	–
286.1	$1/2^+$	286.1	$\xrightarrow[E1]{236.0}$	50.1	0.00(3)	–
		286.1	$\xrightarrow[E2]{256.3}$	29.9	+0.02(4)	+0.02(55)
342.8	$9/2^+$	342.8	$\xrightarrow[E2/M1]{212.6}$	130.2	+0.65(10)	−0.20(10)
		342.8	$\xrightarrow[E2/M1]{281.3}$	61.4	−0.48(8)	+0.10(8)
369.3	$5/2^-$	369.3	$\xrightarrow[E1]{134.5}$	234.8	+0.34(7)	–
		369.3	$\xrightarrow[M1+(E2)]{319.2}$	50.1	−0.30(8)	−0.09(10)
376.3	$7/2^-$	376.3	$\xrightarrow[E1]{141.5}$	234.8	−0.35(3)	–
		376.3	$\xrightarrow[E1]{314.8}$	61.4	+0.50(4)	–
		376.3	$\xrightarrow[E2/M1]{296.5}$	79.7	+0.08(7)	−0.02(8)

Table 5.4: I^{π} assignments and experimental correlation coefficients arising from non-ground state transitions in ^{223}Ra.

from the internal conversion measurements of Briançon *et al.* (1990). The fits to the data from the 281.3 keV transition (342.8 → 61.4) were obtained using $\delta_\gamma > 0$, there is an equally acceptable fit for the hypothesis $5/2 \xrightarrow{\gamma} 7/2$ with $\delta_\gamma < 0$. However, the presence of a dipole component in the 212.6 keV transition between the 342.8 and 130.2 keV levels and an assignment of $9/2^+$ to the 130.2 keV level means that the 342.8 keV level cannot have a spin of $5/2$.

5.3.3 Alpha-Electron Angular Correlations

In order for the α-e correlation data to be useful the transitions involved must be both converted enough so that the electron intensities can be measured and have large enough particle parameters so that their distributions are not isotropic. In the case of E1 transitions although the b_k coefficients are relatively large their conversion will be small. On the other hand, low energy transitions with a large M1 component will be highly converted but will have small b_k coefficients. Thus, the most suitable candidates are low energy transitions that have a large E2 component.

The restrictions imposed by the above criteria limit the usefulness of the α-e correlation data for this particular nucleus. However, the technique can be illustrated by measuring the L conversion and the M conversion of the 113.2 keV transition. Figure 5.8 shows a spectrum of electrons in coincidence with the α group populating the 174.62 keV level. The transition is actually a doublet consisting of an E2 (174.62 → 61.4) and an E1 (174.58 → 61.4) component, however we can expect the electron contribution from the E1 component to be small. Figure 5.9 shows the results of the fits to the four point α-e coincidence data. The fits were performed using the computer code BINPOL (Jones 1990) assuming a parent I^π of $1/2^+$ and a fully aligned intermediate

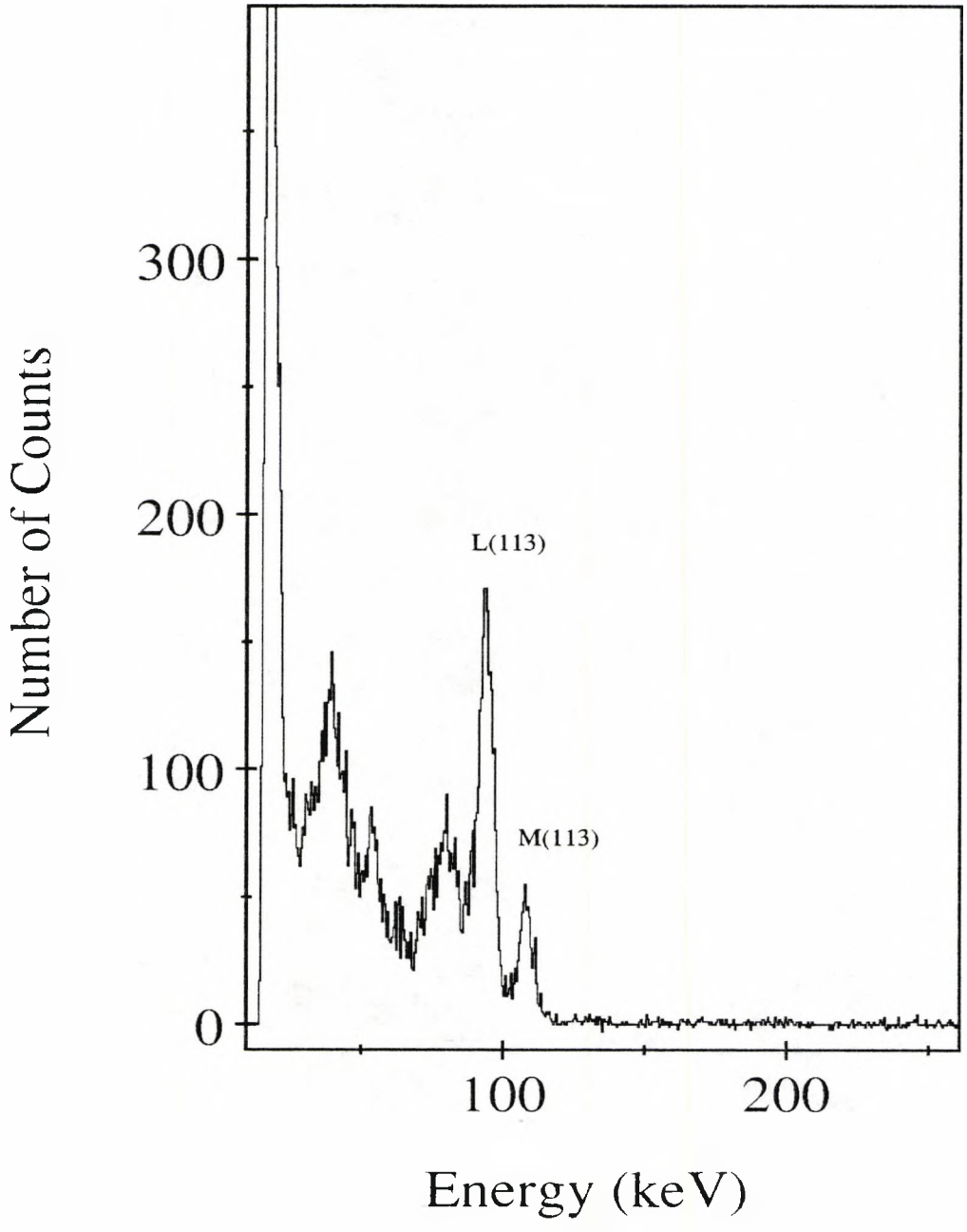

Figure 5.8: Spectrum of internal conversion electrons in coincidence with α-particles in the energy range 5.85 to 5.90 MeV.

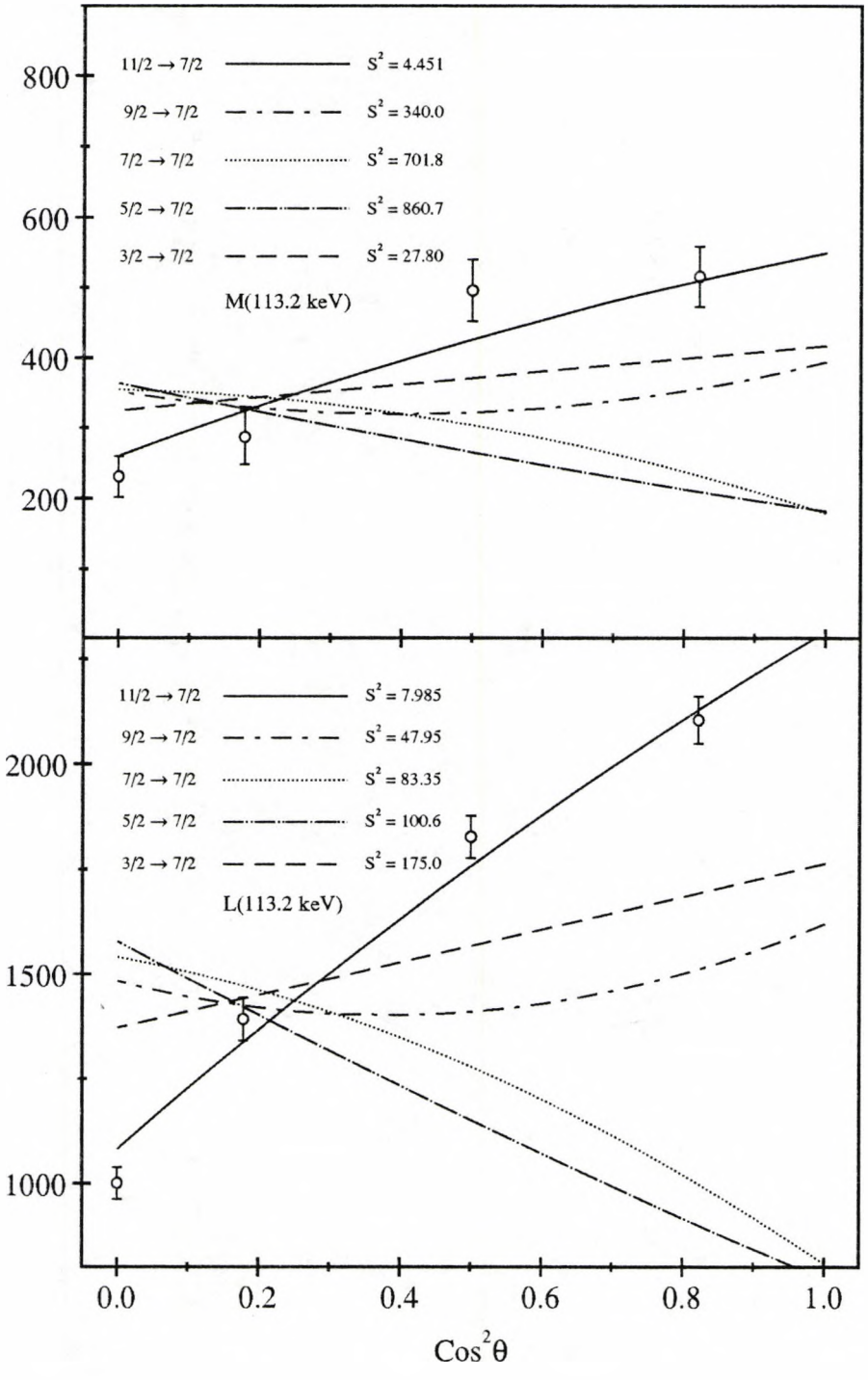

Figure 5.9: Theoretical fits to the four point α-e angular correlation data for L and M conversion of the 113.2 keV (174.62 → 61.4) E2 transition.

state. As can be seen from figure 5.9 the best fit in both cases corresponds to the sequence $11/2 \rightarrow 7/2$, this agrees with the assignment of $11/2$ to the 174.62 keV level obtained from the α-γ angular correlation data.

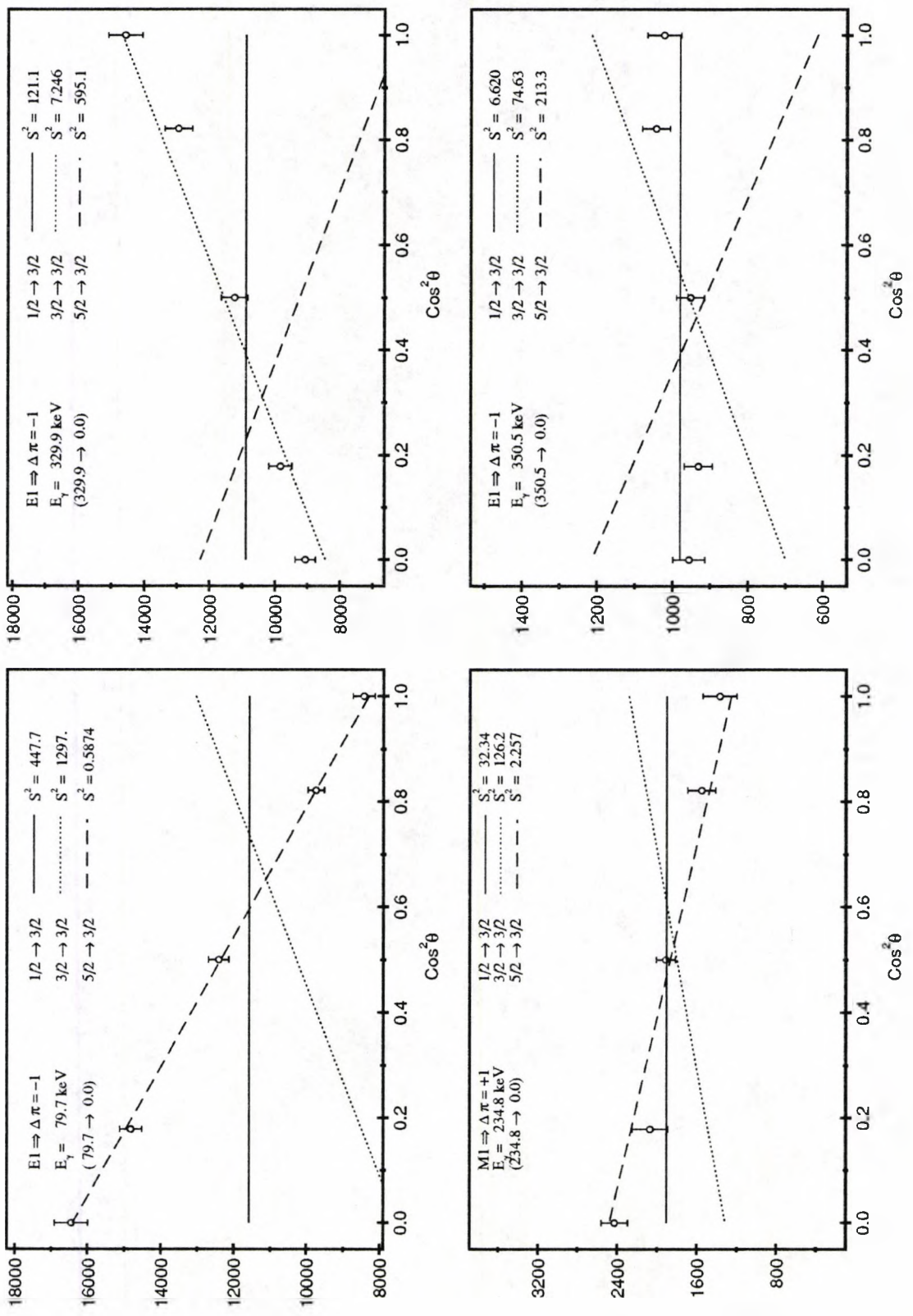

Figure 5.10: Legendre polynomial fits for the 79.7, 234.8, 329.9 and 350.1 keV ground state transitions in ^{223}Ra.

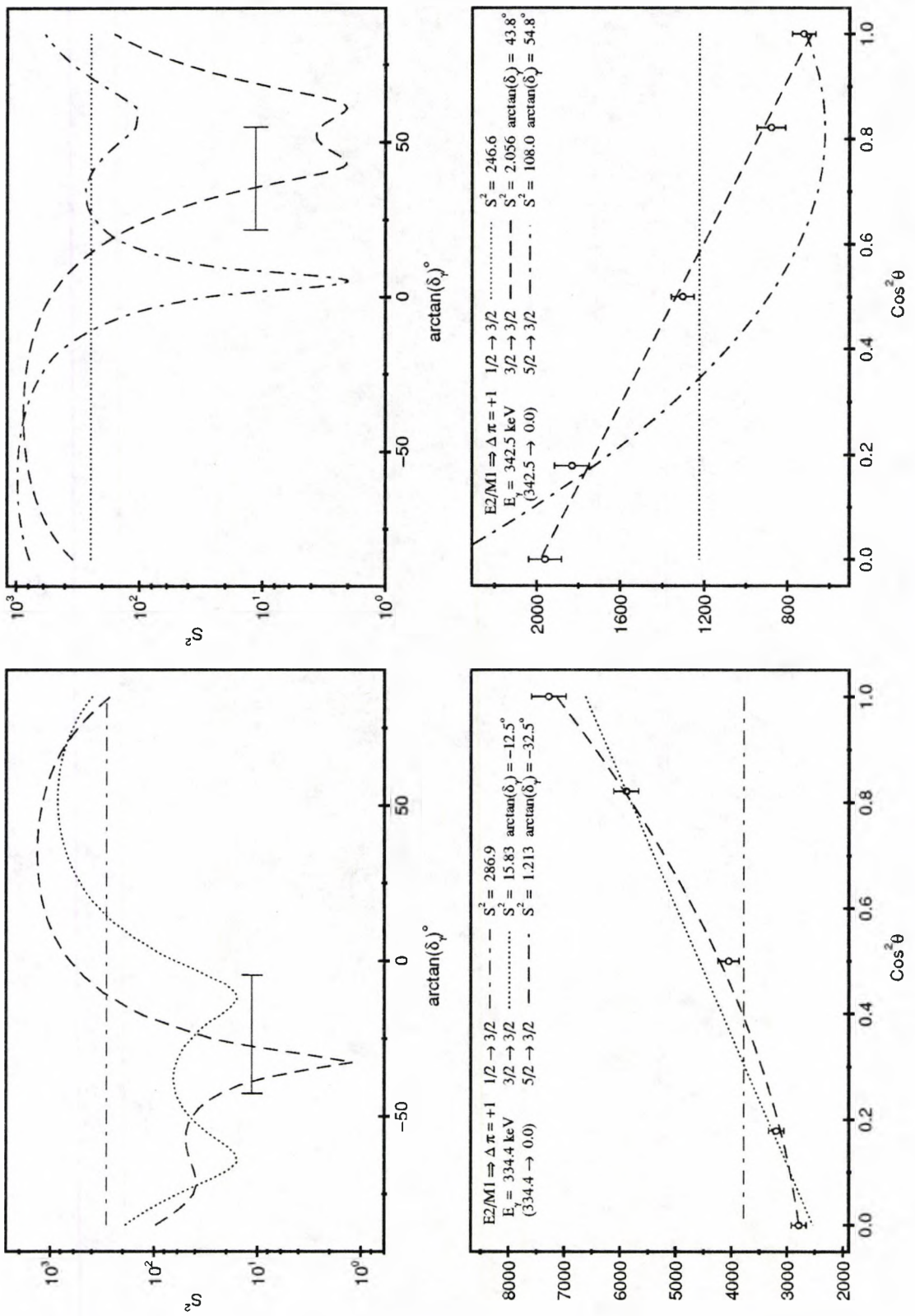

Figure 5.11: Legendre polynomial fits and S^2 vs $\arctan(\delta_\gamma)$ plots for the 334.4 and 342.5 keV ground state transitions in ^{223}Ra.

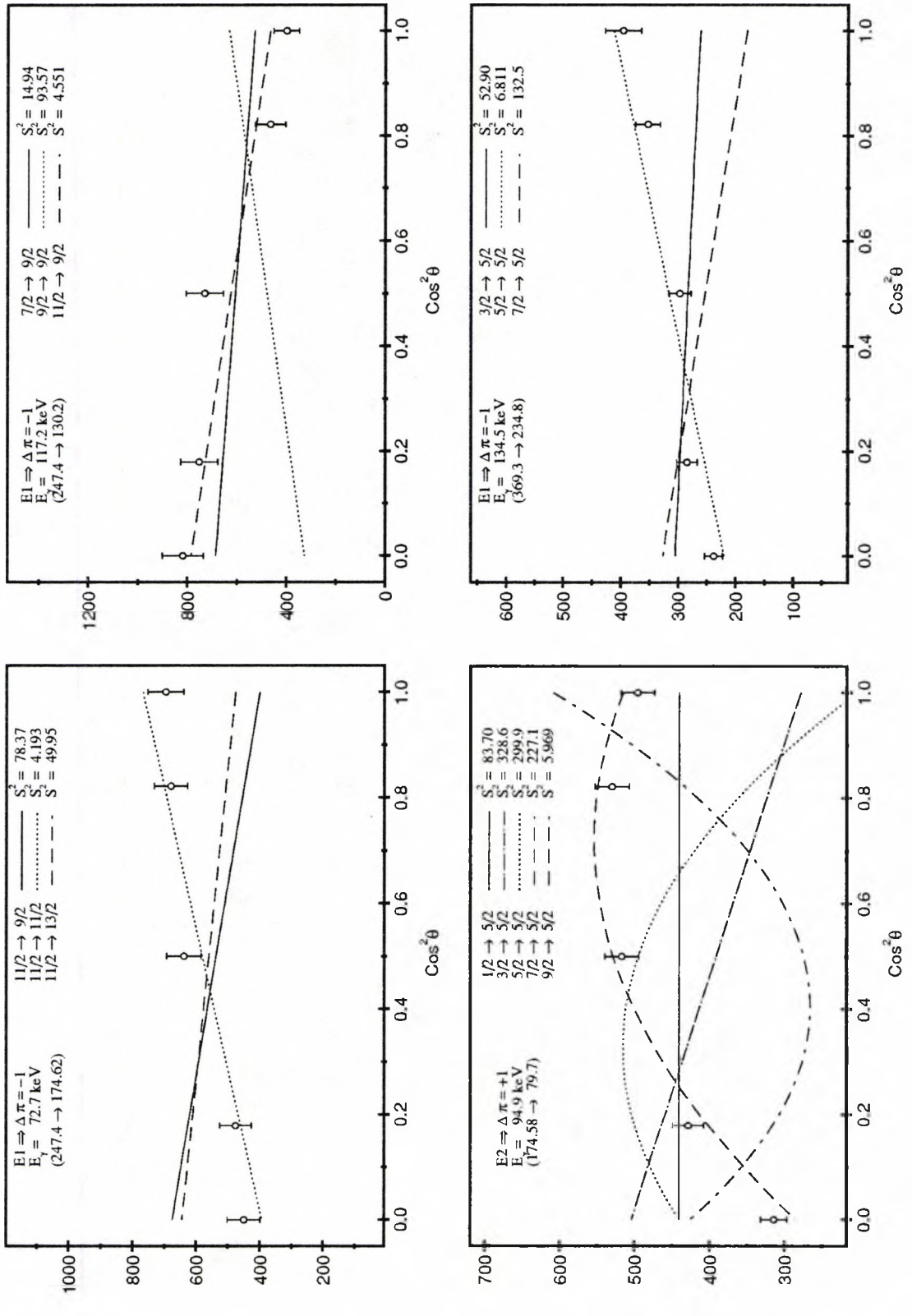

Figure 5.12: Legendre polynomial fits for the 72.7, 94.9, 117.2 and 134.5 keV transitions in ^{223}Ra.

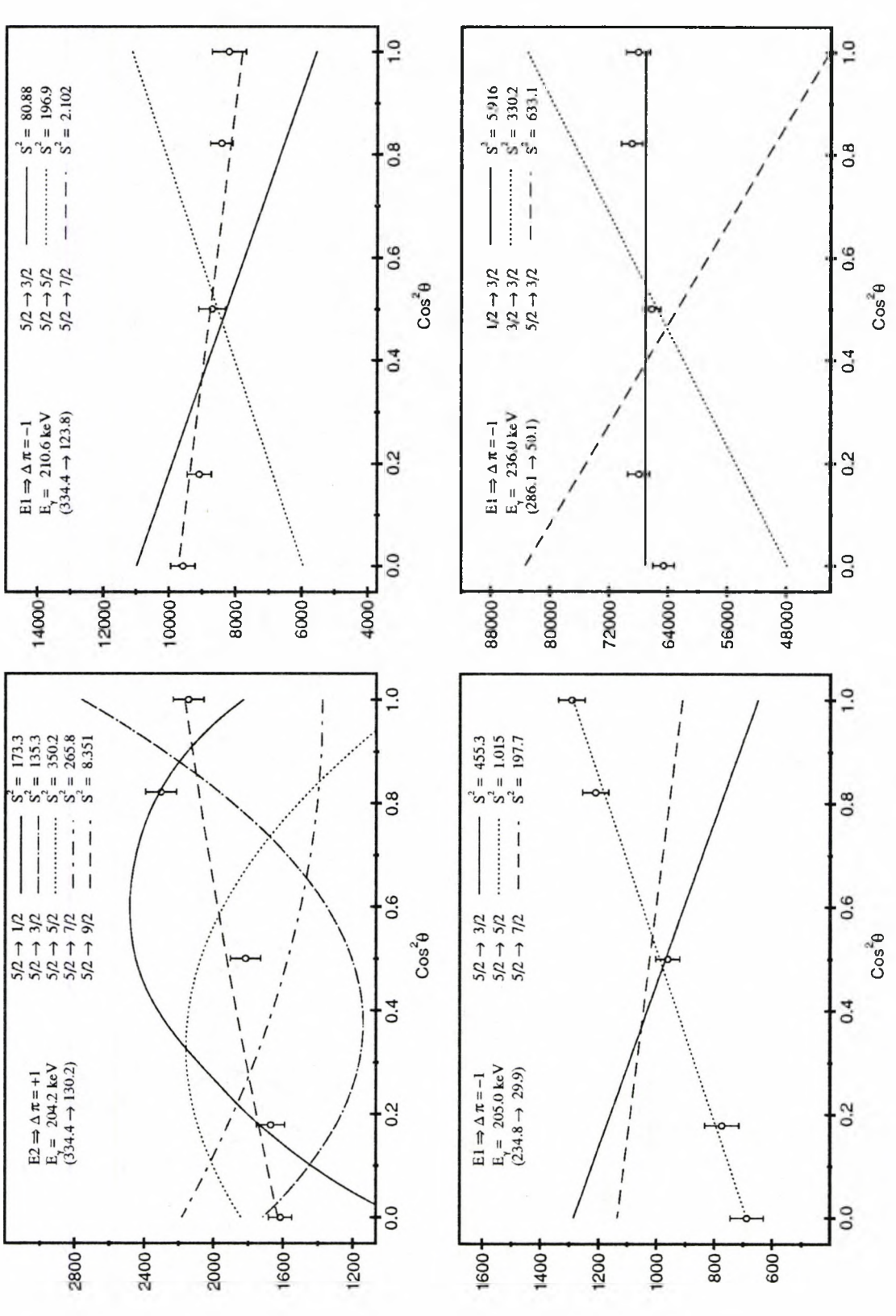

Figure 5.13: Legendre polynomial fits for the 204.2, 205.0, 210.6 and 236.0 keV transitions in ^{223}Ra.

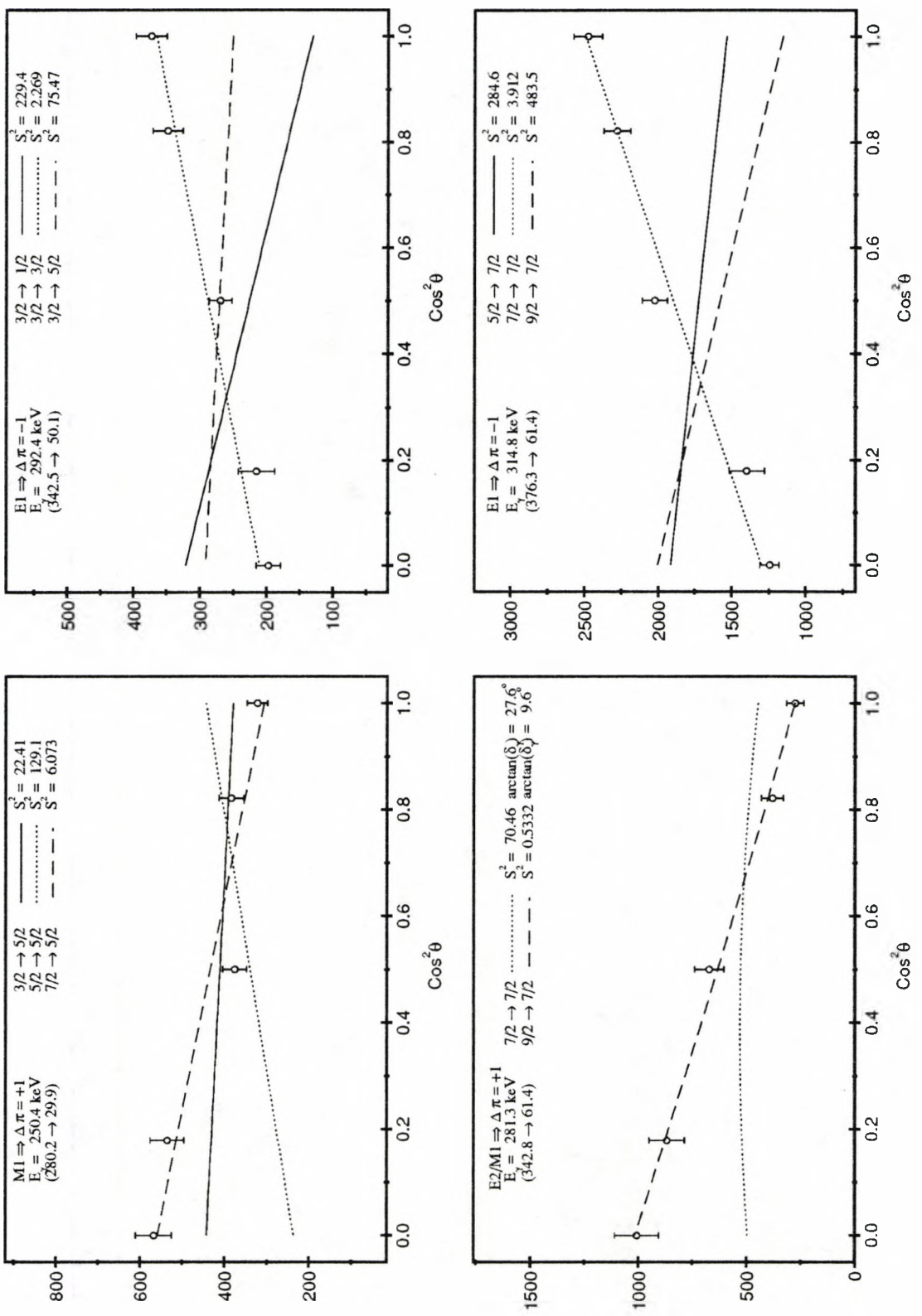

Figure 5.14: Legendre polynomial fits for the 250.4, 281.3, 292.4 and 314.8 keV transitions in ^{223}Ra.

Chapter 6

Discussion

6.1 The ^{223}Th Experiment.

The level in ^{223}Th which has the strongest population by α-decay is the 247 keV level which decays via an M1 transition to the ground state. An α hindrance factor, to an excited state in a daughter nucleus, of less than 4 is usually taken as strong evidence that the excited state has the same I^{π} as the ground state of the parent nucleus. Clearly the hindrance factors calculated in this work may be prone to rather large systematic errors (due to uncertainties in half-lives and branching ratios in neighbouring even-even nuclei, as well as uncertainties in ground state α-decay strength in this nucleus) but the relative hindrance factors are somewhat more reliable. Therefore a value of $I^{\pi} = 3/2^{+}$ is tentatively assigned to the 247 keV level in ^{223}Th as it is the level which is most favoured (lowest hindrance factor) by the α-decay of ^{227}U, for which a ground state $I^{\pi} = 3/2^{+}$ is expected—e.g. figure 4, Leander and Chen (1988).

The N = 133 isotones ^{219}Rn, ^{221}Ra and ^{223}Th are believed to have similar structure and have been treated in the same theoretical framework of octupole deformation by Leander and Chen (1988) where a β_3 deformation of $\sim$0.1 was

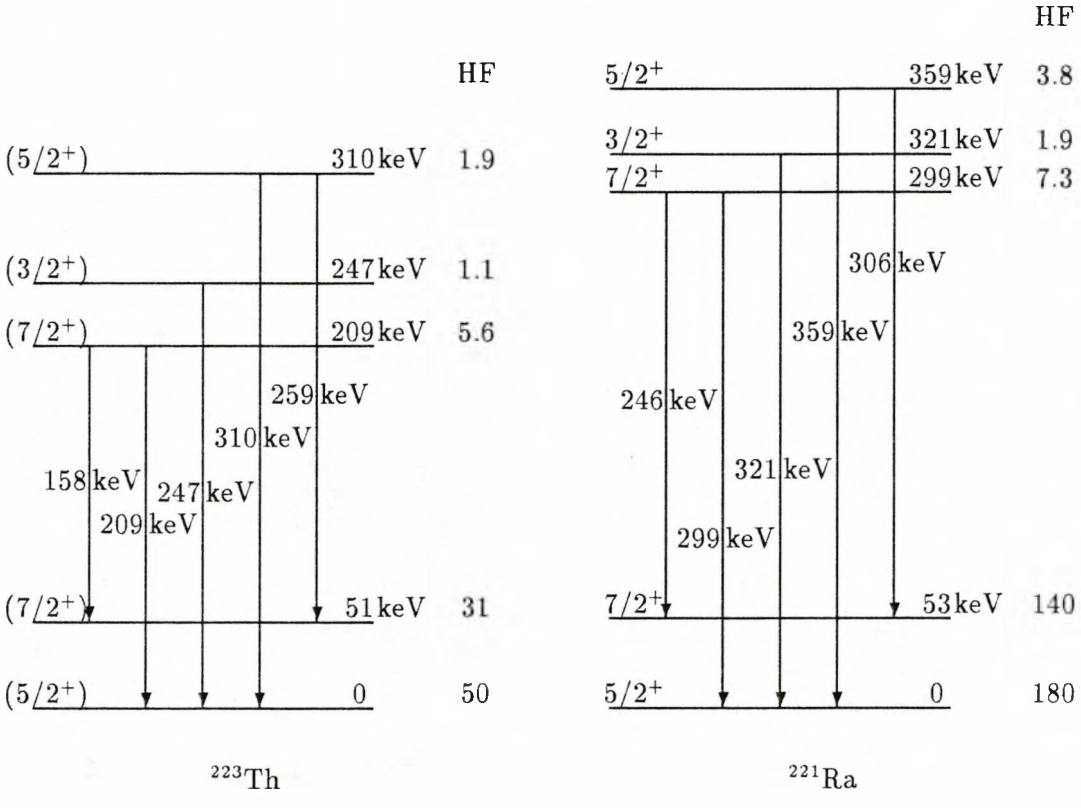

Figure 6.1: Partial level scheme of ^{221}Ra (Ackermann *et al.* 1989) shown for comparison with ^{223}Th.

required to satisfactorily fit the experimental data for ^{219}Rn. Both ^{219}Rn (Maples 1977) and ^{221}Ra (Ackermann *et al.* 1989) have strikingly similar level schemes and structures for those states populated following α-decay. Several of the more strongly excited states have low hindrance and they largely decay by M1 transitions to the ground state and lower excited states.

Figure 6.1 shows a partial level scheme of ^{221}Ra (Ackermann *et al.* 1989) for comparison with ^{223}Th. The relative energy spacings and the relative hindrance factors of the 209 keV (HF = 5.6), 247 keV (HF = 1.1) and 310 keV (HF = 1.9) observed in ^{223}Th bear a remarkable resemblance to the 299.2 keV (HF = 7.3), 321.4 keV (HF = 1.9) and 359.1 keV (HF = 3.8) states observed

in ^{221}Ra and they all decay by M1 transitions to the ground state and first excited state. The 299.2 keV and 359.1 keV states in ^{221}Ra have been assigned $7/2^+$ and $5/2^+$ by Ackermann *et al.* (1989); therefore the same spin parity values can be tentatively assigned to the 209 keV level and the 310 keV level in^{223}Th respectively. These states have been interpreted, both by Leander and Chen (1988) and Ćwiok and Nazarewicz (1990), as arising from two bands with $K = 1/2$ and $K = 3/2$ which lie close to each other and are strongly mixed because of coriolis coupling.

The lower hindrance factors to the ground state and the first excited state in ^{223}Th compared with the corresponding values in ^{221}Ra (Ackermann *et al.* 1989) may suggest that the $K = 3/2$ band is more strongly mixed to the $K = 5/2$ ground band in ^{223}Th than in ^{221}Ra.

6.2 The ^{223}Ra Experiment.

A recently published α-γ angular correlation study of the $^{227}\mathrm{Th} \xrightarrow{\alpha} {}^{223}\mathrm{Ra}$ decay by Briançon *et al.* (1990) indicates the same I^π assignments as found in this work but assuming $3/2^+$ for the ground state spin of the parent nucleus ^{227}Th.

That work appears to show irrefutable evidence that the ground state spin of ^{227}Th cannot be $1/2^+$ due to the observation of γ-ray anisotropies following low temperature, nuclear orientation of ^{227}Th. However, a ^{227}Th ground state assignment of $3/2^+$ raises difficulties which we find hard to reconcile.

For example, using the notation of Rose and Brink (1967) the A_k^α coefficients of chapter 3 are replaced by $B_k(I)$ *statistical tensors* that describe the population of the magnetic substates of the state I. These coefficients can be expressed in terms of *population tensors* S_k. Figure 6.2 shows $B_2(I)$ plotted as a function of $\delta_\alpha/(1+\delta_\alpha^2)$ for a parent spin of $3/2^+$. The values for $B_2(I)$

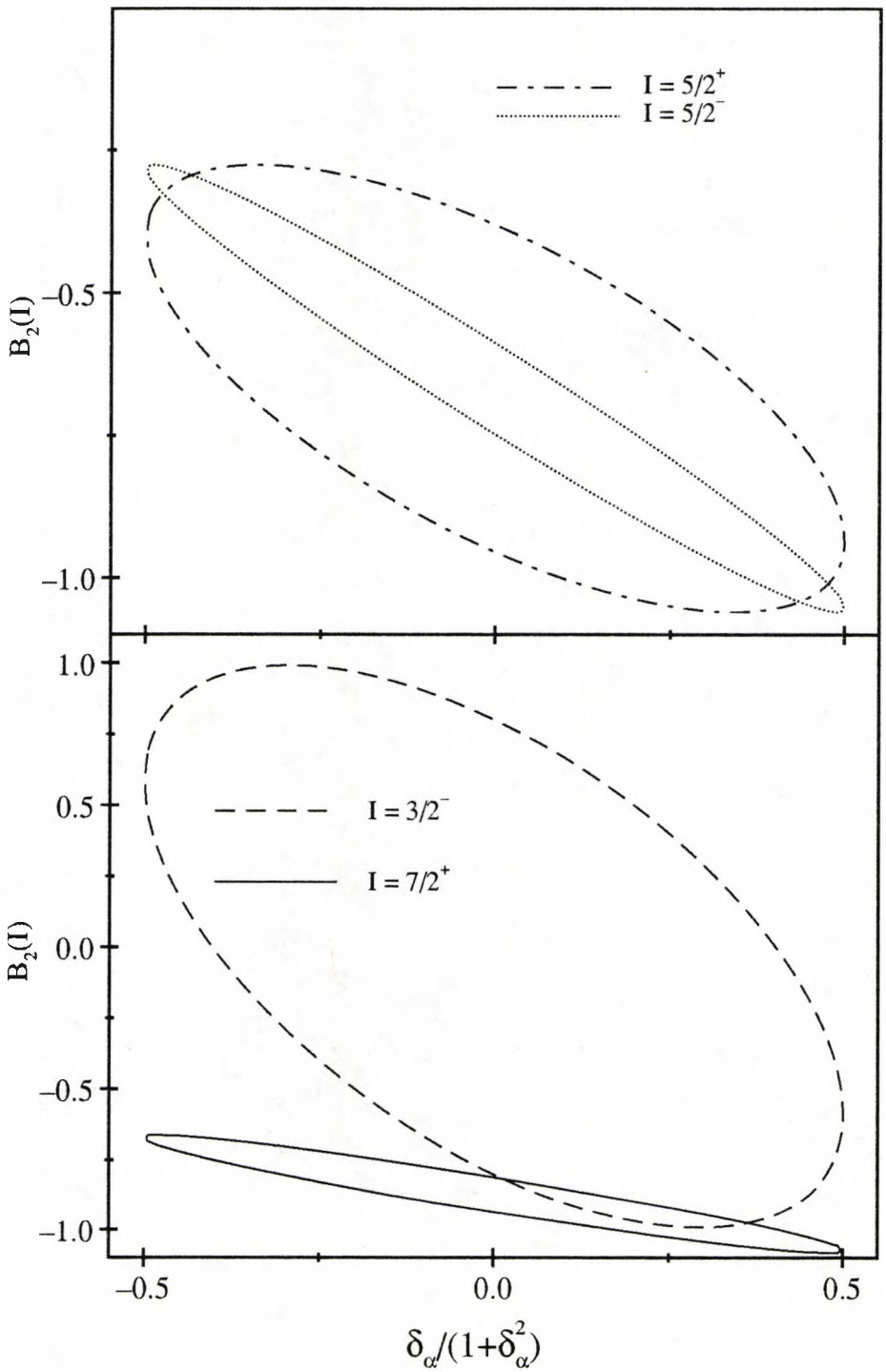

Figure 6.2: Parametric plot of $B_2(I)$ as a function of α-particle mixing ratio.

were obtained using the equations in section 1 of a recent work of Rowley[1] *et al.* (1991) and the tabulated S_k coefficients of Rose and Brink (1967). For a parent spin of $1/2^+$ the $B_2(I)$ coefficients are –1, –1.06904 and –1.09109 for the I values $3/2^{\pm}$, $5/2^{\pm}$, and $7/2^{\pm}$ respectively.

In our analysis of ^{227}Th α-decay we have found no case where α-γ angular correlation data cannot be fitted assuming a spin $1/2^+$ parent nucleus. It is clearly possible to reproduce the large alignment coefficients, $B_k(I)$, that a spin $1/2^+$ parent produces if one assumes a spin $3/2^+$ parent with the appropriate L, L+2 α-wave mixing. However it is difficult to see why α-decay from a spin $3/2^+$ parent should always have the high alignment coefficients commensurate with a spin $1/2^+$ parent nucleus.

In addition, the lowest α hindrance factor for α-decay from the ground state of ^{227}Th is 6.1 (Lederer and Shirley, 1978) to the 286.1 keV ($1/2^+$) level in ^{223}Ra. Although this hindrance factor cannot strictly be used as a strong argument that these parent and daughter states have the same I^{π} (this would require a hindrance factor < 4) it is suggestive that this is indeed the case. Therefore, if ^{227}Th does in fact have a spin $3/2^+$ ground state and the new I^{π} assignments in ^{223}Ra, obtained by Briançon *et al.* (1990), are correct it is extremely difficult to explain why none of the α transitions to $3/2^+$ states in ^{223}Ra have low hindrance factors.

We feel that an independent measurement of the ground state spin of ^{227}Th is warranted.

The two models that incorporate octupole deformation are referred to as the *static* and the *dynamic* reflection-asymmetric rotor models. In odd-A nuclei, where a nucleon is coupled to an octupole deformed core, both models

[1]The equations of this reference relate directly to α-decay, whereas those of Rose and Brink refer to α-capture.

predict a doubling of all spin states with respect to parity. The resulting pairs of bands are known as parity doublets and we can expect to observe enhanced E1 transitions between opposite parity members of the same band (see section 1.6). In the dynamic model the deformation appears in the form of an octupole vibration of a reflection-symmetric core. In this case one half of a parity doublet arises from a reflection symmetric Nilsson orbital of good parity with the opposite parity member coming from a rotational band built on a K = 0 one-phonon octupole vibration of the even-even core, with an energy splitting between the bands equal to the octupole phonon energy. In the static model the core possesses a permanent octupole deformation and the parity doublets are simply different projections of the same intrinsic state. In each of the above situations the octupole mode and a *single* Nilsson orbital are involved, so magnetic moments for parity doublets are expected to approach the same value and, in the case of α-active nuclei, the α hindrance factors to both members of a given parity doublet are expected to be of a similar magnitude, with the lower hindrance factors belonging to the bands that have the same configuration as the parent ground state (eg see Leander and Sheline, 1984). Also, for the $K^{\pi} = 1/2^{\pm}$ parity doublet bands the decoupling parameters (equation 1.14) are expected to approach the same absolute value but with opposite sign.

Prior to the measurement of 3/2 for the ground state spin of ^{223}Ra no evidence has been put forward to support the presence of octupole deformation in this nucleus, despite the fact that it lies in the centre of the region where octupole correlations are expected to be strongest (Sheline 1987). However, in 1988, in publications by Sheline *et al.* (hereafter referred to as S88) and Leander and Chen the energy level structure of ^{223}Ra was calculated assuming the presence of static octupole deformation ($\beta_3 \sim 0.1$). The calculations

predicted that the lowest energy levels would belong to $3/2^{\pm}, 5/2^{\pm}$ and $1/2^{\pm}$ parity doublet bands. Using a ^{223}Ra ground state I^{π} of $3/2^{+}$ and the γ-γ angular correlation results (Maples 1977) for the spin sequence $286.1 \xrightarrow{E1} 50.1 \xrightarrow{E1} 0$, S88 was able to assign new I^{π} values to levels in ^{223}Ra. The assignments were made by considering the decay modes of the levels and, where unique values could not be obtained, on the basis of the expected band structure. In this way the authors were able to demonstrate a one-to-one[2] correspondence between the theoretical and experimental energy levels, with the calculations reproducing the correct level ordering of the parity doublet bands.

The assignments made in the work of this thesis agree with those of S88 and we are able to confirm the assignments of $9/2^{+}$, $1/2^{-}$ and $5/2^{-}$ for the 342.8, 350.5 and 369.3 keV levels, respectively (these values were only tentatively assigned in the above reference). Figure 6.3, reproduced from S88, shows the new I^{π} assignments and experimental level energies compared to the theoretical calculations.

The enhancement of E1 transitions between members of the same parity doublet over other E1 transitions in the same nucleus is illustrated in figure 6.4. The figure, again reproduced from S88, shows the E1 transition strengths as a function of transition energy. The transition strengths are given in Weisskopf units since it is common practice to compare experimental transition strengths to those obtained from the single particle model, in this case the Weisskopf transition probabilities are given as: $3.86 \times 10^{6} E_{\gamma}^{3}$, with E_{γ} in keV. As can be seen from the figure the points fall into two distinct groups, separated by approximately two orders of magnitude, a feature that the theoretical model is able to reproduce.

[2]Neglecting the tentative level at 105 keV which did not fit into the theoretical band structure and was therefore believed to be spurious

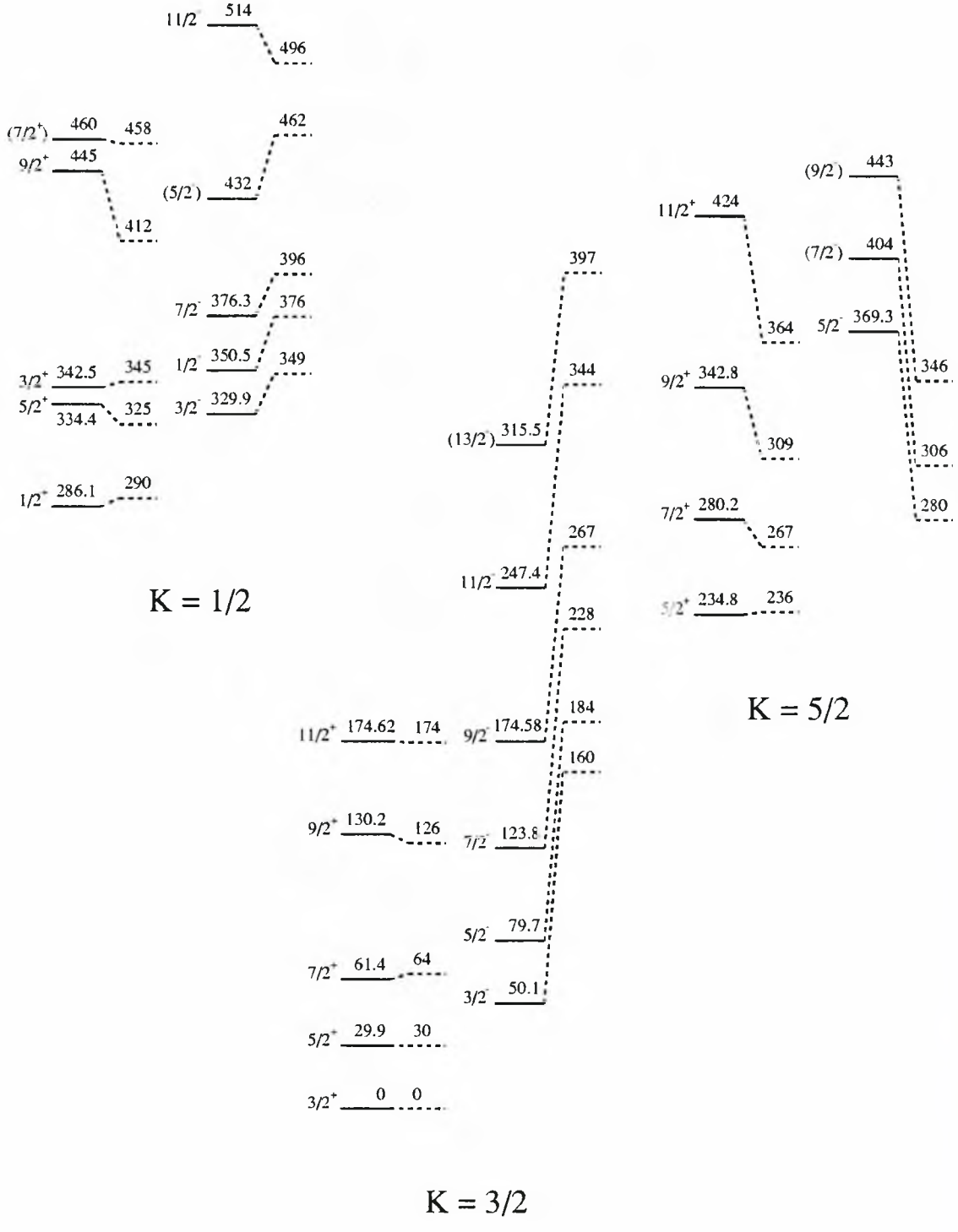

Figure 6.3: Experimental levels up to 514 keV (solid lines) and calculated levels (dashed lines) in ^{223}Ra. The I^{π} assignments to the 315.5 kev level and the levels above 376.3 kev were taken from S88—see text for details.

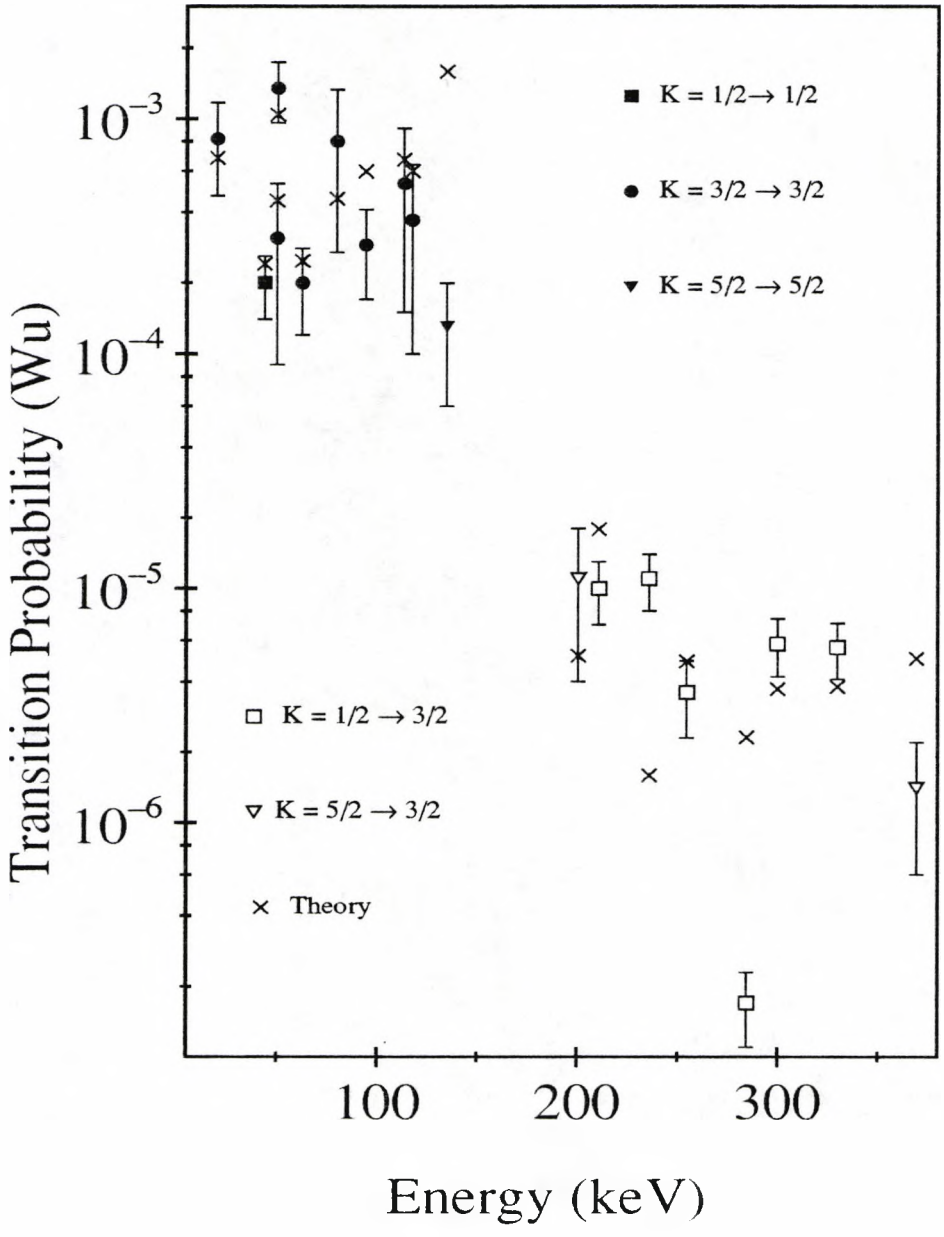

Figure 6.4: E1 transition strengths in ^{223}Ra. The solid points represent transitions between parity doublets. The open points represent transitions from the $K^{\pi} = 5/2^{\pm}$, $1/2^{\pm}$ bands to the ground state band. The crosses represent the theoretical transition probabilities.

		$\beta_3 = 0$		$\beta_3 \neq 0$		
K^π	Nilsson states	μ(nm)	a	μ(nm)	a	Experiment
$3/2^-$	$3/2^-[761]$	–0.06		0.50		0.42 ± 0.06
$3/2^+$	$3/2^+[631]$	0.03				0.28 ± 0.014
$1/2^-$	$1/2^-[770]$		–7.0		–2.7	–2.004
$1/2^+$	$1/2^+[631]$		–0.1		+2.7	1.346
	$1/2^+[640]$		–3.0			

Table 6.1: Experimental and theoretical values of magnetic moments (μ) and decoupling parameters (a) assuming both zero and non-zero values for β_3 in the equilibrium deformation of ^{223}Ra.

The doubling of spin states with respect to parity is a necessary but not sufficient condition for octupole deformation. That is, a parity doublet could also arise from two separate Nilsson orbitals of the same Ω but opposite π. In the case of odd-A nuclei in the actinium region there are many such closely spaced levels. For example, in figure 1.3 (and also in figure 4 of Leander and Chen, 1988) the neutron single particle energy levels corresponding to the Nilsson states $1/2^+[640]$ and $1/2^-[770]$ run almost parallel (as a function of quadrupole deformation), as do the $3/2^+[631]$ and $3/2^-[761]$ Nilsson states. In this situation we can expect the magnetic moments and the decoupling parameters to have quite different values from the octupole deformed case.

Sheline (1986) has compared theoretical and experimental values for the magnetic moments of the $3/2^+$ (ground) and $3/2^-$ (50.1 keV) states and the decoupling parameters for the $K = 1/2^\pm$ rotational bands in ^{223}Ra—see table 6.1. The theoretical values were calculated assuming $\beta_3 = 0$ and $\beta_3 = 0.15$.

As can be seen from the table, although there is no absolute agreement, in each case the experimental values are closer to the theoretical calculations when a non-zero value of β_3 is assumed. It is suggested in the above reference that coriolis coupling between the $1/2^{\pm}$ and $3/2^{\pm}$ bands may explain the discrepancy between the experimental and theoretical ($\beta_3 = 0.15$) magnetic moments. It was also noted that the calculated decoupling parameters were quite sensitive to changes in β_3 a small increase in which would result in a value for $\mid a \mid$ of 1.7, which is intermediate between the experimental values of 1.346 and 2.004.

The conclusions drawn in the above reference are that the experimental values in table 6.1 are what might be expected from an intermediate situation ie. octupole deformation causing mixing between Nilsson orbits of good parity. As to the nature of the octupole deformation, the calculations of S88 are based on static reflection-asymmetry. However, as stated there, this does not mean that the experimental data cannot also be explained in terms of dynamic octupole deformation (ie. the multiphonon method of Piepenbring, 1986). Furthermore, S88 recognises the possibility that the static and the dynamic descriptions of octupole deformation may be similar or even identical.

References

- Ackermann B, Bihn T, Grafen V, Günther C, Marten-Tölle M, Tölle R, Butler P A, Jones G D, White C A, Hughes J R, Wadsworth R, Watson D L, Lauterbach Ch and Maier H J, *Z. Phys.* **A332** 375 (1989).
- Ahmad S A, Klempt W, Neugart R, Otten E W, Wendt K, Ekström C and The ISOLDE Collaboration, *Phys. Lett.* **B133** 47 (1983).
- Bevington P B, *Data Reduction and Analysis for the Physical Sciences*, McGraw-Hill (1969).
- Biedenharn L C and Rose M E, *Rev. Mod. Phys.* **25** 729 (1953).
- Blann M, *Nucl. Phys.* **80** 223 (1966).
- Blatt J M and Weiskopf V F, *Theoretical Nuclear Physics* Willey and Sons (1952).
- Bohr A and Mottelson B R, *Dan. Mat. Fys. Medd.* **27** No. 16 (1953).
- Bohr A and Mottelson B R, *Nuclear Structure, Volume 2*, Benjamin, New York (1975).
- Briançon Ch and Vieu C, *J Physique* **32** 373 (1971).
- Briançon Ch, Ćwiok S, Eid S A, Green V, Hamilton W D, Liang C F and Walen R J, *J. Phys. G.* **16** 1735 (1990).

- Brussard P J and Tolhoek H A, *Physica* **24** 263 (1958).
- Burcham W E, *Elements of Nuclear Physics*, Longman (1979).
- Butler P A, *Ph.D Thesis*, The University of Liverpool (1974).
- Cohen B L, *Concepts of Nuclear Physics*, McGraw-Hill (1971).
- Condon E U and Shortley G M, *The Theory of Atomic Spectra*, Cambridge Univ. Press (1951).
- Ćwiok S and Nazarewicz W, *Phys. Lett.* **224B** 5 (1989).
- Dahlinger M, Kankeleit E, Habs D, Schwalm D, Schwartz B, Simon R S, Burrows J D and Butler P A, *Nucl. Phys.* **A484** 337 (1988).
- Davidson W F and Connor R D, *Nucl. Phys.* **A149** 385 (1970).
- El-Lawindy A M Y, *PhD. Thesis*, The University of Liverpool (1986).
- El-Lawindy A M Y, Burrows J D, Butler P A, Cresswell J R, Holliday V, Jones G D, Tanner R, Wadsworth R, Watson D L, Connell K A, Simpson J, Lauterbach Ch and Mines J R, *J. Phys. G: Nucl. Phys.* **13** 93 (1987).
- Evans R D, *The Atomic Nucleus*, McGraw-Hill (1955).
- Ferentz H and Rosenzweig N, *Argonne National Laboratory Report* 3524 (1954).
- Frauenfelder H and Steffen R M, *Alpha-, Beta- and Gamma-Ray Spectroscopy* (ed. K. Seighbahn), Volume 2, North Holland, Amsterdam (1966).

- Geiger H and Nuttall J M, *Phil. Mag.* **22**, 613 (1911).
- Gooda P H and Gilboy W B, *Nucl. Instr. Meth.* **A255** 222 (1987).
- Hager R S and Seltzer E C, *Nucl. Data* A **4** 1 (1968).
- Hann R L, Roche M F and Toth K S, *Phys. Rev.* **182** 1329 (1969).
- HAMAMATSU, *Hamamatsu Technical Information* SD–08/Nov. 87 (1987).
- Hyde E K, Perlman I and Seaborg G T, *The Properties of the Heavy Elements* Volume 1 Prentice-Hall, Inc., Englewood Cliffs, New Jersey (1964).
- Jain A K, Sheline R K, Sood P C, and Jain K, *Rev. Mod. Phys.* **62(2)** 393 (1990).
- Jones G D, Ekström L P, Kearns F, Morrison T P, Twin P J, Wadsworth R, Ward N J, Collinge B and Wilkinson C L, *Nucl. Instrum. Meth.* **178** 581 (1980).
- Jones G D, Private communication.
- Litherland A E and Ferguson A J, *Can. J. Phys.* **39** 788 (1961).
- Leander G A, Sheline R K, Möller P, Olanders P, Ragnarsson I and Sierk A J, *Nucl. Phys.* **A388** 452 (1982).
- Leander G A and Sheline R K, *Nucl. Phys* **A388**, 375 (1984).
- Leander G A, Nazarewicz W, Bertsch G F and Dudek J, *Nucl. Phys.* **A453** 58 (1986).
- Leander G A and Chen Y S, *Phys. Rev.* **C37** 2744 (1988).

- Lederer C M and Shirley V S, *Table of Isotopes* 7th ed. Wiley, New York (1978).
- Mayer M G, *Phys. Rev.* **78** 16 (1949).
- Myers W D and Swiatecki W J, *Nucl. Phys.* **81** 1 (1966).
- Möller P and Nix J R, *Nucl.Phys.* **A361** 117 (1981).
- Maples C, *Nucl. Data Sheets* **22** 243 (1977).
- Nazarewicz W, Olanders P, Ragnarsson I, Dudek J, Leander G A, Möller P and Ruchowska E, *Nucl. Phys.* **A429** 269 (1984).
- Neergard K and Vogel P, *Nucl. Phys.* **A149** 209 (1970).
- Nilsson G, *Dan. Mat. Fys. Medd.* **29** no. 16 (1955).
- Piepenbring R, *Z. Phys.* **A323** 341 (1986).
- Preston M A, *Phys. Rev.* **71** 865 (1947).
- Preston M A, *Physics of the Nucleus* Adison-Wesley, Reading, Massachusets (1962).
- Rainwater J, *Phys. Rev.* **79** 432 (1950).
- Rasmussen J O, *Phys. Rev.* **115** 1657 (1959).
- Rasmussen J O, *Alpha-, Beta- and Gamma-Ray Spectroscopy* (ed. K. Seighbahn), Volume 1, North Holland, Amsterdam (1966).
- Rose M E, *Alpha-, Beta- and Gamma-Ray Spectroscopy* (ed. K. Seighbahn), Volume 2, North Holland, Amsterdam (1966).
- Rose H J and Brink D M, *Rev. Mod. Phys.* **39** 306 (1967).

- Rowley N, Jones G D and Kermode M W, Submited to *J. Phys. G.* (1991).
- Sheline R K, *Phys. Rev.* **C21** 1660 (1980).
- Sheline R K, *Phys. Lett.* B**166** 269 (1986).
- Sheline R K, *Phys. Lett.* B**197** 500 (1987).
- Sheline R K, Chen Y S and Leander G A, *Nucl. Phys.* **A486** 306 (1988).
- Stephens F S, Asaro F and Perlman I, *Phys. Rev.* **96** 1568 (1954).
- Stephens F S, Asaro F and Perlman I, *Phys. Rev.* **107** 1091 (1957).
- Strutinsky V M, *Nucl. Phys.* **A95** 420 (1967).
- Strutinsky V M, *Nucl. Phys.* **A122** 1 (1968).
- Ter-Akop'yan G M, Private communication.
- Valli K, Hyde E K and Borggreen J, *Phys. Rev.* **C1** 2115 (1970).
- von Weizacker C F Z, *Z. Phys.* **96** 431 (1935).
- Winslow G H, Phys. Rev. **96** 1032 (1954).
- Yamazaki T, *Nucl. Data* A **3** 1 (1967).
- Yates M J L, *Alpha-, Beta- and Gamma-Ray Spectroscopy* (ed. K. Seighbahn), Volume 2, North Holland, Amsterdam (1966).